Reviews

The superior rheological properties (e.g., viscosity, yield stress, shear-thinning behavior, thixotropy, and viscoelasticity) of cellulose nanomaterials (CNMs) have enabled them to be effective rheology modifiers. The dependence of CNM rheology on a wide spectrum of parameters and the application of CNMs as rheology modifiers in several emerging industrial sectors are systematically described.

ADVANCED MATERIALS
www.advmat.de

Rheological Aspects of Cellulose Nanomaterials: Governing Factors and Emerging Applications

Mei-Chun Li, Qinglin Wu,* Robert J. Moon, Martin A. Hubbe, and Michael J. Bortner*

Cellulose nanomaterials (CNMs), mainly including nanofibrillated cellulose (NFC) and cellulose nanocrystals (CNCs), have attained enormous interest due to their sustainability, biodegradability, biocompatibility, nanoscale dimensions, large surface area, facile modification of surface chemistry, as well as unique optical, mechanical, and rheological performance. One of the most fascinating properties of CNMs is their aqueous suspension rheology, i.e., CNMs helping create viscous suspensions with the formation of percolation networks and chemical interactions (e.g., van der Waals forces, hydrogen bonding, electrostatic attraction/repulsion, and hydrophobic attraction). Under continuous shearing, CNMs in an aqueous suspension can align along the flow direction, producing shear-thinning behavior. At rest, CNM suspensions regain some of their initial structure immediately, allowing rapid recovery of rheological properties. These unique flow features enable CNMs to serve as rheological modifiers in a wide range of fluid-based applications. Herein, the dependence of the rheology of CNM suspensions on test protocols, CNM inherent properties, suspension environments, and postprocessing is systematically described. A critical overview of the recent progress on fluid applications of CNMs as rheology modifiers in some emerging industrial sectors is presented as well. Future perspectives in the field are outlined to guide further research and development in using CNMs as the next generation rheological modifiers.

1. Introduction

In recent years, to minimize environmental health and safety concerns, the development of nanotechnology in a sustainable, environmentally friendly manner has been highly desired.[1,2] One of the most promising strategies for sustainable development involving nanotechnology is the isolation and utilization of nanomaterials from green, low-cost, abundant, renewable, and biodegradable natural resources. One such attractive bioresource is cellulose, the most abundant biopolymer on earth, which is widely present in various forms of renewable biomass, such as trees, plants, tunicates, and bacteria.

Structurally, cellulose is a linear, high molecular weight polysaccharide with repeating glucose units linked by 1–4 glycosidic bonds. Owing to the presence of hydroxyl groups, those linear chains of glucose units link together through van der Waals forces and intermolecular hydrogen bonding to form elementary fibrils, which are further packed into larger aggregates known as microfibrils.[3] Cellulose fibrils consist of disordered (amorphous) regions and highly ordered (crystalline) regions. In the crystalline regions, cellulose chains are closely packed together in highly ordered fashion (parallel to the direction of fibril length), dictated by the intricate intra- and intermolecular hydrogen bonding; whereas in the amorphous regions, cellulose chain stacking is less ordered and not as closely packed. Therefore, the amorphous regions are more vulnerable to both physical disintegration and chemical hydrolysis in comparison with crystalline regions. When cellulose is prepared in nano-scale fibrillar or crystalline forms, it is broadly referred to as cellulose nanomaterials (CNMs).

The isolation, characterization, modification, and application of CNMs are currently receiving much attention. Understanding

Prof. M.-C. Li, Prof. Q. Wu
School of Renewable Natural Resources
Louisiana State University AgCenter
Baton Rouge, LA 70803, USA
E-mail: mli@njfu.edu.cn; wuqing@lsu.edu
Prof. M.-C. Li
Co-Innovation Center of Efficient Processing and Utilization of Forest Resources
College of Materials science and Engineering
Nanjing Forestry University
Nanjing 210037, P. R. China
The ORCID identification number(s) for the author(s) of this article can be found under https://doi.org/10.1002/adma.202006052.

DOI: 10.1002/adma.202006052

Dr. R. J. Moon
Forest Products Laboratory
USDA Forest Service
Madison, WI 53726, USA
Prof. M. A. Hubbe
Department of Forest Biomaterials
North Carolina State University
Raleigh, NC 27695-8005, USA
Prof. M. J. Bortner
Department of Chemical Engineering
Virginia Polytechnic Institute and State University (Virginia Tech)
Blacksburg, VA 24061, USA

the processing–structure–property relationship is essential to be able to design and produce CNMs with suitable properties for various emerging applications. The methodologies and cellulosic sources used for CNM production as well as properties of CNMs have been well documented.[3,4] The morphology and characteristics of CNMs, e.g., crystallinity, elastic modulus, thermal stability, colloidal behavior, liquid crystallinity, self-assembling, optical effects, and barrier properties, are greatly dependent on the origin of cellulose and production methods. CNMs possess an abundance of hydroxyl groups, providing a facile platform for modification and functionalization of their surfaces through various chemical and physical strategies.[5–7] Those techniques not only offer solutions to many challenges of CNMs facing practical applications, but also enable fabrication of CNM-based products with high added values. During the past decade, CNMs have been explored for potential applications as functional fillers, templates or building blocks in a large variety of emerging areas, reflected in recently published review articles on polymer composites,[8,9] hydrogels and aerogels,[10,11] water treatment,[12] food science,[13,14] catalysis,[15] liquid crystal template,[16] electronics,[17] and energy devices.[18–20] More recently, the rheological aspects of CNM suspensions (e.g., viscosity, yield stress, shear-thinning behavior, thixotropy, and viscoelasticity) have attracted significant interest.[21–23] In particular, at appropriate concentrations, CNMs can form highly viscous suspensions in aqueous medium due to the occurrence of percolation networks and chemical interactions (e.g., van der Waals forces, hydrogen bonding, electrostatic attraction/repulsion, and hydrophobic attraction) as well as entanglement. Under continuous shearing, CNMs orient along the flow direction, producing profound shear-thinning behavior, i.e., viscosity decreasing with increased shear rate. At rest, CNMs regain much of their initial structure in a short time (i.e., good thixotropic performance), allowing rapid recovery of steady-state viscosity and viscoelastic properties. These attractive flow features allow CNMs to serve as effective rheological modifiers in a wide range of applications, whereas a comprehensive review in this topic is missing.

Herein, we focus on the recent progress of rheological behaviors of CNM suspensions and using CNMs to formulate advanced fluids and materials for different emerging applications (**Figure 1**). The differences in cellulosic sources and production methods account for the diverse morphology and surface chemistry of CNMs, and directly impact the rheology of CNM suspensions. Accordingly, a brief overview on the sources, production methods, and general characteristics of CNMs is outlined in Section 2. Section 3 provides a brief outline of rheology principles in relation to CNM suspensions, as well as a comprehensive summary of the flow behaviors, and their dependence on test protocols, CNM inherent properties, suspension environments, and post processing. In Section 4, a critical overview of recent progress in applications of CNMs as rheological modifiers in: i) inks for 3D printing, ii) materials for oilfield and construction services, iii) food additives, iv) coatings, and v) cosmetics and personal care products is outlined. Finally, future perspectives are provided to further guide research and development in using CNMs as the next generation rheological modifiers for diverse industry applications.

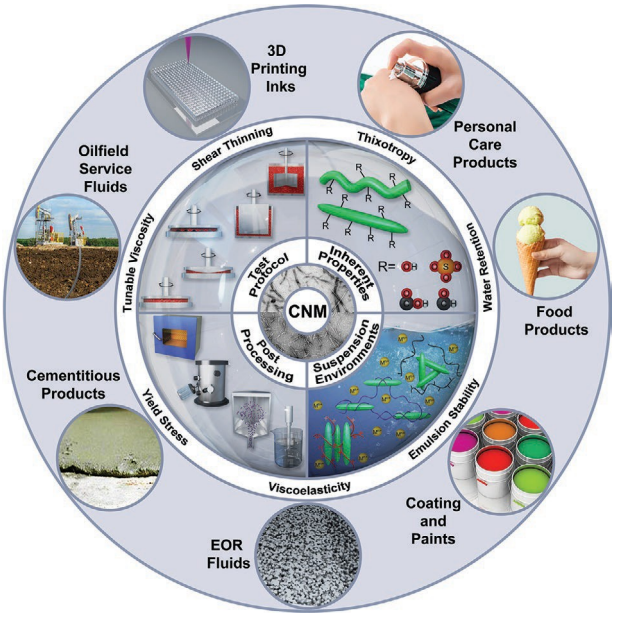

Figure 1. An overview of key factors in cellulose nanomaterial (CNM) rheology and their influence on CNM's emerging applications. At the center is the morphology of two typical CNMs (i.e., fiber-like NFC and rod-like CNCs), which are the focus of this review paper. Several governing factors, including test protocols, inherent CNM properties, suspension environment, and post processing, affect the rheological properties of CNM suspension (i.e., viscosity, yield stress, viscoelasticity, shear thinning, thixotropy, water retention, and emulsion stabilization) that must be further tailored for use in the given CNM's emerging applications (i.e., 3D printing inks, personal care products, food products, coating and paints, enhanced oil recovery or EOR fluids, cementitious products, and oilfield service fluids).

2. General Characteristics of CNMs

"CNMs" is a general term designated by the International Standards Organization (ISO) to describe a class of cellulose-based particles that have at least one dimension in the nano-size scale (1–100 nm). There are many different varieties of CNMs, presenting a wide spectrum of particle morphologies (e.g., shape, size, and aspect ratio), properties and surface chemistries, all of which affect the rheology, colloidal behavior, and self-assembly of CNM suspensions, colloids, and mixtures. As a result, when working with CNMs, it is critical to have a comprehensive and accurate characterization of the particle morphology, size, surface characteristics, and rheological properties prior to investigating potential applications of CNMs as rheological modifiers.

Variations in CNMs arise from three main factors: i) cellulose source material, ii) isolation or production method, and iii) surface chemistry. The influence of cellulose source on the resulting CNMs arises from the cellulose biosynthesis process, which is highly specific to the cellulose-producing organism, affecting the cellulose chain stacking and bundling that make up CNMs and subsequently govern the degree of crystallinity, particle aspect ratios, lengths, widths, and cross-sectional morphologies. A wide variety of cellulose source materials (e.g., trees, plants, algae, bacteria, tunicate) have been used to produce CNMs.[3,24–27] The focus here is on CNMs produced from trees and plants.

The processes for producing CNMs typically consist of pretreatment and refinement steps that are tailored for the specific cellulose source. Pretreatments (e.g., mechanical, chemical, or enzymatic) typically purify and homogenize the starting material so that it reacts more consistently to facilitate fragmentation of the cellulose source material during the refinement step. There are two main refinement approaches to fragment cellulose source materials into nanosized particles: mechanical shear and acid hydrolysis.[28] Refinement by mechanical shear tears apart the cellulose source material (e.g., fibrillating the material),[27] creating nano-sized particles with fibril-like morphologies (e.g., microns in length, nanometers in width, and often branched). In contrast, refinement by acid hydrolysis preferentially dissolves the disordered regions of the material,[29] creating nano-sized particles with spindle-like morphologies (e.g., nanometers in length and width, with tapered ends). As a consequence of the large differences in particle morphology from these two refinement approaches, they subsequently define two classifications of CNMs, nanofibrillated cellulose (NFC) and cellulose nanocrystals (CNCs). The term cellulose nanofiber (CNF), as designated by the ISO nomenclature, can be regarded as a synonym for the traditionally established term NFC.[30]

The surface chemistry of CNMs can critically affect how they interact with the environment, controlling such things as dispersion in solvents or polymers, rheology, self-assembly, and agglomeration. The surface chemistry can result as an artifact from a given CNM production method, or after subsequent chemical modification. A wide variety of chemistries and modification routes have been explored.[5–7]

With large differences in particle morphology of NFC versus CNCs, it is necessary that their rheological behaviors be discussed separately, as being done throughout this review. By comparing and contrasting NFC and CNCs, further insight on the role of CNM morphology on rheology can be gained. Additionally, not all NFC or CNCs are the same, and considerable variation in particle morphology and surface chemistry can result from differences in the production/refinement process. Sections 2.1 and 2.2 provide some additional description on the processing and morphologies of NFC, and CNCs, respectively.

2.1. NFC

In general, NFC refers to cellulosic particles that have fibril-like morphology (e.g., microns in length, nanometers in width, with aspect ratios usually greater than 50), are flexible, semicrystalline, nanosized, and often exhibit longitudinal splits (e.g., branching), and form entanglements between cellulose fibrils (e.g., network-like structures). However, it is necessary to appreciate that there is an extremely wide spectrum in the degree of fibrillation and branching of these objects.[25,27,31–35] They can range from fine isolated fibrils of ≈4–10 nm in width, to coarse materials (20–100 nm wide) with extensively branched/interconnected network structures, and most typically they lie somewhere in between (**Figure 2**). In this review, NFC is used to generally refer to particles produced via mechanical refinement to fibrillate wood and plant cellulose.[30] It should be noted that such materials have been named as nanofibrillated cellulose, microfibrillated cellulose, cellulose microfibrils, cellulose nanofibers, cellulose microfibers, and highly refined cellulose in the literature.

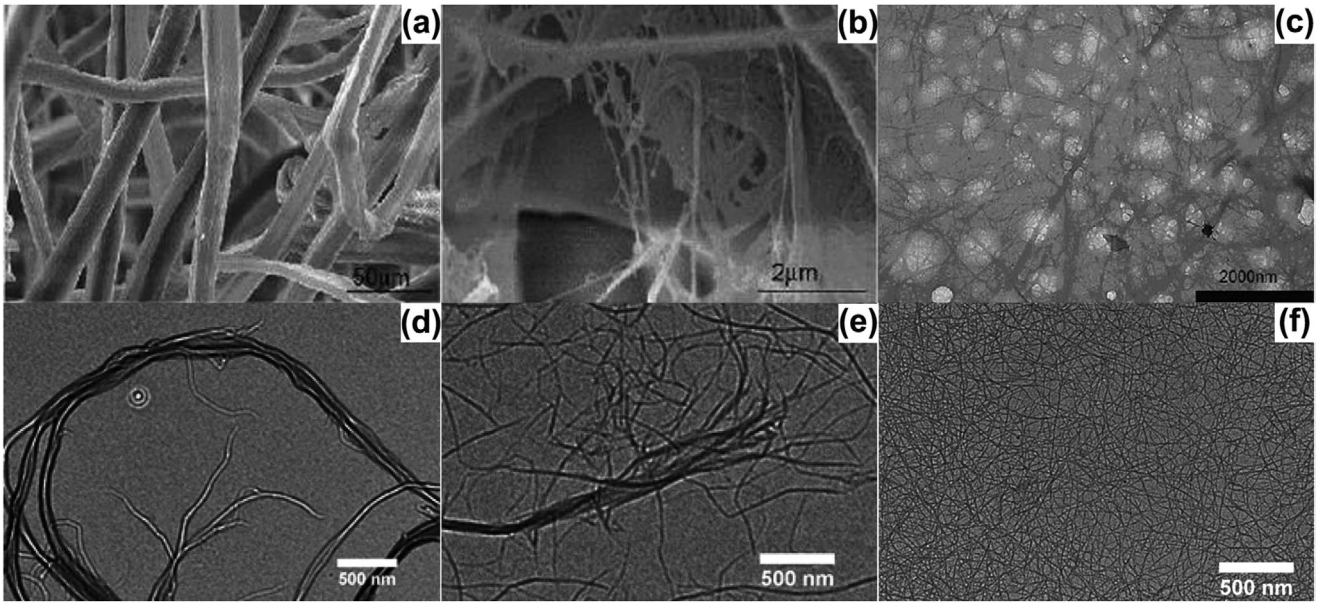

Figure 2. Morphology of cellulose fibers and NFC from various processing approaches. a–c) By comparing: a) bleached kenaf bast pulp, b) bleached kenaf bast pulp after cryocrushing and refining; and c) UN-NFC from bleached kenaf bast pulp through cryocrushing, refining, and HPH using a homogenizer; it is apparent that finer size-scale of the cellulose fibrils were produced as a result of increased mechanical refinement. a–c) Reproduced under the terms of the CC-BY Creative Commons Attribution 4.0 International License (http://creativecommons.org/licenses/by/4.0/).[40] Copyright 2009, The Authors, published by BioResources. d–f) Contrasting results were obtained for: d) UN-NFC, e) E-NFC, and f) TO-NFC from commercial wood pulp. d–f) Reproduced with permission.[41] Copyright 2014, American Chemical Society. Note: a,b) SEM images; c–f) TEM images.

The fibrillation process from wood and plant cellulose typically results in a complex mixture of particles of various shapes, morphologies, and sizes, encompassing nanoscale particles, nanofibrillated fibers, microfibrillated fibers, and residual micron to millimeter sized fibers. As a result, it has been extremely difficult to quantify or systematically describe the morphology (e.g., aspect ratio, degree of fibrillation, level or branching, etc.) and the distributions produced from a given fibrillation process. Approaches are outlined by Desmaisons et al., and Kangas et al. that offer some guidance on the use of multiple characterization methods to gain a more collective description of the objects produced (e.g., fractionation, light scattering, rheology, crystallinity, water retention, specific surface area, surface chemistry, etc.).[36,37]

The challenge here is that the NFC's rheological behavior is highly dependent on the NFC morphology (and its distribution), and thus it is challenging to link changes in NFC preparation parameters to changes in NFC morphology and then to the resultant rheological behavior. This hinders efforts to link mechanisms to the differences (or similarities) in rheological behavior when comparing results. This is made even more challenging when comparing results in the published literature, where the details of NFC particle characterization can vary substantially. An approach to partially deal with this is to broadly subcategorize NFC, which could be based on coarseness of structure (e.g., cellulose nanofibrils, cellulose microfibrils), differentiation in processing, and/or surface chemistry. Though not ideal, as there is still a high level of ambiguity, such an approach makes it possible to identify similar or dissimilar comparisons in the NFC literature, but extreme caution is needed to avoid over-stating the relevance of such comparisons. In this review we have subcategorized NFC based on whether it has undergone mechanical refinement alone compared to NFC that underwent various types of pretreatments (e.g., enzymatic or chemical) prior to mechanical refinement. We have done this to inform the reader about differences in processing of the NFC material, and the reader should infer the potential for differences in the resulting NFC morphology and surface chemistry, and thus differences in rheological behavior. We define each NFC subcategory and distinguish them with one or two letters preceding NFC; for example, mechanical refinement without pretreatments, i.e., untreated, is represented by UN-NFC.

The resulting NFC morphology is influenced by i) pretreatments, ii) mechanical disintegration techniques and processes used, and iii) the extent of the mechanical fibrillation (i.e., energy input, or number of cycles). Prior to mechanical disintegration, there are three general approaches to pretreating cellulose source materials for NFC production: mechanical, enzymatic hydrolysis, and chemical. Mechanical pretreatments (e.g., refining, cryocrushing) reduce the length of the cellulose fibers and also delaminate fiber surface layers, thus facilitating the fibrillation (Figure 2a–c). The enzymatic pretreatments degrade the cellulose using a set of cellulases (e.g., exoglucanases and endoglucanases).[38] NFC produced with enzymatic pretreatments prior to mechanical disintegration are referred to as E-NFC. Certain chemical pretreatments alter cellulose fibers to provide abundant ionic charges on the surface, leading to the formation of strong repulsion forces between cellulose fibers, which are beneficial for subsequent mechanical disintegration. The most commonly reported chemical pretreatment is carboxylation via TEMPO oxidation,[39] but there are many other chemical pretreatment options (e.g., periodate–chlorite oxidation, carboxymethylation, sulfonation and cationization).[27,31] NFC produced with TEMPO, periodate–chlorite oxidation, carboxymethylation, sulfonation and cationization pretreatments prior to mechanical disintegration are referred to as TO-NFC, PC-NFC, CM-NFC, S-NFC and CA-NFC, respectively. TO-NFC and CM-NFC are carboxylated forms of NFC, referred to as C-NFC. It should be noted that the chemical pretreatments not only alter NFC morphology, but also change NFC's surface chemistry and charges.

Three of the more prevalent mechanical disintegration approaches used to fibrillate cellulose materials to NFC are high-pressure homogenization (HPH), grinding, and ultrasonication. As shown in Figure 2d–f, NFC morphology (e.g., thickness and length) is influenced by different pretreatments and mechanical disintegration methods. UN-NFC, E-NFC, and TO-NFC have large, moderate, and small sized (diameter) nanofibril, respectively. In general, the production method (e.g., pretreatment and mechanical fibrillation) has a more profound influence on the dimension of resultant NFC than the cellulosic source.

2.2. CNCs

CNCs have a spindle morphology (e.g., rod-like, nanometers in length and width, aspect ratios less than 50, tapered ends, no branching, and no entanglement). CNCs are rigid and highly crystalline nanoparticles extracted from wood, plants, algae, bacterial and tunicate cellulose source materials.[3,4] There are various isolation methods to produce CNCs, including hydrolysis with mineral acid, organic acid, enzyme, and subcritical vapor, treatment through oxidation, ionic liquids, deep eutectic solvents, mechanical forces, and their combinations.[26] Mineral acid hydrolysis with sulfuric acid is the predominant process. The resulting CNC morphology is influenced by i) cellulose source material, ii) pretreatments, and iii) acid hydrolysis parameters (e.g., type of acid, concentration, time, temperature). The resultant surface chemistry and charge are also determined by the acid hydrolysis conditions.[26,42] Independent of any differences in processing, the current International Standards Organization (ISO) nomenclature standard for CNMs has grouped this under a single name of CNCs.[30] Herein, CNCs hydrolyzed using sulfuric acid, hydrochloric acid, phosphoric acid, and formic acid are referred to as S-CNCs, H-CNCs, P-CNCs, and F-CNCs, respectively.

The effect of sulfuric acid hydrolysis parameters, including time, temperature, acid concentration, and acid-to-cellulose ratio on the dimension, crystallinity, surface characteristics, and yield of CNCs has been widely studied.[43–45] The amount of sulfate groups has been found to gradually increase as the acid concentration is increased,[43] but is relatively independent of hydrolysis time.[45] In addition, lower temperatures were shown to favor a higher number of sulfate groups, whereas at higher temperatures, de-esterification of the sulfate groups occurred.[44] One major disadvantage of S-CNCs is that sulfate group catalyzes the thermal decomposition of cellulose, resulting in poor thermal stability.[46] The use of other acids to hydrolyze CNCs can

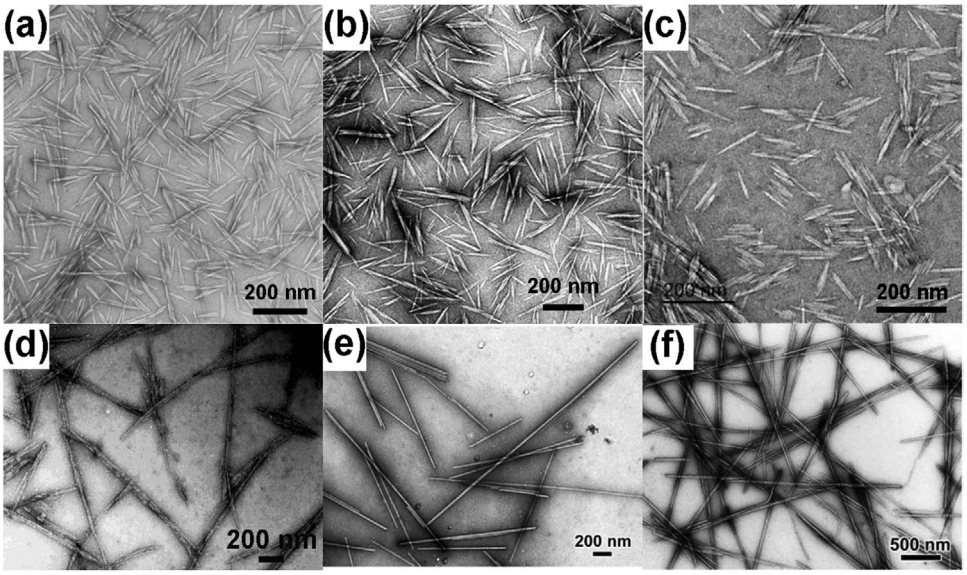

Figure 3. TEM morphology of S-CNCs isolated from different cellulosic sources. a) Wood; b) ramie fibers; c) cottonseed hulls; d) bacterial cellulose; e) green algae; f) tunicate. a) Reproduced with permission.[42] Copyright 2015, Springer Nature. b) Reproduced with permission.[48] Copyright 2008, Royal Society of Chemistry. c) Reproduced with permission.[49] Copyright 2016, Elsevier. d) Reproduced with permission.[46] Copyright 2004, American Chemical Society. e) Reproduced with permission.[50] Copyright 2012, American Chemical Society. f) Reproduced with permission.[51] Copyright 2007, American Chemical Society.

produce different negatively charged groups on the CNC surface, leading to increased thermal stability of CNCs. For example, P-CNCs isolated from cotton using phosphoric acid showed superior thermal stability compared with that of S-CNCs.[47]

Cellulosic source origin for CNCs can have a large influence on their dimensions and crystallinity, as shown in **Figure 3**. CNCs hydrolyzed from wood (Figure 3a) and plants (Figure 3b,c) are generally 5–20 nm in width and 50–350 nm in length,[42,48,49] whereas those from bacteria (Figure 3d), algae (Figure 3e), and tunicates (Figure 3f) can possess widths of 10–50 nm and lengths up to several micrometers.[46,50,51]

3. Rheological Behaviors of CNM Suspensions

Due to diverse morphology and surface chemistry of CNMs, their suspensions exhibit very complicated flow behaviors. A fundamental understanding of the principle of rheology becomes critically essential for a better interpretation of the complex rheological responses of CNM suspensions. When CNMs are suspended in an aqueous medium, NFC and CNCs show flocculation and lyotropic phase behaviors, respectively. Upon continuous shearing, both NFC and CNCs can gradually align along the flow direction, exhibiting typical shear-thinning behavior. The flocculation of NFC, lyotropic phase of CNCs, and shear-induced orientation behaviors are critically relevant for their rheological properties.

3.1. Principle of Rheology in Relation to CNM Suspensions

Fluids such as CNM suspesnions can be generally classified into Newtonian and non-Newtonian fluids (**Figure 4**a,b). Newtonian fluids exhibit a constant viscosity, while the incorporation of a dispersed phase into a Newtonian fluid can lead to the occurrence of several types of non-Newtonian behaviors, i.e., Bingham plastic, Bingham pseudoplastic, shear thinning (pseudoplastic), and shear thickening (dilatant). Bingham plastic fluids behave as rigid solids until a yield value of shear stress, and above this value they flow as Newtonian fluids. Bingham pseudoplastic fluids also exhibit a yield stress, but they show shear-thinning behavior above the yield stress. The viscosity of shear thinning fluids gradually decreases with increased shear rate. Conversely, shear thickening fluids show increased viscosity with increased shear rate. Non-Newtonian fluids also include thixotropic and rheopectic fluids. A thixotropic fluid is a time-dependent shear thinning fluid, which becomes less viscous over time after being sheared, shaken, or agitated. A rheopectic fluid is a time-dependent shear thickening fluid, which becomes more viscous or even solidified over time after being sheared, shaken, or agitated.

The viscoelatic behavior of fluids such as CNM suspesnions can be determined by oscillatory shear measurements as functions of strain, γ, (strain sweep) and frequency, ω, (frequency sweep). In the linear region, the strain sweep curve of CNM suspensions generally exhibits stable $G'$and G'' independent of the applied strain under a fixed frequency (Figure 4c). Above a critical strain (γ_c), a nonlinear region appears, in which the dynamic moduli become a function of the strain (i.e., in most of cases, the dynamic moduli decresase with increase in strain).[52] It is worth noting that overshoots in G'' have been reported in specific cases, particularly in electrolytes.[53,54] The decrease in $G'$and G'' beyond the critical strain (γ_c) is attributed to the structural breakdown under high deformation. The value of γ_c is therefore widely used to contrast the stability of structure for different samples. The shape of the frequency sweep curves depends on the microstructure of viscoelastic materials

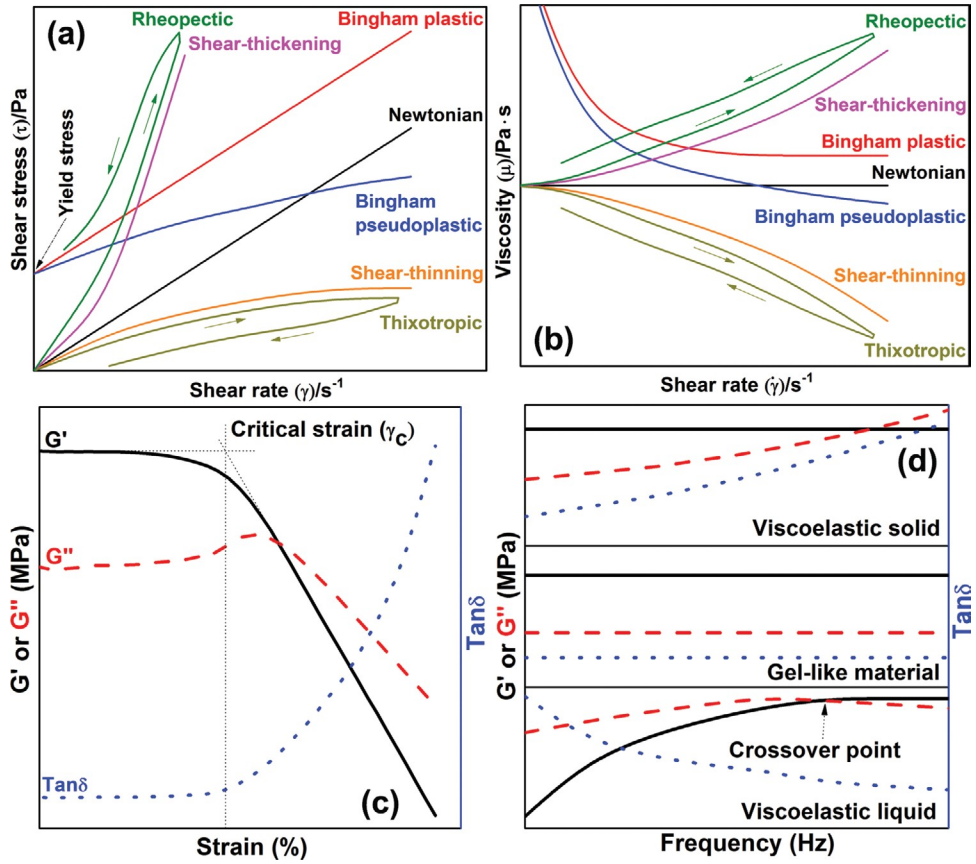

Figure 4. a–d) Typical rheological curves for different types of ~~fluids: a) shear~~ stress and b) viscosity cu~~lasticity curves as functions of strain, and d) frequency. The lines of black solid, red dash, and blue do~~ modulus (G''), and tan δ, respectively.

(Figure 4d). For viscoelastic solids, G' is independent of the frequency, whereas G'' is linearly proportional to the frequency ($G' \approx \omega^0$, and $G'' \approx \omega$). For gel-like materials, both G' and G'' are independent of the frequency ($G' \approx \omega^0$, and $G'' \approx \omega^0$). For viscoelastic liquids, G' and G'' gradually increase as the frequency increases ($G' \approx \omega^2$, and $G'' \approx \omega$).

Rheological properties of fluids are generally governed by shear rate, time, temperature and physicochemical properties of included particles. For rod- and fibril-like CNMs, shear rate and aspect ratio are the most two critical governing parameters. Numerous rheological models have been used to describe the complicated flow behavior of CNM suspensions (**Table 1**).

In general, shear rate-dependent models can be classified into two-parameter[55–57] and three-parameter[58–65] models. The two-parameter models are simple to use, but they can lead to inaccurate results for simulating complex fluids such as CNM suspensions (especially for NFC suspensions with physically entangled network). For example, the Bingham plastic model[55] assumes that a fluid behaves in Newtonian manner after the yield stress is exceeded. However, CNM suspensions exhibit strong shear-thinning behaviors above the yield stress.[63] The power-law model[56] can only accurately fit the shear thinning region with a constant logarithmic decrease in viscosity as a function of shear rate, and it cannot capture Newtonian viscosity plateaus at low (zero shear) or high shear rates of NFC suspensions.[73] On the other hand, models wi
applied to describe t
shear stress and shea
as their fluid mixture
include Herschel–Bu
Mizrahi–Berk,[61] Robert
Berg,[64] and Ellis[65] mo
Herschel–Bulkley ~~model, combined Bingham plastic and power-law models,~~ is popula
minimum stress applie
the model described t
only when the shear ra
transition in the middle
fluids (WDFs) contain
and bentonite (BT),[78]
most accurate fitting re
curves for S-CNC/PAC/
at low and intermediate
at high shear rate regio
well describe the flow behavior of S-CNC suspensions at very high shear rates ranging from 10^4 to 10^6 s^{-1}, suggesting a shear thinning behavior (represented by the flow index, n) followed by transition to a high shear Newtonian viscosity plateau.[80] For cement pastes containing S-NFC,[79] the Vom Berg model was shown to perform the best in accurately capturing yield stress

Wiley-VCH
2021-04-14 23:11:59
---
rate; c,d) viscoelasticity curves as functions of strain (c) and frequency (d). The black solid lines, red dashed lines, and blue dotted lines

Wiley-VCH
2021-04-14 23:14:11
---
model (combined Bingham plastic and power-law m

Table 1. Common rheological models for describing the flow behavior of CNM suspensions as functions of shear rate, aspect ratio and volume fraction (Note: τ is shear stress, τ_0 is yield stress, μ_p is plastic viscosity, K is flow consistency coefficient, n is flow behavior index, μ_0 is zero-shear viscosity, $\tau_{1/2}$ is value of shear stress at $\frac{0}{2}$, μ_∞ is viscosity at infinite shear rate; $[\mu]$ is intrinsic viscosity, μ_r is relative viscosity, ν is the number density of CNMs, L is the CNM length, β is a measure of the release of the CNM tube constraints, ε is a parameter indicating the degree of "log-jamming," D is the rotational diffusion coefficient, ϕ is volume fraction, ϕ_m is maximum packing fraction, which is dependent on f of CNMs. The ϕ_m has been estimated as a function of f of CNMs (i.e., $\phi_m = 96f^{-2}$).[71]

Parameters	Rheological models	
	Name	Equation
Shear rate (γ)	Bingham plastic[55]	$\tau = \tau_0 + \mu_p\gamma$
	Power law[56]	$\tau = K\gamma^n$
	Casson[57]	$\tau^{0.5} = \tau_0 + K\gamma^{0.5}$
	Herschel–Bulkley[58]	$\tau = \tau_0 + K\gamma^n$
	Sisko[59] Heinz–	$\tau = \mu_\infty\gamma + K\gamma^n$
	Casson[60]	$\tau^n = \gamma_0^n + K\gamma^n$
	Mizrahi–Berk[61]	$\tau^{0.5} = \tau_0 + K\gamma^n$
	Robertson–Stiff[62]	$\tau = K(\gamma_0 + \gamma)^n$
	Vocadlo[63]	$\tau = (\tau_0^{1/n} + K\gamma)^n$
	Vom Berg[64]	$\tau = \tau_0 + b\sinh^{-1}\left(\frac{\gamma}{c}\right)$
	Ellis[65]	$\tau = \frac{\mu_0\gamma}{1+\left(\frac{\tau}{\tau_{1/2}}\right)^{n-1}}$
Aspect ratio (f)	Onsager[66]	$[\mu] = \frac{4f^2}{15\ln f}$
	Simha[67]	$[\mu] = \frac{f^2}{15[\ln(2f)-1.5]} + \frac{f^2}{5[\ln(2f)-0.5]} + \frac{14}{15}$
	Batchelor[68]	$[\mu] = \frac{8f^2}{45\rho\ln(2f)}\left\{\frac{\ln(2f)+0.64}{\ln(2f)-1.5} + \frac{1.659}{[\ln(2f)]^2}\right\}$
	Wierenga–Philipse[69]	$\mu_r = \left(1 + \frac{\pi}{90\ln f}\nu L^3 + \frac{\pi}{30\beta\ln f}\right)\nu L^3)^3$
	Sato–Teramoto[86]	$\mu_r = 1 + \frac{\pi}{90\ln f}\nu L^3 + \frac{\pi}{30\beta\ln f}\left[1 + \frac{\gamma L}{\beta^{0.5}(1-\varepsilon^{\nu DL_2}}\right]\nu L^3$
	Krieger–Dougherty[70]	$\mu_r = \left(1 - \frac{\phi}{\phi_m}\right)^{-2.5\phi_m}$

and shear thinning response over the broadest range of compositions and shear rates.

Depending on the volume fraction (ϕ) and aspect ratio (f) of CNMs, CNM suspensions can be classified into three regimes: i) dilute regime, $\phi \le f^{-2}$; semi-dilute regime, ii) $f^{-2} \le \phi \le f^{-1}$; and iii) concentrated regime, $\phi \ge f^{-1}$.[81] In the dilute regime, the hydrodynamic forces and particle–particle interaction are negligible, and the relationship between intrinsic viscosity $[\mu]$ and f follows the Onsager,[66] Simha,[67] and Batchelor[68] equations. Among these models, the Simha equation has been widely used to predict the f of CNMs using $[\mu]$ of CNM suspensions.[72,82–84] However, the negative charge on the surface of CNCs created strong electro-viscous effects, which caused a non-negligible increase in the $[\mu]$. As a result, the Simha model led to much higher f than that determined from microscopic techniques (e.g., AFM and TEM). The presence of a small amount of salt is an effective approach to screen the electric double layers of S-CNCs, leading to remarkable reduction in the $[\mu]$.[85] With the Batchelor equation and revised $[\mu]$, the derived f value was close to that determined by TEM. The Onsager and Simha models were also used to describe the $[\mu]$ of UN-NFC suspensions as a function of f, and simulation results showed that these two models provided almost the same fitting results.[84] In the semi-dilute regime, the hydrodynamic and particle–particle interactions are not negligible. The model developed by Wierenga and Philipse[69] is more applicable. In the concentrated regime, the particle–particle interaction becomes dominant, the Krieger–Dougherty[70] and Sato–Teramoto[86] models can well describe the relationship between relative viscosity (μ_r) and f. In comparison with Wierenga–Philipse model, the Sato–Teramoto model performed better in fitting the μ_r of the S-CNC suspension in the concentration range from 1.3 to 8.0 vol%.[87] Furthermore, the viscosity of S-CNC suspensions at volume fraction less than 10% increased much faster with concentration increase than the simulated results by Batchelor and Krieger–Dougherty models for spherical particles due to the higher f of S-CNCs, highlighting the need for selection of proper f values to obtain accurate fitting results.[88]

3.2. Flocculation and Shear-Induced Orientation Behaviors of NFC Suspensions

Because of extremely long fibrils and stiff inter-fibrillar interactions, NFC tends to become highly entangled, forming flocculated microstructures. The formation of NFC flocs and shear-induced orientation governs the rheological behaviors of NFC suspensions both at rest and under steady shearing conditions.

To monitor microstructure changes in situ of NFC flocs during shear rheology, [illegible] digital imaging,[89,90] [illegible] sonic speckle velocimetry,[34] and a [illegible]

For example, Saarinen [illegible] the relationship betw [illegible] and their rheological [illegible] a cylindrical, transpa [illegible] changes of flocs were [illegible] shear stress with incr [illegible] ultrasonic speckle velocimetry (USV) coupled to rheometry, the 2D spatial and time-resolved characterization of the shear flow of NFC suspensions was realized.[34] For E-NFC suspensions, the spatial velocity maps recorded at different times were very erratic (Figure 5e), suggesting the presence of flocs and change in the microstructure of flocs under shearing. For TO-NFC suspensions, although the velocity was also heterogeneous, its spatial and temporal variations were smoother and much less erratic (Figure 5f), confirming the absence of mesoscale flocs at the micrometric scale. These differences were ascribed to the distinctively different dispersion states of E-NFC and TO-NFC

Wiley-VCH
2021-04-14 22:42:07
---
of NFC flocs in situ
Wiley-VCH
2021-04-14 22:43:10
---
using

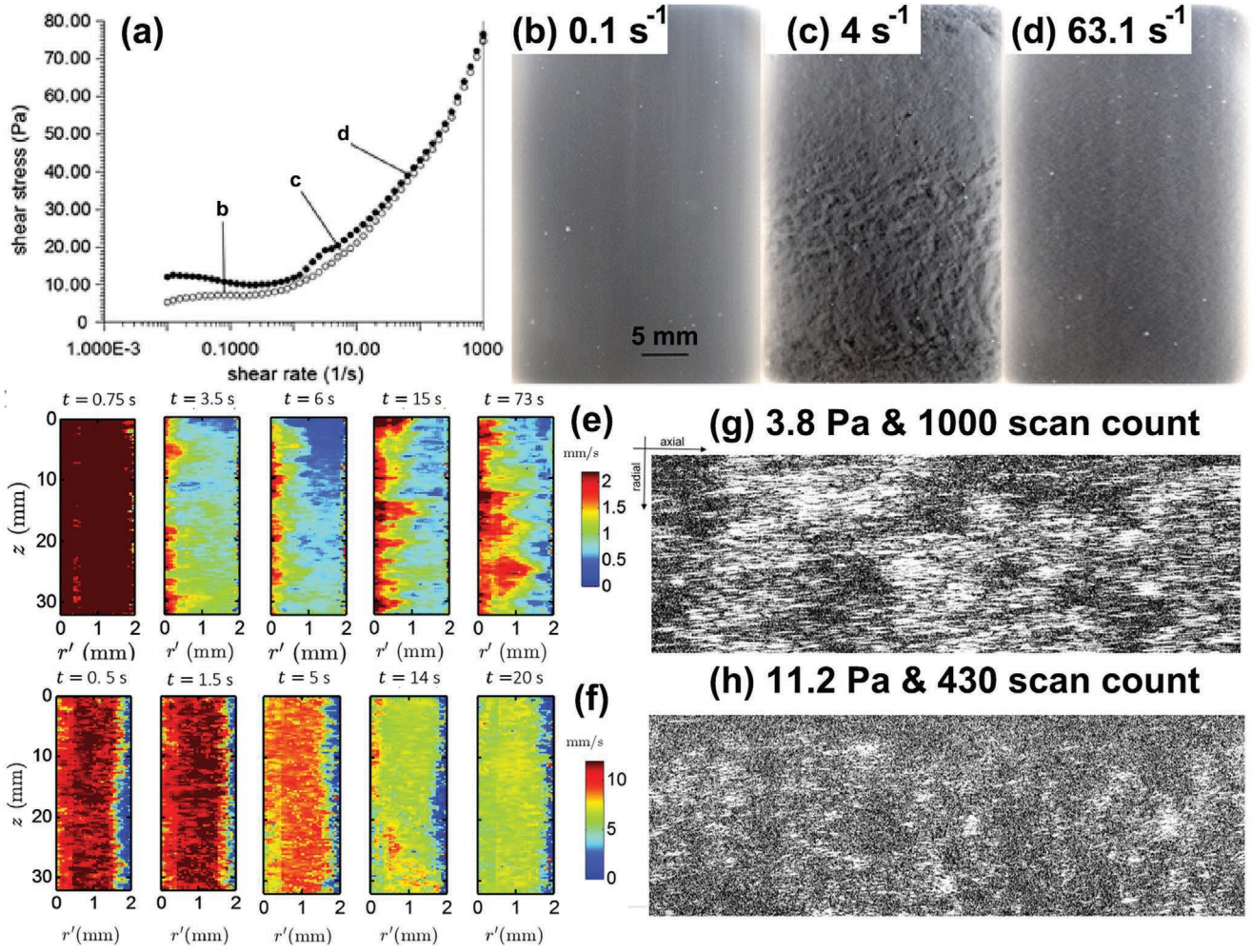

Figure 5. Concentration-dependent flocculation and shear-induced orientation behaviors of NFC in an aqueous suspension. a) Shear stress versus shear rate curves for TO-NFC suspension measured using the transparent (empty circles) and metal (filled circles) cups. b–d) The corresponding microstructures of NFC flocs at shear rates of 0.1, 4 and 63.1 s^{-1}, respectively. a–d) Reproduced under the terms of the CC-BY Creative Commons Attribution 4.0 International license (http://creativecommons.org/licenses/by/4.0/).[90] Copyright 2012, The Authors, published by Springer. e,f) Spatial velocity maps taken at different times for E-NFC suspension and TO-NFC suspension, respectively. e,f) Reproduced with permission.[34] Copyright 2015, Royal Society of Chemistry. g,h) Optical coherence tomography images showing microstructure of flocs in UN-NFC suspension with the shear stress and scan count of 3.8 Pa & 1000 and 11.2 Pa & 430, respectively. g,h) Reproduced under the terms of the CC-BY Creative Commons Attribution 4.0 International license (http://creativecommons.org/licenses/by/4.0/).[92] Copyright 2018, The Authors. ~~(g,h) is 120 μm × 290 μm.~~ In all images, NFC flow from left to right.

Wiley-VCH
Wiley-VCH
2021-04-14 23:01:24
is

suspensions. Due to the highly charged surface, TO-NFC suspensions are more homogeneously dispersed, and thus they do not display evident flocculation. The combined uses of an optical coherence tomography device and a rotational rheometer[91] or a pipe rheometer[92] to examine the flocculation dynamics and rheological properties of UN-NFC suspensions were also reported. The highly elongated flocs flowed along the shearing direction below the yield stress (Figure 5g). Above the yield stress, the flocs became almost spherical (Figure 5h). The size of spherical flocs was monotonically reduced as the shear stress was increased. Assuming that the birefringence of the fibrils is the same as CNCs, the birefringence can directly indicate the alignment of the fibrils.[73] Through in situ measuring of the birefringence using a parallel-plate geometry associated with a photo-elastic modulator, the shear-induced orientation of fibrils [illegible]. The fibrils became alig[illegible] in the intermediate she[illegible]

3.3. Lyotropic Phase an[illegible] Shear-Induced Orientation Behaviors of CNC Suspensions

CNC suspensions display concentration-dependent lyotropic phase behavior.[44,94] With a gradual increase in CNC concentration, the dispersion microstructure of CNCs readily transits from isotropic to biphasic containing both isotropic and liquid crystalline, to fully liquid crystalline, and ultimately to a gel. Aspect ratio and surface chemistry are two important parameters governing the lyotropic phase formation. Furthermore,

CNCs are more prone to align along the shear direction in suspension compared with NFC due to their smaller dimensions and moderate aspect ratios, which notably affect the rheological behaviors of CNC suspensions.

The formation of a liquid crystalline phase in a CNC suspension as a function of CNC concentration can be observed using polarized optical microscopy (POM). For example, cross-polarized microscopy images of S-CNCs from cotton cellulose[94] showed that the transition from isotropic to biphasic occurred at concentrations of 4.2 wt%, 4.05 wt% and 4.5 wt% at 4 °C, 20 °C and 45 °C, respectively, agreeing well with the critical concentration reported by Dong et al.[95] With an increase in the S-CNC concentration, the portion of liquid crystalline phase gradually increased (**Figure 6**a). The POM images further revealed that a biphase of isotropic and liquid crystalline (Figure 6b), entirely liquid crystalline phase (Figure 6c) and gel microstructure (Figure 6d) gradually appeared with increases in the S-CNC concentration. Through optical microscopy in crossed polarization geometry, Bercea and Navard observed the first birefringent liquid crystalline domains in S-CNC suspension at an extremely low concentration of around 0.8 wt% (or 0.53 vol%).[81] Using the rigid rod approximation, the critical transitions of S-CNC suspension from dilute regime to semi dilute regime and from demi dilute regime to concentrated regime were predicted to be at volume fractions of f^{-2} and f^{-1}, respectively.

The shear-induced orientation of CNCs in suspension was intuitively confirmed through several techniques, including small angle X-ray scattering (SAXS),[96] small angle neutron scattering (SANS),[97] small angle light scattering (SALS),[98] scanning electron microscopy (SEM),[99] and POM[100] observations. Ebeling et al. used SAXS to characterize the alignment of 6.9 wt% S-CNCs in a colloidal aqueous suspension at different shear rates.[96] At a lower shear rate of 0.05 s^{-1}, an isotropic ring pattern was observed from the radial position (Figure 6e); whereas when the shear rate was increased to 500 s^{-1}, anisotropic interference peaks along the lateral arcs appeared (Figure 6f), indicating the alignment of S-CNCs along the shear direction. The azimuthal tracing results from scattering patterns further demonstrated that when the shear rate was higher than 5 s^{-1}, alignment along shear direction occurred, which was evidenced by the development of two peaks at 90° and 270° (Figure 6g). The shear-induced orientation of S-CNCs was also confirmed through SEM observations (Figure 6h,i).[99] S-CNC suspensions were cast into a 50 mL glass vial, which was rotated horizontally at a speed of 500 rpm.

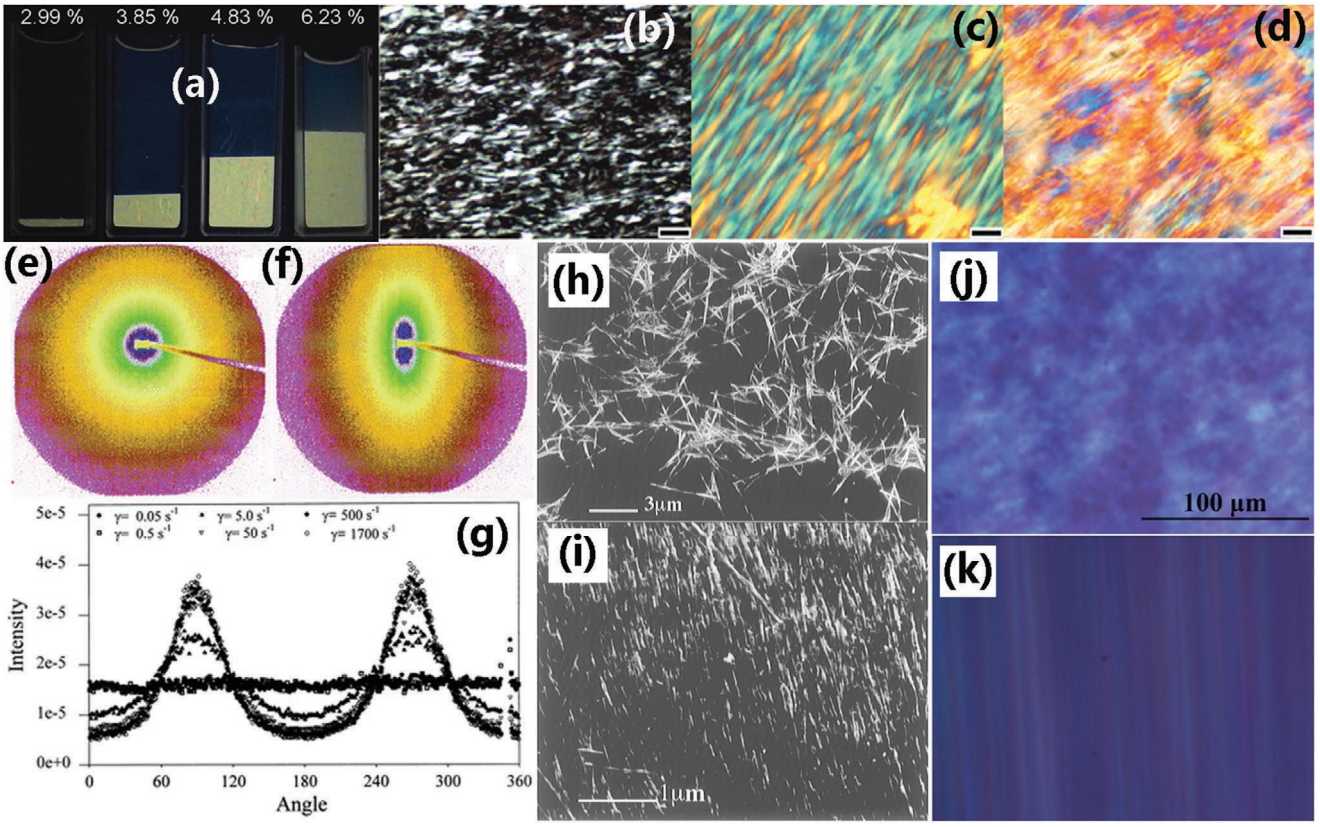

Figure 6. Concentration-dependent lyotropic phase and shear-induced orientation behaviors of CNCs in an aqueous suspension. a) Cross-polarized photos showing phase separation of S-CNC suspensions at different concentrations. b–d) POM of S-CNC suspensions at 4.3, 6.8 and 10.2 wt%, respectively. a–d) Reproduced with permission.[94] Copyright 2011, American Chemical Society. e,f) 2D scattering patterns of S-CNC suspension collected at 0.05 and 500 s^{-1}, respectively. g) Azimuthal traces from scattering patterns at different shear rates. e–g) Reproduced with permission.[96] Copyright 1999, American Chemical Society. h,i) SEM images of S-CNC films prepared from S-CNC suspension without and with rotation treatment at 500 rpm for 12 h, respectively. h,i) Reproduced with permission.[99] Copyright 1997, American Chemical Society. j,k) POM images of S-CNC suspension at shear rates of 0.01 and 1 s^{-1}, respectively. j,k) Reproduced with permission.[100] Copyright 2012, American Chemical Society.

After 12 h of rotation, a gel layer was created and then dried to obtain S-CNC film. SEM observations confirmed that S-CNCs were highly oriented along to the rotation direction on the surface of dried film (Figure 6i). More recently, the alignment of S-CNCs in suspension was in situ monitored as a function of shear rate during rheological tests through POM observation.[100] At a shear rate of 0.01 s^{-1}, a birefringent microstructure was observed, indicating the uniform dispersion of S-CNCs at a lower shear rate (Figure 6j). With increase in the shear rate to 1 s^{-1}, notable alignment of ordered domains along the shear direction appeared (Figure 6k).

3.4. Aspects Governing the Rheological Properties of CNM Suspension

Many factors, including test protocols (e.g., rheometer geometry, shear rate, and time), CNM inherent properties (e.g., concentration, morphology and surface characteristics), suspension environments (e.g., ionic strength, pH, temperature, magnetic and electric strength and water-soluble polymer interactions), and post processing (i.e., drying and redispersion), govern the flow behaviors of CNM suspensions. These aspects are crucial for understanding the CNM's diverse rheological behaviors, making it possible to more effectively utilize CNMs as rheological modifiers in a wide range of applications.

3.4.1. Rheometer Geometry

Common geometries for rotational rheometers include parallel plate, cone- and-plate, serrated plate, concentric cylinder, and concentric vane (**Figure 7**a). Parallel plate and cone-and-plate geometries are usually used for measuring small volume samples with intermediate to high viscosity. Concentric cylinder geometry is for measuring larger volume samples with low viscosity; this geometry has less sensitivity to particle settling and solvent evaporation effects, assuming that appropriate geometry and gap size are employed.

The rheological properties of NFC suspensions have a strong dependence on the rheometer geometry types and sizes.[101] The cone-and-plate geometry with a much smaller gap (especially diminutive near the tip of the cone) constrains the mobility of the fibrils more profoundly, and hence yields higher G' for UN-NFC suspensions (Figure 7b). With a cone and plate geometry, the maximum particle size in the fluids should be less than approximately 10% of the gap height between the truncated cone and bottom plate. With a parallel plate geometry, the measured G' progressively increases with decreasing measurement gap, which is contradictory to the viewpoint that wall depletion effects become more dominant as the measurement gap declines, resulting in a reduction in the measured viscosity.[89,109,110] Therefore, some other factors, e.g., geometrical constraint and gap-dependent floc size, might be more dominant, especially for thick fibrils.

In general, when fibrous suspensions undergo a continuous shearing with a smooth geometry, heterogeneous flows (e.g., wall depletion and shear banding) take place.[89,102,110–112] Wall depletion is a phenomenon in which the particles in suspension are susceptible to migrate away from the wall of the measurement device, leaving a suspending medium layer with a lower particle concentration and thus a much lower viscosity than the bulk viscosity. This phenomenon originates from various forces, including steric, hydrodynamic, chemical, viscoelastic and gravitational forces being exerted on the disperse phase immediately adjacent to smooth boundaries.[109] In other words, it is energetically favorable to have a low-viscosity layer in the proximity of geometry wall. The wall depletion can further induce shear banding—the occurrence of fast and slow flowing regions despite loading under the same shear rate. These flow instabilities cause inaccurate measurement of the rheological properties. Solid-depleted areas are likely to be present not only at the walls but also at other points within a sheared CNM suspension.

The use of serrated plate or concentric vane can help minimize the wall depletion effects, producing more accurate viscosity and G' values.[113,114] For a bucket vane viscometer with a wide gap, high stress near the vane edge maintained a good contact to fibrils, while low stress at the cup edge prevented the slippage.[115] The presence of a profiled surface in a concentric cylinder was shown to yield substantially higher values of both viscosity and moduli of 2 wt% CM-NFC suspensions due to elimination of wall slippage.[116] Comparative studies with smooth and serrated cone-plate and concentric cylinder geometries showed that the serrated concentric cylinder was the most suitable geometry to measure the rheology of TO-NFC suspension (Figure 7c).[102] In addition, microcapillary viscometry has also been applied to help mitigate the effects of wall slippage and turbulent flow that may be observed at high rates in rotational geometries, although viscous heating effects became a concern at shear rates $>10^5$ s^{-1}.[80] Overall, although the use of serrated geometry is essential to reduce wall slippage, the complete elimination of the slippage depends on types of serrated geometry and NFC, NFC concentration and shear rate.

3.4.2. Shear Rate

CNM suspensions exhibit typical shear-thinning behavior, i.e., decrease in viscosity with increase in shear rate. For UN-NFC suspensions, shear-thinning curves often can be divided into four distinctive regions, corresponding to the gradual changes in microstructure of UN-NFC flocs as a function of shear rate (Figure 7d).[72] At low shear rates, shear-thinning behavior is significant (Region I) due to the breakdown and orientation of UN-NFC flocs. At intermediate shear rates, a plateau can be observed (Region II) because of the formation of more entangled UN-NFC flocs, which prohibits the continuous decrease in viscosity. With further increase in shear rate, more severe shear-thinning appears (Region III), due to the breakdown of the entangled flocs as well as the orientation of small flocs parallel to the shear direction. At high shear rates, the viscosity becomes less dependent on the shear rate with most of entangled flocs disintegrated and oriented (Region IV).

For S-CNC suspensions, the pattern of shear-thinning curves is highly dependent on the S-CNC concentration (Figure 7e).[103] In the dilute (or isotropic) regime, the flow curves include a Newtonian plateau at low shear rates, a shear thinning region at intermediate shear rates, and another plateau at high shear

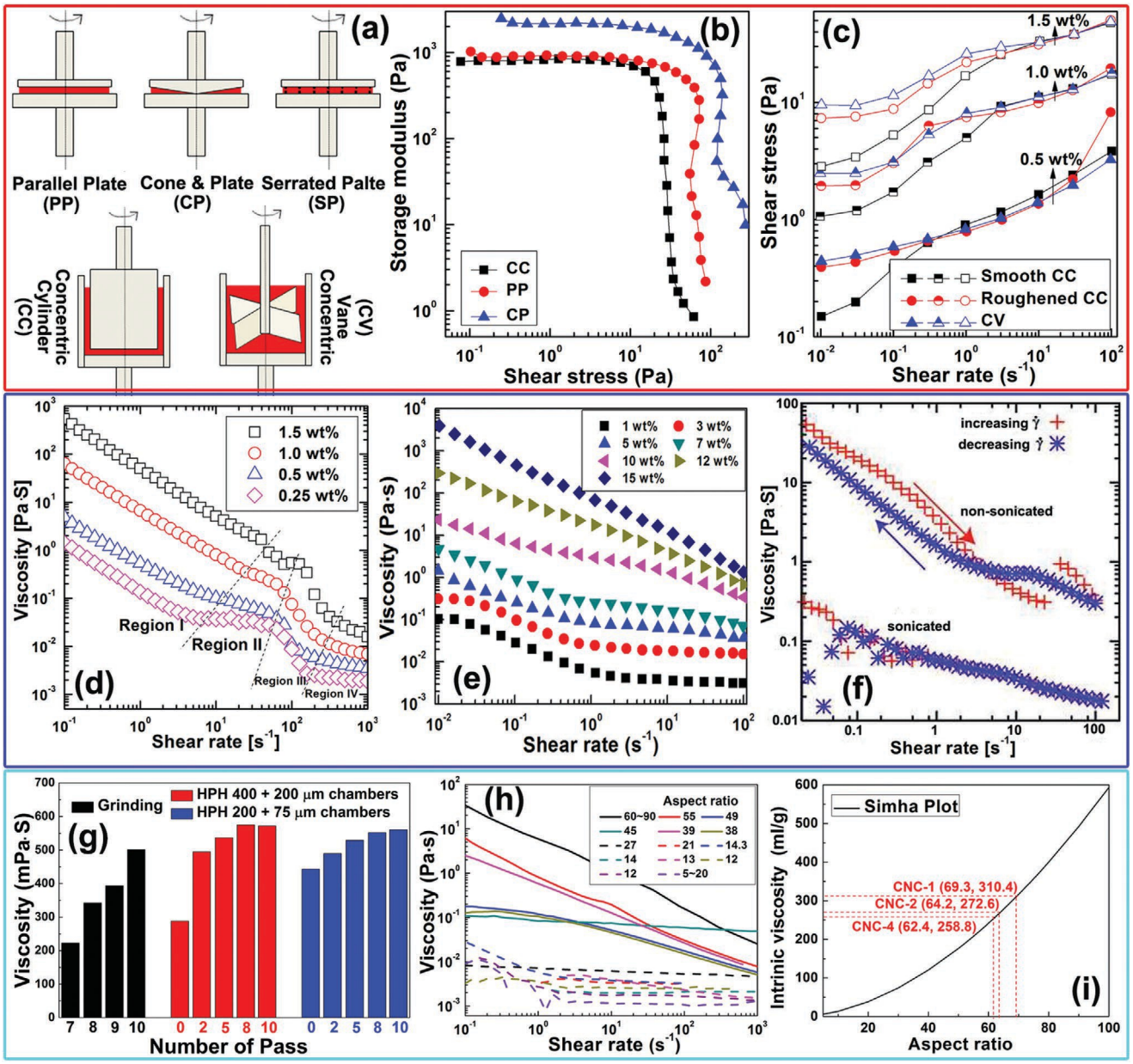

Figure 7. Rheological properties of CNM suspensions. a) Five typical geometries used in the rotational rheometer. b) G' of UN-NFC suspensions measured using three different smooth geometries of concentric cylinder (CC), parallel plate (PP), and cone-and-plate (CP). b) Reproduced with permission.[101] Copyright 2009, Nordic Rheology Society. c) Shear stress of TO-NFC suspensions measured using smooth/roughened CC and CV geometries at concentrations of 0.5, 1.0, and 1.5 wt%. Reproduced with permission.[102] Copyright 2015, Springer Nature. d) Viscosity of UN-NFC suspensions as functions of shear rate and concentration. Reproduced with permission.[72] Copyright 2015, American Chemical Society. e) Viscosity of S-CNC suspensions as functions of shear rate and concentration. Reproduced with permission.[103] Copyright 2014, Springer Nature. f) Thixotropic behavior of TO-NFC influenced by sonication. Reproduced with permission.[73] Copyright 2008, Springer Nature. g) Viscosity of UN-NFC suspensions produced using a grinder or high shear homogenizer with different passes. Reproduced with permission.[104] Copyright 2014, Springer Nature. h) f-dependent viscosity curves of 1 wt% S-CNC suspensions based on 10 typical literature reported previously.[21,49,72,88,98,103,105–108] i) Prediction on f of S-CNCs from intrinsic viscosity using the Simha model. i) Reproduced with permission.[72] Copyright 2015, American Chemical Society.

rates. In the semi-dilute (or liquid crystal) regime, the steady-state flow curves consist of a shear-thinning region at low shear rates, a plateau at intermediate shear rates, and another shear-thinning region at high shear rates. In the concentrated (or gel) regime, only a single shear-thinning region is observed. More detailed discussion on this subject is presented in Section 3.3.4.

3.4.3. Time

CNM suspensions show thixotropic behavior, i.e., a time-dependent rheological phenomenon. After being shaken, agitated, or sheared, CNM suspensions become less viscous, and time is needed for the fluids to recover the lost viscosity. The

presence of highly entangled networks in TO-NFC suspensions is responsible for their thixotropic behavior,[73] and ultrasound treatment that disrupts TO-NFC network can lead to less thixotropic behavior (Figure 7f). For CNC suspensions, the thixotropic behavior is dependent on surface charge and concentration.[83] The lack of charges on the surface of H-CNCs led to formation of aggregates, and therefore the thixotropic behavior appeared when the concentration was higher than 0.5% (w/v). No thixotropic behavior was observed for S-CNC suspension even at a much higher concentration.

3.4.4. CNM Concentration

Concentration is considered as one of the most important factors governing the rheological properties of CNM suspensions. For example, it was shown that the increase in the concentration from 0.25 to 1.5 wt% led to a gradual increase of both viscosity and G' for UN-NFC suspensions, suggesting the formation of a strong network (Figure 7d).[72] The G' was independent of ω and always higher than G'' for the UN-NFC suspensions studied. These observations revealed that the UN-NFC suspensions created gels even at the lowest concentration of 0.25 wt%. Similar results were observed for E-NFC suspensions,[117] forming gel structure at a concentration of 0.125 wt%. The extremely high aspect ratio and superior water retention ability enabled E-NFC to create highly entangled networks at an extremely low concentration.

The relationship between G' and concentration of NFC (C) often follows a power law, i.e., $G' = kC^n$, in which k depends on the characteristics of fibril, and n indicates the concentration-dependent network in the NFC suspensions. High n values show more concentration dependence of NFC network. For UN-NFC suspensions prepared from fresh sugarbeet, the relationship between G′ and C was expressed as $G' = 235.5C^{2.58}$.[118] For E-NFC suspensions prepared from Kenaf pulp, the relationship between G' and C was expressed as $G' = 8.71C^{3.03}$.[114] Interestingly, this exponent value of 3.03 is very close to that reported by Paakko et al.,[117] for E-NFC from bleached sulfite softwood cellulose pulp. Chemical pretreatments change the surface characteristics of NFC, resulting in a broad range of the exponent values, e.g., 2.5,[119] 3,[120] 4.1,[121] 4.5,[122] 4.6,[123] 4.51,[124] and 4.62[124] for TO-NFC, as well as 2.4[125] and 5.2[126] for CM-NFC. The presence of repulsive forces among charged nanofibrils generates distinctive bond dynamics, leading to different concentration-dependent network in NFC suspensions.[121] Moreover, the dimension (Section 3.3.5) and surface charge density (Section 3.3.6) of NFC significantly influences the obtained exponent values.

For S-CNC suspensions, two transitions were shown to take place with a gradual increase in S-CNC concentration from 1 to 15 wt% (Figure 7e).[103] The first transition concentration (C^*) from isotropic to liquid crystal occurred between 3 and 5 wt%, and the second transition concentration (C^{**}) from liquid crystal to gel occurred between 10 and 12 wt%. In the isotropic (or dilute) regime (e.g., 1 and 3 wt%), the steady-state flow curves consisted of a Newtonian plateau at low shear rates, a shear thinning region at intermediate shear rates (due to the shear-induced orientation of individual crystals), and another plateau at high shear rates (due to the complete orientation of individual crystals). In the dilute region, Brownian diffusion was dominant; the extent of the Brownian diffusion can be detected by calculating the rotary Peclet number (Pe_{rot}). Since the Pe_{rot} is proportional to the shear rate (γ), a Newtonian plateau at low shear rates is observed due to the predominant Brownian diffusion. A nearly Newtonian plateau over the shear rates from 0.1 to 100 or 1000 s^{-1} at low concentrations was also seen.[72,127,128] In the liquid crystal (or semi dilute) regime (e.g., 5, 7, and 10 wt%), the steady-state flow curves consisted of a shear-thinning region at low shear rates, a plateau at intermediate shear rates, and another shear-thinning region at high shear rates, which is attributed to the disassociation of liquid crystal clusters into individual crystals and subsequent orientation of individual crystals along the shear direction. This is known as the three-region shear behavior, a typical feature for many liquid crystals.[129,130] In the gel (or concentrated) regime (e.g., 12 and 15 wt%), only a single shear-thinning region was observed. The single shear-thinning behavior can be well described by the power-law model during the flow consistency coefficient (K) and

The formation of ge
centrations was furth
lastic measurements.[10
S-CNC suspensions sh
like behavior. At a co
overlapped, demonstr
concentration of 15 wt
ation of stiff gel. Therefore, with the dynamic viscoelastic measurements, the critical concentration for gel phase formation was also determined at 12 wt%, which was in a good agreement with the steady-state flow measurements.

Additionally, the Cox–Merz rule was applied to correlate the viscosity from steady-state flow measurement with complex viscosity obtained from oscillatory measurement.[94,100,128] It was found that the applicability of the Cox–Merz rule for S-CNC suspensions is also concentration-dependent. When the S-CNC suspension is isotropic, the Cox–Merz rule applies, i.e., the complex and steady shear viscosities of S-CNC suspensions are almost identical. When the S-CNC suspension is anisotropic, the Cox–Merz rule is only applicable after a shift factor is included.

3.4.5. CNM Morphology

The morphology of CNMs is another important factor determining the rheological properties of CNM suspensions. UN-NFC and E-NFC are extensively branched with a high degree of entanglement, where there are filaments that extend off the central core of the fibril. The enhanced degree of fibrillation by mechanical disintegration and enzymatic pre- treatment thus causes more entangled networks, leading to higher viscosity and viscoelastic properties. However, vigorous treatment can result in fibril shortening and lower degree of entanglement, which reduces the viscosity and viscoelastic properties. TO-NFC and S-CNCs, due to repulsion between negative charges and minimal branching, are expected to have lower viscosity and viscoelasticity. To the extent that their

effective length in suspension is proportional to their measured length, their rheological properties are directly proportional to their length divided by their width, i.e., their aspect ratio. The relationship between the intrinsic viscosity, [μ], and aspect ratio, f, of CNMs can be described using the Simha model, highlighting the critical role of morphology on the rheological properties of CNM suspensions.

The sources and production methods have significant influence on the morphology of NFC, as discussed in Section 2.1. For UN-NFC suspensions, increased number or time of grinding and HPH treatment (up to 5–8 passes) resulted in a higher degree of fibrillation, yielding a stronger NFC network and higher viscosity of the suspension (Figure 7g).[104] Similarly, for TO-NFC suspensions, their viscosity gradually increased with increased Waring Blender treatment time.[73] For E-NFC suspensions, G' increased as the homogenizing pressure increased from 500 to 1000 bars during the HPH process as well.[116] In contrast to the above studies, Shogren et al. reported the maximum G' of UN-NFC suspensions produced after only 2 passes through the HPH treatment, and G' decreased asymptotically with subsequent passes.[131] This behavior was attributed to the strong interaction of large fibrillar aggregates (microns in size) in the fluids, which were broken up into smaller fibrils and fragments with additional HPH passes, resulting in lower G'. Thus, there is a strong need to characterize the NFC morphology across different length scales, so that one can be aware of the presence of large-scale agglomerates that may skew the results.

Enzymatic pretreatments not only enhanced the degree of fibrillation, but also reduced the fibril length. The fibril length reduction had a predominant influence on the rheological properties, impairing the entangled network of E-NFC suspensions. Therefore, G' of E-NFC suspensions was progressively decreased as the dosage of enzymes increased, although the degree of fibrillation was increased.[111] In comparison with the enzyme FiberCare R (a monocomponent endoglucanase), the enzyme Celluclast 1.5 L (an enzyme mixture containing endoglucanases, exo-glucanases, cellobiohydrolases, and β-glucosidases) produced weaker NFC networks through the strong decomposition of fibril. The exo-glucanases and cellobiohydrolases brought about the decomposition of amorphous or crystalline regions, yielding di- and tetrasaccharides, and β-glucosidases, which further converted the di- and tetrasaccharides into monomeric glucose.[27] Overall, it can be concluded that rheological properties of NFC suspension depend on both NFC diameter and length (i.e., f). Unfortunately, because NFC generally is extremely long and highly flexible, an accurate determination of the length for f calculation remains a big challenge.

The rod-like CNCs have much smaller dimensions, and their f can be more easily estimated through morphological analyses such as AFM and TEM observations. Several studies have demonstrated the f-dependency of CNC rheological properties, e.g., 1 wt% S-CNC suspensions with a notable f-dependency (Figure 7h). The data suggest a critical f value of around 30, above which the pronounced shear-thinning behavior appeared together with relatively high viscosities at low shear rates. The f-dependent viscosity of S-CNC suspensions in a wide range from 10^{-3} to 10^{2} Pa s allows them to be utilized as tunable rheological modifiers in distinctive commercial applications.

The relationship between the intrinsic viscosity and f of rod-like particles has been well established using several theoretical models. For rod-like CNCs, the Simha model is applied to predict the f of CNCs from their intrinsic viscosity.[72,82–84] For example, the Einstein equation was used to derive the intrinsic viscosity, and the data were used with the Simha equation to calculate f of both S-CNCs and H-CNCs.[83,84] For S-CNCs, the predicted f was in a good agreement with TEM measurement, whereas much higher f was derived for H-CNCs due to severe aggregation in the longitudinal direction arising from the absence of charges on the surface. Huggins and Kraemer equations were applied to obtain the intrinsic viscosity, which was used in the Simha equation to predict the f of S-CNCs with different f and sulfate group density (Figure 7i).[72] The theoretically predicted f values of S-CNCs with higher f and lower sulfate group density were within the range of f determined from TEM. For S-CNCs with lower f and higher sulfate group density, the strong electroviscous effects caused a non-negligible increase in the intrinsic viscosity, and thus the derived f was much higher than that determined from TEM. To overcome the electroviscous affects, a small amount of NaCl was used to screen the electric double layers of S-CNCs, remarkably reducing the intrinsic viscosity.[85] Using the Batchelor equation, the predicted f of S-CNCs was very close to that determined by TEM.

3.4.6. CNM Surface Chemistry Characteristics

The CNM surface chemistry characteristics (e.g., sign of charge, charge density, functional groups, hydrophilicity and hydrophobicity) affect rheological properties by altering chemical interactions (e.g., electrostatic attraction, electrostatic repulsion, hydrogen bonding, van der Waals attraction, hydrophobic attraction, etc.) and physical interactions among neighboring CNMs. As presented in Section 2, CNMs with different surface chemistries (**Figure 8**a) can be manufactured depending on the isolation or production method. Effects of changes in attractive or repulsive forces between cellulose surfaces in a suspension on rheology vary, depending on a contiguous structure of reinforcing particles within the mixture.[23] When such a contiguous structure exists or can be formed, increased attractions increase the yield stress.[134] But in systems where multi-particle structures are discontinuous, broken, or absent, net attraction between particles can reduce viscosity.[126]

In general, the introduction of charges on the NFC surface enhances the degree of fibrillation, leading to the formation of stronger fibrous networks and higher viscosity and G'.[111,132] For example, G' values of TO-NFC suspensions from *Posidonia oceanica* (a sea grass) progressively increased when the carboxyl content of TO-NFC was increased from 0.25 to 0.45, 0.55, and 0.65 mmol g^{-1} (Figure 8b).[132] However, as the NFC surface charge increases, the electrostatic repulsion force becomes stronger, which further diminishes the strength of net chemical attractions among nanofibrils, and thereby lowers viscosity and G'. Furthermore, chemical pretreatments can shorten the fibril, decreasing the f of NFC. When these two factors become more pronounced, the strength of a NFC network is weakened, thereby lowering the viscosity and G'. A periodate–chlorite oxidation method was used to treat wood

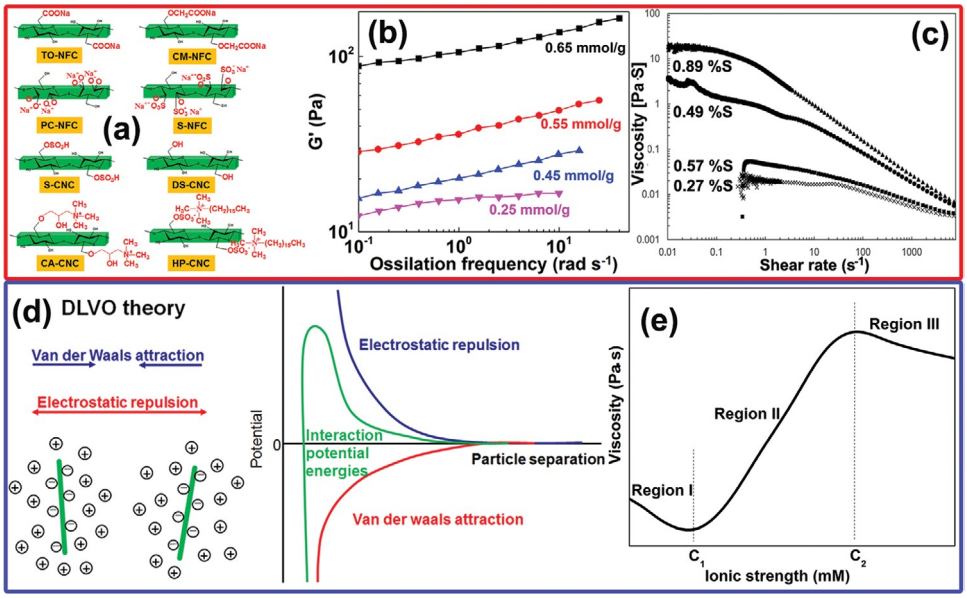

Figure 8. Rheological properties of CNM suspensions. a) Schematic illustration on surface chemistry of CNMs. b) Influence of carboxyl contents on the *G'* of TO-NFC suspensions. c) Influence of sulfur content on the viscosity of S-CNC suspensions. d) Schematic illustration on the DLVO theory application to CNMs. e) Proposed viscosity plot as a function of ionic strength. b) Reproduced with permission.[132] Copyright 2015, Elsevier. c) Reproduced with permission.[133] Copyright 2018, American Chemical Society.

pulp prior to nanofibrillation.[135] With increase in oxidation time from 0.25 to 0.5, 1, 2 and 3 h, the carboxyl content on the surface of PC-NFC increased from 0.38 to 0.69, 0.75, 1.20 and 1.75 mmol g^{-1}, respectively. Interestingly, PC-NFC suspension with the carboxyl content of 1.20 mmol g^{-1} had the highest viscosity due to the high degree of fibrillation. At a higher content (e.g., 1.75 mmol g^{-1}), the strong electrostatic repulsion force and low *f* became dominant, leading to a reduction in viscosity. S-NFC[136] and CM-NFC[137] (Figure 8a) displayed similar surface chemistry-dependent rheological behaviors with TO-NFC and PC-NFC.

In contrast, for CNCs, increased density of charged functional groups usually decreases viscosity and dynamic moduli due to the weakened chemical attraction among neighboring CNCs as well as the improved dispersion state of CNCs via electrostatic repulsion.[83,133,138,139] The rheological properties of CNC suspensions can be further tuned through post-modification, e.g., cationization,[140,141] desulfonation,[142] and hydrophobization.[143–149]

In comparison with H-CNC suspensions, S-CNC suspensions exhibited superior colloidal stability as well as lower viscosity due to the presence of negatively charged sulfate groups.[83,138] In addition, the content of sulfate group content on surface of S-CNCs affected the rheology of S-CNC suspensions significantly.[133,139] The viscosity of S-CNC suspensions gradually decreased with increase in sulfur content on the surface of S-CNCs from 0.27 to 0.49, and 0.57 and 0.89% (Figure 8c).

Post-treatments of CNCs via chemical reaction have been found to influence the rheology of CNC suspensions. One post-treatment of particular interest is the cationic functionalization of CNCs through etherification with a cationic reagent (2,3-epoxypropyl)trimethylammonium chloride (EPTMAC).[140,141] Two types of cationic CNCs (CA-CNCs, Figure 8a) with different degree of substitution (DS) were prepared through controlling the water content during the etherification reaction. The suspension of CA-CNCs with a lower DS (dCNCs) exhibited higher viscosity than an unmodified CNC suspension due to the formation of aggregates arising from declined surface charge. Furthermore, the dCNC suspension exhibited a typical three-region shear-thinning behavior, indicating the presence of shear-induced liquid crystalline domains in suspension resulting from poor dispersion of dCNCs. However, for the suspension of CA-CNCs with a higher DS (cCNCs), the three-region shear-thinning behavior disappeared along with a remarkable reduction in viscosity, highlighting the critical role of surface charge on the dispersion state and flow behavior of CA-CNC suspensions.

When surface charges are eliminated from CNCs, the attractive chemical interactions (e.g., hydrogen bonds and van der Waals attraction) become more dominant between neighboring CNCs, generating viscoelastic gels. For example, a novel hydrothermal desulfation treatment was used to prepare CNC gels (DS-CNCs, Figure 8a) from S-CNC suspensions.[142] Dynamic viscoelastic studies revealed that the transition from liquid to gel took place at a hydrothermal treatment temperature between 70 °C and 80 °C. Further increase in the hydrothermal treatment temperature to 90 °C significantly enhanced the strength of gel, as evidenced by a notable increase in *G'*. When the hydrothermal desulfation was carried out at 120 °C, most of sulfate groups were removed, producing a free-standing gel even at a low concentration of 2 wt%.

More robust CNC gels can be achieved through the introduction of hydrophobic groups by absorption of amphiphilic surfactant or chemical modification with hydrophobic moieties.[143,144] The amphiphilic surfactant contains a head with a

charged group and a tail with a hydrophobic group. CNCs with negatively charged surfaces can be attached to the positively charged head of a cationic surfactant through electrostatic attraction, producing hydrophobized CNCs (HP-CNCs, Figure 8a). The influence of cetyltrimethylammonium bromide (CTAB) adsorption on the rheology of S-CNC suspension was studied.[143] Results showed that CTAB-CNC suspensions had more pronounced shear-thinning behavior as well as much higher viscosity than neat S-CNC suspensions at the same concentrations ranging from 1 to 4 wt%. The formation of strong hydrophobic interactions between surfactant tails of adjacent CTAB-CNC and the increase in volume fraction arising from the extended conformation of the surfactant in ethanol were responsible for the gelation. A two-step chemical reaction, i.e., periodate oxidation of S-CNCs, and reductive amination reaction between aldehyde groups of the oxidized S-CNCs and octylamine, was reported to synthesize HP-CNCs and mechanically robust gels.[144] The hydrophobization significantly enhanced both viscosity and $G'$of S-CNC suspensions. Furthermore, different thermo-responsive polymers, e.g., poly(*N*-isopropylacrylamide),[145] Jeffamine polyetheramine,[146] poly(*N*-vinylcaprolactam),[147] methylcellulose,[148] and poly(poly(ethylene glycol) methylacrylate)s,[149] were successfully grafted onto the surface of S-CNCs though surface-initiated atom transfer radical polymerization (SI-ATRP).[150] Above the LCST, the thermo-responsive polymer chains around the S-CNCs transitioned from hydrophilic to hydrophobic, leading to gelling through hydrophobic interactions as well.

3.4.7. Ionic Strength

The classical Derjaguin–Landau–Verwey–Overbeek (DLVO) theory states that an electrical double layer is present on the surface of charged particles in a colloidal system, and the interaction potential energies between two charged particles are the sum of van der Waals attractions plus electrical double layer repulsion (Figure 8d).[151] One of the most important parameters governing the DLVO interaction energies is the ionic strength. Variation in ionic strength alters the electrical double layer repulsion greatly, whereas the London dispersion components of van der Waals attraction arising from temporary fluctuating dipoles is insensitive to the ionic strength.[152] As a result, the balance between van der Waals attraction and electrical double layer repulsion is disrupted, leading to alteration in the colloidal stability, dispersion state, as well as rheological properties of charged nanoparticle suspensions. Theoretically, at a low ionic strength, the electrical double layer repulsion is dominant, and the charged nanoparticle suspension is less viscous with stable, homogeneous dispersion. At a high ionic strength, on the contrary, the van der Waals attraction becomes dominant due to the screening of electrical double layer repulsion by counter-ions. As a result, nanoparticles have a high tendency to collide and form aggregates, creating a strong network. However, a detailed literature review on the influence of ionic strength on the rheological properties of CNM suspensions reveals more complicated trends, as illustrated in Figure 8e.

Ideally, UN-NFC and E-NFC do not possess surface charge, and thus they should have high ionic strength tolerance. However, even after purification, the cellulosic pulps used for NFC production still contain slight impurities (e.g., hemicellulose and pectin), leading to the presence of some sugar acids, e.g., uronic acids on the surface of resultant NFC.[118,153] The negatively charged uronic groups were thought to be responsible for the ionic strength-dependent rheological behaviors of UN-NFC and E-NFC suspensions.[154–156] For example, Sim et al. prepared UN-NFC suspensions from commercial eucalyptus bleached kraft pulp through mechanical grinding.[154] The values of viscosity, yield stress and G' increased with an increase in the concentration of salts (Region II in Figure 8e). It was proposed that the presence of salt screened the electrostatic repulsion between negatively charged nanofibrils arising from uronic groups, leading to the formation of aggregates. However, there was a critical point (C_2 in Figure 8e) beyond which further increase in ionic strength caused a reduction in the viscosity of NFC suspensions (Region III in Figure 8e).[155,156] For instance, for UN-NFC suspension from Norway spruce, the complex viscosity reached the maximum when $\approx 60 \times 10^{-3}$ m NaCl was incorporated.[155] Further adding NaCl resulted in a gradual decrease in the complex viscosity due to the formation of precipitated flocs rather than a continuous network.

For chemically pretreated NFC, the introduction of more negative charges on the surface causes more significant electroviscous effects, i.e., a more profound increase in the apparent viscosity of chemically pretreated NFC suspensions compared with UN-NFC and E-NFC suspensions. The electroviscous effects are due to the flow-induced distortion of the electrical double layer (primary effect) and the overlapping of electrical double layers between neighboring nanofibrils (secondary effect).[23,82] The presence of dilute salts hence reduced the thickness of electrical double layer (also known as the Debye length), leading to the suppression of the electroviscous effects, i.e., a reduction in the apparent viscosity (Region I in Figure 8e).[126,157–159] When the applied ionic strength was high enough, chemically pretreated NFC suspensions displayed an analogous trend to the UN-NFC suspensions.[120,160,161] The viscosity of 0.1 wt% TO-NFC suspension increased with increasing NaCl concentration from 0×10^{-3} to 10×10^{-3}, 50×10^{-3} and 100×10^{-3} m but then decreased at 200×10^{-3} and 400×10^{-3} m.[160] Furthermore, the increase in cation valence induced more rigid networks.[161,162] The strength of cation-induced TO-NFC gels increased in the following order: $Fe^{3+} > Al^{3+} > Cu^{2+} > Zn^{2+} > Ca^{2+}$ driven by the screening of electrical double-layer repulsion as well as the formation of metal–carboxylate complexation.[162]

CNC suspensions have similar ionic strength-dependent rheological behaviors to chemically pretreated NFC suspensions (Figure 8e). Especially when a low concentration of ions is incorporated, the suppression of electroviscous effects prevails, leading to a reduction in viscosity of CNC suspensions.[82,128,163–165] When the electroviscous effects are completely eliminated by ions, a further increase in ionic strength shields the electrical double layer repulsion. As a result, the van der Waals attractions become dominant, resulting in gelation of CNC suspensions.[106,166,167] A phase diagram for S-CNCs was proposed to correlate NaCl concentration to a dimensionless suspension concentration based on aspect ratio and volume fraction of CNCs.[168] The phase diagram suggests a range of

potential conditions based on ionic strength, geometry and concentration of CNCs in suspension to target specific phases for a desired rheological response and application. G' progressively increased with increases in both valence (i.e., $Na^+ < Mg^{2+} < Al^{3+}$) and radius (i.e., $Mg^{2+} < Ca^{2+} < Sn^{2+}$) of the cation.[76,169] Moreover, the valence of the cation had more significant influence on the rheology of S-CNC suspensions than radius of cation, suggesting that the gelation of S-CNC suspension can be primarily ascribed to the intermolecular bridging capacity of multivalent cations. However, although divalent cations induced gelation at lower concentrations than monovalent cations, both valence and radius of cations can have minimal impact on the maximum strength of S-CNC gels.[167] These phenomena demonstrated that the gelation of CNCs was independent on valence and radius of cation, but results can be attributed to net intermolecular attraction induced by charge screening.

3.4.8. pH

The rheology of CNM suspensions is also dependent on the pH value, as a result of the combined actions of deprotonation and protonation of surface functional groups and counter-ion effects.[106,117,119,164] The change in pH value above and below p*K*a (i.e., the negative decadic logarithm of the acid dissociation constant) causes the deprotonation and protonation of functional groups on the surface of CNMs, respectively, which subsequently alters rheology. When the pH is well above the p*K*a, the surface functional groups are deprotonated, generating strong electrical double layer repulsion, leading to the formation of a weaker network. When the pH is well below the p*K*a, the surface functional groups are protonated, which makes the attraction forces dominant, resulting in the formation of a stronger network. It is worth noting that different functional groups have distinctive p*K*a values. For example, the carboxyl groups associated with cellulose have p*K*a values in the range of 3 to 4, whereas the p*K*a value of the sulfate groups is as low as −3. In addition, the incorporation of NaOH or HCl to change the pH value also generates counterion effects (i.e., the suppression of electroviscous effect and the screening of electrical double layer repulsion), as discussed in Section 3.4.7. Overall, the combined effects of these two mechanisms contribute to the pH-dependent rheology of CNM suspensions.

For UN-NFC suspensions, the change in pH from 4.5 to 9 had little influence on their viscoelastic properties at 1 wt% concentration, presumably due to the extremely low surface charge content and high solid content of UN-NFC.[118] For E-NFC suspensions, the viscosity of a 0.25 wt% NFC suspension gradually increased as pH decreased from 10.0 to 5.9, 3.8 and 2.0 because of the presence of negative charges (i.e., 44.2 μeq g^{-1}) originated from hemicellulose with uronic acids.[117] Since the carboxyl groups have a p*K*a of 3 to 4, a gradual increase in viscosity with decrease in pH from 10.0 to 3.8 can be ascribed to the screening of electrical double layer repulsion. Further increase in viscosity with decrease in pH from 3.8 to 2.0 was then attributed to the protonation of carboxyl groups. A more profound change in the rheological behavior was observed from highly charged TO-NFC suspensions. When the pH of 0.1 wt% TO-NFC suspensions was shifted from 8 to 2, the suspension became more elastic.[119]

Because sulfate groups have an extremely low p*K*a value of -3, S-CNCs are always deprotonated in suspensions. Therefore, the counter-ion effects dominate pH-dependent rheological behavior of S-CNC suspensions. Due to strong counter-ion effects, viscosity first increased with increasing pH from 2 to 6, and then steadily decreased with further pH increase from 6 to 12.[106] These results are consistent with the fact that the ionic strength increases with the addition of strong acid to adjust the pH, especially at the lowest values of pH considered. Interestingly, when 100×10^{-3} m NaCl was added prior to a change in pH using NaOH or HCl solutions, the viscosities became independent of pH over a larger range from 1 to 13, which can be ascribed to the complete screening of counter-ion effects by 100×10^{-3} m NaCl. These phenomena strongly supported the assumption that the pH-dependent rheology of S-CNC suspension was primarily attributable to the counter-ion effects. For C-CNCs, because their carboxyl groups have a relatively high p*K*a value of 3 to 4, both the deprotonation/protonation of carboxylated groups and counter-ion effects should be taken into account for their pH-dependent rheological properties.[164]

3.4.9. Temperature

Temperature has a lesser influence on the rheological properties of CNM suspensions compared with other factors. Especially, NFC particles with high aspect ratio create physically entangled networks in aqueous suspension, and hence they show very stable rheology upon temperature change from 20 °C to 80 °C. For UN-NFC suspensions, their moduli were shown to be independent of temperature between 20 °C and 60 °C.[156] Further temperature increase (up to 80 °C) caused a slight decrease in moduli.[118] Additionally, a UN-NFC suspension showed superior thermo-reversibility, i.e., moduli almost returning to the original value after being cooled from 80 °C to 20 °C. By contrast, Herrick et al.[170] and Iotti et al.[113] observed that increasing temperature from 25 °C to 60 °C decreased the viscosity of UN-NFC suspensions, possibly due to the reduced viscosity of water in UN-NFC suspension as well as the deswelling of fibril. It should be pointed out that the dynamic moduli were examined in the linear viscoelastic regime, where the network of UN-NFC was well preserved; whereas the viscosity was detected under continuous shearing condition, in which the network of UN-NFC was disrupted. Therefore, conflicting results from dynamic moduli and viscosity measurements further highlighted the critical role of an entangled network in maintaining the viscoelasticity of UN-NFC suspensions upon change in temperature. E-NFC has a similar temperature dependence of rheology with UN-NFC. Their moduli displayed no dependence with increasing temperature from 20 °C to 40 °C, but they were slightly increased when being heated to 80 °C.[117] The viscosity and moduli of both E-NFC and CM-NFC suspensions were negligibly affected with a rise in temperature from 5 to 50 °C.[171] The suspensions of CM-NFC with higher surface charge content exhibited superior thermally stable rheology over the suspensions of E-NFC with lower surface charge

content, which can be ascribed to the formation of a more rigid network as a result of an increased degree of fibrillation.

In contrast, CNC suspensions are more susceptible to temperature owing to the absence of physically entangled networks, where significant increases in viscosity of CNC suspensions can be achieved when aged at temperatures higher than 100 °C for several days. A possible explanation is progressive hydrolysis of the sulfate groups, thus decreasing the charge density. This aging-related viscosity change can be altered through the use of a small amount of radical scavengers.

Above the critical concentration, CNCs can form temperature-sensitive liquid crystalline phases.[100,172,173] Temperature increase reduced the volume fraction of the liquid crystalline phase within S-CNC suspensions, resulting in a notable alteration in viscosity depending on the concentration of S-CNCs.[94] In addition to the concentration, changes in shear rate impacted the microstructure of S-CNC suspension as well, generating distinctive temperature-dependent flow behavior.[100] At intermediate shear rates (e.g., 1 and 10 s^{-1}), the viscosity of 5 wt% S-CNC suspension gradually decreased as temperature increased from 5 to 55 °C. However, at low shear rates (e.g., 0.1, 0.3, and 0.5 s^{-1}), an abrupt increase in viscosity appeared in the temperature region between 30 °C and 40 °C. POM images indicated that the sudden increase in the volume fraction of isotropic domains was responsible for the abrupt upturn behavior. Generally, when liquid crystals orient in the flow direction, viscosity undergoes an abrupt increase at the nematic-isotropic transition point.[173]

The effect of heat aging with higher temperatures and longer durations on the viscosity of S-CNC suspensions was also investigated.[174,175] Viscosity measurements with aged 2 wt% S-CNC suspensions showed that the aging treatment significantly increased the viscosity of S-CNC suspensions.[174] The highest viscosity was achieved when the aging temperature and time was 120 °C and 48 h, respectively. The aging treatment enhanced the delamination of the S-CNC crystallites, which not only increased the surface area of S-CNCs but also exposed more hydroxyl groups to the surrounding medium, resulting in a profound viscosity increase. However, extravagant prolonging of the aging time to 168 h caused a notable reduction in viscosity because of the degradation and hydrolysis of S-CNCs under the severe conditions. To overcome this bottleneck, radical scavengers (e.g., sodium formate and cesium formate) were applied. The presence of radical scavengers greatly enhanced the aging resistance of S-CNC suspensions, yielding very close viscosity curves before and after aging treatment.[175]

3.4.10. Magnetic and Electric Field Strength

CNMs exhibit anisotropic diamagnetic susceptibility due to the presence and alignment of magnetic dipoles of C□O, C□H, and O□H bonds in cellulose chains.[176,177] The direc- tion perpendicular to the polymer chain axis displays a larger diamagnetic susceptibility than the parallel direction.[178] With the presence of a magnetic field, CNMs can orient in the direction perpendicular to magnetic field direction. Consequently, CNM suspensions exhibit promising magnetorheological (MR) behavior, i.e., the rheological properties can be well tuned as a function of magnetic strength. Such MR behaviors take place in CNC suspensions more easily due to the smaller dimension of CNCs than NFC.[176] For example, it was reported that both the viscosity and G' of S-CNC suspensions at 0.1 and 0.5 wt% increased as the magnetic strength was increased from 0 to 1 T.[179] Moreover, the S-CNC suspension at higher concentrations showed less pronounced MR behavior than that at lower concentrations due to the steric hindrance effect.

Additionally, owing to the absorption of water molecules on the surface, CNMs show semiconducting properties and electrorheological (ER) responses.[180] Under an electric field, CNMs can construct fibrillated structures because of the difference in dielectric constant between CNMs and a dispersing solvent (e.g., silicon oil), resulting in the reversible phase transition from liquid-like to solid-like. In comparison with microcrystalline cellulose (MCC), S-CNCs exhibited more profound ER responses in methyl-silicone oil.[181] In addition, the acid hydrolysis time affected the ER properties of S-CNC fluid significantly.[182]

3.4.11. Polymer Interaction

The combined use of CNMs and polymers leads to significant changes in the stability and microstructure of the suspensions, resulting in distinctive rheology. The surface of the added polymer chain plays a crucial role in such hybrid systems. Understanding the complex interactions among CNMs and different polymers can help in formulating cost-effective fluids, whereas CNMs serve as the rheological modifier or as the main fluid additive. Generally, depending on the nature of surface functional groups, a water-soluble polymer can be classified as a cationic polyelectrolyte, an anionic polyelectrolyte or a nonionic polymer.

Effects of polymer addition on interactions between particulates in suspension—and by extension the rheological behavior—tend to fall into a few main classes, depending on the net charge, molecular mass, and dosage of the polymer. Since many CNMs of interest have a negative surface charge, the discussion here will assume such a situation. Relatively low addition levels of cationic polyelectrolytes can be expected to adsorb onto the CNM surfaces, thereby reducing and possibly neutralizing repulsive electrostatic forces between the surfaces. If the molecular mass is large enough, a cationic polyelectrolyte may induce strong attachments among suspension particles by either a charged patch mechanism[74,134,183,184] or a bridging mechanism.[185,186] The distinction between these two mechanisms is that the charged patch mechanism assumes reversible behavior, for instance if a suspension is intermittently sheared to break the particles apart. By contrast, intensive shearing of polymer bridges is understood to break polymer chains.[187,188] An overdose of cationic polymer can in some cases lead to charge reversal and stabilization of suspended particles.[189] Adding an anionic polyelectrolyte to the same negatively charged particle suspension also can affect rheology, often to a less dramatic extent; sometimes the effects can be attributed to the anionic polyelectrolyte acting as a dispersant, as a steric stabilizer, or through depletion flocculation.[190–198] Nonionic polymers usually contain abundant hydroxyl groups on the

surface, which can form extensive hydrogen bonding with the hydroxyl groups of CNMs. They are thus extensively attached to the surface of CNMs, and act as an effective "bridging" role to flocculate CNM suspensions, leading to notable enhancement in the rheology of CNM suspensions.[193,199] Based on the above analyses, the microstructures of CNMs in the presence of cationic polyelectrolytes, anionic polyelectrolytes, and non-ionic polymers are schematically illustrated in **Figure 9**a.

For example, the influence of cationic polyacrylamide (CPAM) and anionic carboxylmethyl cellulose (CMC) on the dispersion and viscosity of UN-NFC suspensions was studied.[200,201] Optical microscopy images showed that the presence of CPAM created dense and large agglomerates through electrostatic attraction and polymer bridging.[200] On the contrary, a notable improvement in the distribution of UN-NFC was achieved by adding anionic CMC. This was ascribed to the absorption of negatively charged CMC on the surface of fibrils, which dispersed the agglomerated fibrils and also induced steric stabilization. As a result, the presence of CPAM and CMC increased the viscosity of UN-NFC suspensions, and CPAM enhanced the viscosity of UN-NFC suspensions more effectively than CMC due to the formation of larger agglomerates.[201] In another example, the gelation behavior of S-CNC suspensions in the presence of cationic polyelectrolytes (e.g., high molecular weight chitosan, low molecular weight chitosan, and polydiallyldimethylammonium chloride), anionic polyelectrolytes (e.g., sodium carboxylmethyl cellulose, sodium alginate and gum arabic), and non-ionic water-soluble polymers (e.g., polyvinyl alcohol, polyethylene glycol and hydroxypropyl methylcellulose) was systematically compared (Figure 9b–d).[88] At the 5 wt% S-CNC concentration, the addition of the polymers increased the value of G', suggesting the formation of more rigid network through different flocculation mechanisms, i.e., electrostatic attraction, entropic depletion and polymer bridging (Figure 9a). Particularly, the cationic polyelectrolytes exhibited much stronger flocculating ability than anionic polyelectrolytes and non-ionic polymers, since the presence of only 0.1 wt% of cationic polyelectrolytes led to even higher G′ than the introduction of 1 wt% of anionic polyelectrolytes and non-ionic polymers, highlighting the effectiveness of electrostatic attraction on the flocculation of S-CNC suspensions. Furthermore, the anionic polyelectrolytes had a greater thickening effect than non-ionic polymers (except for hydroxypropyl methylcellulose), which is probably due to the predominant entropic depletion forces considering that those anionic polyelectrolytes did not absorb on the S-CNC surface.

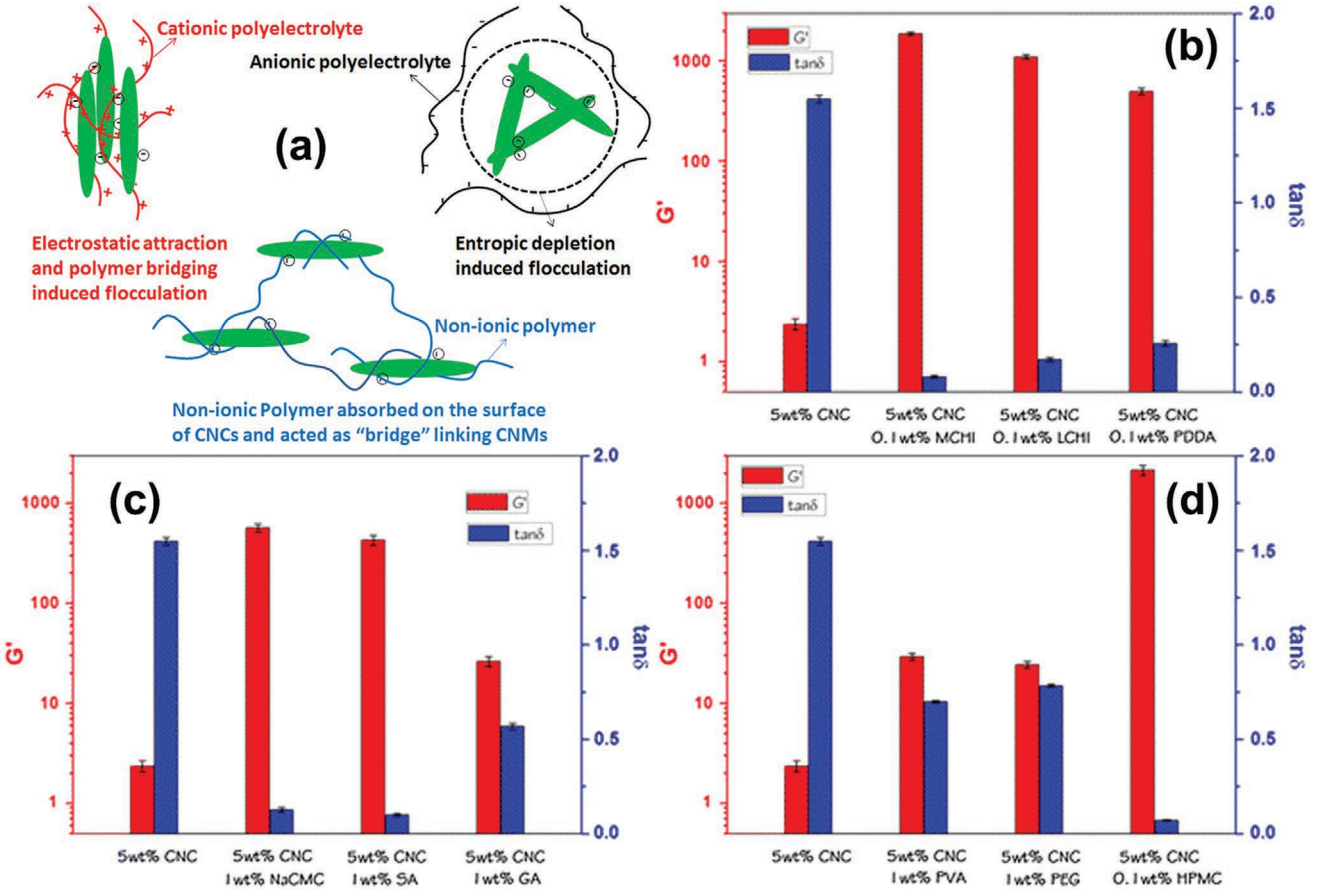

Figure 9. Influence of water-soluble polymer addition on the microstructure and rheology of CNM suspensions. a) Schematic illustration on microstructures of CNMs in the presence of cationic polyelectrolytes, anionic polyelectrolytes, and non-ionic polymers. b–d) G' and tan δ of S-CNC suspensions in the absence/presence of cationic polyelectrolytes, anionic polyelectrolytes, and nonionic polymers, respectively. b–d) Reproduced with permission.[88] Copyright 2018, Springer Nature.

More recently, lignin-containing CNMs (LCNMs) have emerged as cost and performance competitive CNMs.[202,203] LCNMs are directly produced from unbleached lignocellulosic biomass, offering advantages of less chemical usage, cost effectiveness, and environmental friendliness. The residual lignin either attached on the CNM surface or as free structures can act as a binder among CNMs through hydrophobic interaction, which affects the rheological properties of CNM suspensions.[204–206] Strong gel-like rheological behavior was observed for the lignin-containing NFC (LNFC) suspensions, especially for the finely fractioned samples. For lignin-rich samples that had coarser fibril morphology, dilatant behavior was found in the high deformation region. The deformation-induced flocculation/aggregation of the weakly surface-charged LNFC greatly confined the freedom of movement in the shearing direction because of created entanglement and hydrophobic properties of lignin.[204]

3.4.12. Postprocessing

Postprocessing (e.g., drying and redispersion) is practiced in industry to make CNMs more cost-effective for shipping and storage. The processes, however, generally have an adverse influence on the rheological properties of redispersed CNM suspensions. Current drying technologies includes oven-drying, freeze-drying, spray-drying, and supercritical drying.[207] Upon drying, CNMs form dense agglomerates, which exhibit poor redispersibility because of the formation of extensive and organized hydrogen bonding among dried CNMs. As a consequence, redispersion of the fully dried CNMs in an aqueous suspension does not enable a complete recovery of the rheological properties of the original suspension. Several strategies have been applied to overcome this bottleneck through preventing the formation of strong hydrogen bonding, including freezing–defreezing, carboxymethylation, addition of water-soluble polymers, and addition of salts.[23]

Among the published work, the viscosity of E-NFC suspensions was shown to be reduced by almost threefold after being oven dried and redispersed.[208] The increase in drying rate lowered viscoelastic properties of redispersed CMC/UN-NFC materials because of the formation of denser NFC agglomerates.[156] Freeze drying, supercritical drying and spray drying techniques were also applied, aiming to obtain less dense CNM agglomerates with highly porous microstructures.[207,209–211] However, notable loss of the rheological properties of CNM suspensions occurred as well. For example, freeze drying led to 55% and 72% reduction in the G' of redispersed 0.5 and 1 wt% UN-NFC suspensions, respectively.[118] The freeze-defrosting method offers certain advantages for the storage of CNM suspensions in terms of maintaining their rheology. The defrosted sample showed very similar rheological properties as compared with original sample.[118]

For more efficient and cost-effective drying and redispersion of CNMs, techniques including carboxymethylation,[212] addition of water-soluble polymers,[156,208,213–215] and addition of salts[216,217] have been developed. For example, CM-NFC were manufactured from refined, bleached beech pulp through carboxymethylation prior to mechanical disintegration.[212] The obtained CM-NFC after being dried exhibited good redispersibility in an aqueous suspension. The presence of a small amount of water-soluble polymers before drying effectively enhanced the water-redispersibility of CNMs as well. Various water-soluble polymers, such as CMC, CPAM, sodium polyacrylate (PAA),[156] PEO,[213] pectin, hemicellulose,[214] and tannic acid[215] have been used. The anionic CMC outperformed PAA and CPAM in the preparation of water-redispersible NFC with less loss in rheology. The coating of a layer of CMC films around NFC greatly weakened the hydrogen bonding between NFC during drying.[156] Furthermore, water-redispersibility of dried NFC was dependent on the amount of absorbed CMC on NFC, which was governed by treatment temperature and feeding ratio between CMC and NFC.[208] Particularly, higher temperature and feeding ratio yielded a higher amount of CMC absorbed onto NFC, leading to better water-redispersibility of dried NFC, which was reflected in the most effective recovering of viscosity after redispersion of the dried sample (i.e., NFC-CMC-HT-100). Salt was also shown to effectively act as a hydrogen bonding blocker, preventing the formation of CNM agglomerates during drying, producing fully water-redispersed CNMs.[216,217]

4. Emerging Applications of CNMs as Rheology Modifiers

CNMs have emerged as effective rheological modifiers with widely tailorable viscosity and viscoelastic properties, high viscosity at rest, profound shear-thinning behavior, good thixotropic properties, outstanding water retention capacities, and superior ability to stabilize emulsions. These rheological characteristics have the potential to be well suited for specific applications, as outlined below. For example, thixotropic behavior can be advantageous, in principle, in applications where the mixture first needs to be able to flow readily at one stage, but then it needs to become thickened or immobilized when the flow ceases.[218] As another example, the water-holding tendency of CNMs can be an inherent advantage in paper coating formulations.[219] This is because the coating formulation needs to hold onto water long enough to avoid formation of crumbs on coating blades. Also, the strength, chemical stability, and nontoxic nature of most cellulosic materials may be important for the final product performance in various applications. Recent advances in establishing the influential factors on CNMs' rheological behaviors, including CNM inherent properties and suspension environment, have led to their diverse industrial applications.

4.1. Inks for 3D Printing

3D printing, also known as additive manufacturing (AM), is an advanced manufacturing technology to rapidly fabricate a wide range of 3D constructs in a layer-by-layer manner.[220] Among the 3D printing technologies,[221,222] specifically relevant for CNMs is a subset of material extrusion AM called direct ink writing (DIW). The rheological feature of inks is considered to be the most important factor for DIW in terms of the

printability and shape fidelity. An ideal DIW ink should: i) possess shear-thinning capability, enabling the ink to smoothly flow through small diameter deposition nozzles under shear; ii) have a sufficient zero-shear viscosity and high yield stress to maintain the structural stability of printed 3D constructs, thereby avoiding the deformation or collapse under their own weight; and iii) show superior thixotropic property, allowing a rapid recovery in viscoelastic properties after printing. CNM-based hydrogels meet the above requirements and thus have been emerging as novel inks or rheological modifiers in multicomponent ink formulation for printing of 3D structural constructs in biomedical and electronic applications.[223–229] **Table 2** shows a summary of recent studies on CNM-based bioinks for 3D printing with respect to characteristics of CNMs, ink composition and rheology, printers, gelation or solidification methods, and given biomedical and electronic applications.

4.1.1. Biomedical Applications

The applications of 3D printing technology in biomedicine are growing exponentially and are expected to revolutionize the health care industry.[264] CNM-based hydrogels can be: i) biocompatible, sharing many similarities to the natural extracellular matrix; ii) not cytotoxic against a series of cell lines, providing suitable environment for cell growth and proliferation; iii) biodegradable, allowing the natural decomposition of printed constructs and subsequent formation of new extracellular matrix; and iv) mechanically robust and able to be further physically or chemically crosslinked using heat, UV, cations, and various chemical cross-linkers. These attractive features further allow CNM-based hydrogels to serve as perspective bioinks for 3D printing scaffolds in biomedical applications, particularly in tissue engineering and wound dressing fields.

Among the studies, a bioink composed of E-NFC and alginate for 3D printing of living soft tissue with cells has been commercialized as CELLINK (CELLINK AB, Sweden) and is a promising bioink for 3D printing constructs together with diverse living cells for cartilage tissue engineering.[230–234] The NFC has an average width of 20 nm and negative surface charge of 24 μeq g^{-1} produced through a combined enzymatic pretreatment and HPH. The presence of E-NFC in alginate inks greatly increased their viscosity at low shear rates (e.g., ≈10^4 Pa s at 10^{-2} 1 s^{-1}), but it also induced a more profound shear-thinning behavior (e.g., ≈10^5–10^{-1} Pa s), leading to enhancement in shape fidelity and printing resolution (**Figure 10**a,b). The printed scaffolds were further ionically crosslinked by $CaCl_2$ to prevent the 3D structure from collapse after printing (Figure 10c), and 2D structures (e.g., grid) and 3D constructs (e.g., human ear and sheep meniscus) were successfully fabricated.

In addition to alginate, some other natural biopolymers and their derivatives, such as hyaluronic acid,[235] xylan,[236] glycerin,[247] gelatin,[237] and gelatin methacrylamide,[238] were also used to formulate bioinks together with NFC for 3D printing of tissue. The addition of NFC also yielded more profound shear-thinning properties with improved printability and shape fidelity compared with pure polymer inks. Depending on the characteristics of the polymer matrix, different gelation or solidification strategies were reported. For example, the E-NFC/alginate bioinks were crosslinked using $CaCl_2$,[230–233,247] whereas H_2O_2 was employed to crosslink the bioink composed of E-NFC and hyaluronic acid with 5% tyramine substitution.[235] The minimum amounts of horseradish peroxidase (HRP) and H_2O_2 required for gelling E-NFC/tyramine-modified xylan bioink were found to be highly dependent on the substitution degree of tyramine, further highlighting the critical role of tyramine on their gel formation.[236] To crosslink the UN-NFC/gelatin bioink, genipin, a natural crosslinker derived from the fruit of *Gardenia jasminoides*, was used.[237] Alternatively, a chemically crosslinked UN-NFC/gelatin methacrylamide bioink was obtained using an ammonium persulfate/tetramethylethylenediamine (APS/TEMED) initiating system.[238] Gelation time was controllable by tuning the loading of initiator APS, which greatly facilitated the 3D printing process.

The NFC reported in the above literature was mostly manufactured through enzymatic pretreatment and mechanical disintegration approaches, and therefore they have weak surface charge and large dimension. For highly charged NFC with ultrafine diameters (e.g., C-NFC),[240–242,245,247,265] their superior stability and high gel ability allowed the production of bioinks in the absence of biopolymers. For example, 3D NFC aerogels with highly deformable, shape recoverable, and functionalizable properties were fabricated through the DIW method followed by freeze-drying and crosslinking.[240] Commercial NFC was subjected to TEMPO oxidation and HPH treatment, producing C-NFC ink with a suitable viscosity (i.e., 515 cP) at a concentration of 2.8 wt% for 3D printing of stable constructs without collapsing over time. In another example, C-NFC was manufactured from bagasse, through multi-step treatment of pulping, TEMPO oxidation, and homogenization.[241] The resultant C-NFC was 20 nm in width with carboxylic acid group content of 1.15-1.67 mmol g^{-1} depending on the applied conditions of pulping and TEMPO oxidation. 2D grid and 3D ear and nose scaffolds were fabricated using 2 or 2.6 wt% C-NFC inks, and their shape fidelity was improved when C-NFC was more oxidized and nanofibrillated. A more recent study revealed that TO-NFC and acetylated NFC (A-NFC) yielded more dimensionally stable scaffolds than UN-NFC because of the higher surface charge and axial aspect.[248]

In comparison with NFC, CNCs have gained less attraction as bioinks for 3D printing with living cells for tissue engineering, probably because of the relatively low viscosity of CNCs. For instance, to obtain self-standing, 3D printed constructs, the required concentrations of C-NFC and S-CNCs in bioinks without adding biopolymer were reported to be 2.8 and 11.8 wt%, respectively.[240,249] However even at a concentration of 11.8 wt%, the CNC bioink had a low viscosity of ≈0.24 Pa s, which caused the printed constructs to sag within a few minutes. With increase in the CNC concentration to 15, 20 and 30 wt%, the viscosity was raised to 0.79, 1.79, and 7.68 Pa s, respectively. The improved viscosity effectively overcame the observed sagging issue, leading to fabricating constructs with a higher shape fidelity and smoother edges. Different cartilage models, such as octet cube, nose, ear and honeycomb in the forms of gel and aerogel were successfully fabricated using 20 wt% CNC gel as ink through DIW.

CNCs were also combined with polymers (e.g., alginate, gelatin, and PEGDA)[250,251,253,255,256] or functional additives

Table 2. Summary of the reported studies on CNM-based ink for 3D printing for biomedical and electric applications.

Characteristics of CNMs				Ink formulation and rheology			Printer	Gelation or solidification method	applications	Refs.
Type	Dimension		Surface charge density	Formulation	Viscosity [Pa s]	Storage modulus [Pa]				
	Diameter [nm]	Length [nm]								
E-NFC	20	N/A	24 μeq g^{-1}	1.50–2.25 wt% E-NFC, 0.25–1.00 wt% alginate	≈10^5 @ 10^{-3} 1 s^{-1}	N/A	3D Discovery (regenHU Ltd., Switzerland)	Crosslinking by $CaCl_2$	Constructs for cartilage tissue growth	[230–233]
				1.36 wt% E-NFC, 0.5–1.0 wt% alginate or alginate sulfate	≈4×10^3–10^4 @ 10^{-2} 1 s^{-1}	N/A	3D Discovery (regenHU Ltd., Switzerland)	Crosslinking by $CaCl_2$	Constructs for cartilage tissue growth	[234]
				3 wt% E-NFC, 1.29 wt% hyaluronic acid	N/A	N/A	3D Discovery (regenHU Ltd., Switzerland)	Crosslinking by H_2O_2	Adipose tissue model for metabolic diseases test	[235]
				2.6–3.0 wt% E-NFC, 5.11–10.6 wt% Xylan	N/A	≈2.5×10^3–10^4 @ 1 Hz	3D Discovery (regenHU Ltd., Switzerland)	Crosslinking by horseradish peroxidase and H_2O_2	Constructs proposed for tissue engineering and wound dressings	[236]
UN-NFC	24.6 ± 1.2	2.8 ± 0.1	N/A	0.15–1 wt% UN-NFC, 3–7 wt% gelatin	4–30 @ 10^2 1 s^{-1};	2×10^3–5×10^3 @ 1% strain and 1 Hz	Bio-Architect-Pro (Hangzhou Regenovo Biotechnology Co., Ltd., China)	Crosslinking by genipin	Scaffolds for neural tissue engineering	[237]
	N/A	N/A	N/A	0.5–2 wt% UN-NFC, 5 wt% gelatin methacrylamide	≈10^2–3×10^3 @ 10^{-2} 1 s^{-1}	≈10–10^3 @ 1 Hz	Custom-built 3D printer	Crosslinking by APS and TEMED initiating system	Constructs for cartilage tissue growth	[238]
	20–30	N/A	N/A	1.47 wt% UN-NFC	N/A	N/A	Fab@Home experimental 3D printer (Fab@Home, USA)	Crosslinked by glutaraldehyde	Threads for would healing	[239]
C-NFC	N/A	≈5×10^4	0.83 mmol g^{-1}	2.8 wt% C-NFC, 0.06 wt% polyamido-amine epichlorohyrin	≈300 @ 0.2 1 s^{-1}	N/A	Ultimus V Dispenser (Nordson EFD, USA)	Freeze-drying and heating	Aerogels proposed for cartilage tissue growth, oil/water separation, and electronics	[240]
	<20	N/A	1.15–1.67 mmol g^{-1}	2 wt% C-NFC	N/A	N/A	Regemat3D 1.0 (Regemat3D, Spain)	Not crosslinking	Scaffolds for tissue engineering and wound dressings	[241]
	5–15	N/A	515 μeq g^{-1}	1.6 wt% C-NFC, 0.4 wt% CNTs	≈10^5 @ 10^{-3} 1 s^{-1}	≈500 @ 1 Hz	3D Discovery (regenHU Ltd., Switzerland)	Not crosslinking	Conductive scaffolds for neural tissue engineering	[242]
	N/A	N/A	1.14 mmol g	1 wt% C-NFC	N/A	≈300@3 rad s^{-1}	KIMM SPS1000 Bioplotter (Machtronics 4 Technology, Korea)	Crosslinking by $CaCl_2$ and 1,4-butanediol diglycidyl ether	Scaffold for wound healing, skin regeneration and tissue repair approaches	[243]
	N/A	N/A	1.14 mmol g	1 wt% C-NFC, 0.2–1 wt% gelatin methacrylate	≈10^3 @ 10^{-3} 1 s^{-1}	≈100–150	KIMM SPS1000 Bioplotter (Machtronics 4 Technology, Korea)	Crosslinking by $CaCl_2$ and UV (365 nm) irradiation	Scaffold for wound healing and soft tissue regeneration	[244]

Table 2. Continued.

Characteristics of CNMs				Ink formulation and rheology			Printer	Gelation or solidification method	applications	Refs.
Type	Dimension		Surface charge density	Formulation	Viscosity [Pa s]	Storage modulus [Pa]				
	Diameter [nm]	Length [nm]								
	<20	<200	0.39 mmol g^{-1}	3.9 wt% C-NFC	≈10 @ 10 1 s^{-1}	N/A	3D-Bioplotter (EnvisionTEC, Germany)	Crosslinking by $CaCl_2$ and freeze-drying	Scaffolds for wound dressings	[245]
	N/A	N/A	1040–1128	2 wt% C-NFC, 20 wt% alginate (based on the dry content of C-NFC)	16–18@1 RPM	N/A	Regemat3D printing unit (Granada, Spain)	Crosslinking by $CaCl_2$ and freeze-drying	Scaffolds for wound healing	[246]
	3–10	N/A	1.1 mmol g^{-1}	0.5–1.65% C-NFC, 3.3–4.5% alginate, 0–50% glycerin	≈10^5 @ 10^{-4} 1 s^{-1}	N/A	Custom-built microdispensing system	Crosslinking by $CaCl_2$	Constructs for customized implant, wound-healing, and biosensors	[247]
A-NFC	2–5	N/A	N/A	0.5 wt% A-NFC	≈10^5 @ 10^{-2} 1 s^{-1}	≈400 @ 0.5% strain and 1 Hz	BIO X Bioprinter (CELLINK, Gothenburg, Sweden)	Not crosslinking	Scaffold for cardiac myoblast cell growth	[248]
S-CNC	30	400	0.34 mmol g^{-1}	11.8–30 wt% S-CNC, 2 wt% Kymene (based on dry S-CNC mass)	≈0.24–7.68 @ 400 1 s^{-1}	N/A	Ultimus V (Nordson EFD, USA)	Freeze-drying and heating	Aerogels proposed for tissue engineering	[249]
	10–20	200–400	0.25 mmol g^{-1}	1–4 wt% S-CNC, 2 wt% alginate	≈30–100 @ 10^{-1} 1 s^{-1};	≈30–300 @ 0.1% strain and 1 Hz	FlashForge Creator Pro (FlashForge, China)	Crosslinking by $CaCl_2$	Constructs for liver-mimetic tissue growth	[250]
	3 ± 1	246 ± 100	N/A	0–1.2 wt% S-CNC, 75 wt% PEGDA, 0.765 wt% PI	N/A	N/A	Form 2 SLA (Formlabs, USA)	UV curing	Constructs proposed for cartilage tissue engineering	[251]
	23	183	0.34 mmol g^{-1}	5 wt% S-CNC, 1 wt% graphene quantum dots	N/A	266 @ 0.1% strain and 1 Hz	PRUSA i3 (Prusa Research s.r.o., Czech Republic)	Physical crosslinking by interfacial bonding	Fluorescent thread proposed for tissue engineering	[252]
	5–10	150–200	0.33 mmol g^{-1}	3.7–13.0 wt% S-CNC 71.1–20.0 wt% PEGDA	≈1000–5000@10^{-1} 1 s^{-1}, ≈0.8–2 @ 10^2 1 s^{-1}	N/A	Cellink BIO X (Cellink, USA)	UV curing	Gradient scaffolds for tissue engineering and potential stem cell embedment	[253]
C-CNC	5	547	0.106 mmol g^{-1}	15 wt% C-CNC	≈10^4 @ 10^{-1} 1 s^{-1}	≈10^5 @ 1 Hz	F4200N robot (Fisnar, USA)	Freeze drying	Porous structure proposed for tissue engineering and flexible electronics	[254]
	<10	N/A	N/A	3.76 wt% C-CNC, 1.09 wt% alginate, 0.55 wt% gelatin	6.92×10^4 @ 10^{-3} 1 s^{-1}	1.98×10^4 @ 0.1% strain and 1 Hz	Discovery Complete (Structur3D Printing, Canada)	Crosslinking by $CaCl_2$	Scaffolds proposed for tissue regeneration	[255]
D-CNC	N/A	N/A	49.39%	2 wt% D-CNC, 4 wt% gelatin	≈550 @ 0.1 1 s^{-1}	90.12–5297.23 as function of incubation time @ 1% strain and 1 Hz	Bio-Architect-Pro (Hangzhou Regenovo Biotechnology Co., Ltd., China)	Self-crosslinking via a Schiff base reaction	Scaffolds for tissue engineering	[256]

Table 2. Continued.

Characteristics of CNMs				Ink formulation and rheology			Printer	Gelation or solidification method	applications	Refs.
Type	Dimension		Surface charge density	Formulation	Viscosity [Pa s]	Storage modulus [Pa]				
	Diameter [nm]	Length [nm]								
NFC	100	2000	N/A	36 wt% silver nanowire in NFC	$\approx 10^5$ @ 10^{-3} l s^{-1}	$\approx 10^3$ Pa @ shear stress of 1 Pa	3D printing system (SHOT mini 100Sx and ML-808GX, Musashi Engineering, Inc.).	Drying in air	Ion detectable sensor	[257]
E-NFC	N/A	N/A	N/A	2 wt% NFC, 0–50 wt% LS	$\approx 10^5$ @ 10^{-3} l s^{-1}	N/A	Model 3 (Seraph Robotics, USA)	Freeze-drying or drying in air, pyrolysis	Porous electrodes for energy storage devices	[258]
C-NFC	N/A	N/A	N/A	5.1 wt% NFC, 10 wt% $LiFePO_4$	$\approx 5 \times 10^4$ @ 10^{-2} l s^{-1}	$\approx 5 \times 10^4$ @ 10 Pa shear stress	F4200N robot (Fisnar, USA)	Annealing	Electrodes for lithium metal microbattery	[259]
	15	300–500	N/A	1.2 wt% T3C2/NFC mixture with Ti3C2/NFC weight ratios of 10/90, 30/70 and 50/50	$\approx$7–100 @10^2 s^{-1}	5–30 @ 0.1% strain	3D printer (JDX01, Changsha Nayi Co., Ltd)	Drying in air	Smart fibers and textiles with excellent responsiveness to electrical/ photonic/ mechanical stimuli	[260]
	N/A	N/A	N/A	2 wt% NFC, 0.2 wt% CNT, 0.2 wt% CTAB	$\approx 10^5$ @ 10^{-3} l s^{-1}	N/A	3D Discovery (regenHU Ltd., Switzerland)	Drying in air	Packaging, textiles, biomedical devices, and furniture with conductive parts	[261]
	$\approx$20	> 1000	N/A	0.5 wt% NFC, 0.5 wt% CNT	$\approx$100 @ 0.03 l s^{-1}	$\approx$20 @ 0.1% strain	Benchtop robot F4200n (Fisnar, USA)	Drying in air	Wearable electronic and energy storage devices	[262]
	3.5–5	500–1000	600 ± 50 μmol g^{-1}	NFC/alginate = 80:20	N/A	N/A	BIO X Bioprinter (CELLINK, Gothenburg, Sweden)	Drying in air; in situ polymerization of conductive polymers	Energy storage materials, pressure, and humidity sensors	[263]

(e.g., graphene quantum dots)[252] to prepare high-performance bioinks. The presence of S-CNCs increased the viscosity of polymers, leading to better printability and shape fidelity (Figure 10d,e).[250] The introduction of polymers not only reduced the amount of CNCs required to print self-standing gels, but also imparted crosslinking ability to the hybrid ink. A UV-curable ink with S-CNCs, poly(ethylene glycol) diacrylate (PEGDA), and photoinitiater (PI) was formulated for 3D printing using the stereolithography technique.[251] The S-CNC provided good printability, shape fidelity and mechanical integrity to PEGDA resin, while PEGDA was cured by UV to retain the 3D structure after printing. Further, a series of PEGDA/S-CNC/PI ink formulations with sufficient rheology for DIW was demonstrated with S-CNC compositions of 3.7–13.0 wt%. Multiple formulations with varying PEGDA/S-CNC ratios were extrusion printed into representative tissue scaffolds with gradient properties.[253] These formulations possessed sufficient yield stress and strong shear thinning response to generate dimensionally stable prints that were UV post-cured into the final form. A Schiff base reaction was reported to crosslink a bioink composed of dialdehyde CNCs (D-CNCs) and gelatin.[256] D-CNCs were prepared through oxidation of CNCs using sodium periodate as oxidant. The ink 4:8-DAC/GEL incubated for 3 h exhibited the best performance in terms of breaking strength, G' and viscosity; and therefore, it was considered as the optimal ink formulation for 3D printing. Furthermore, a multifunctional gel with injectable and fluorescent features was developed using S-CNCs and graphene quantum dots (GQDs).[252] The formation of gel was ascribed to the hydrogen bonding and hydrophobic interactions between S-CNCs and GQDs. The 3D printed thread showed a precise pattern, fluorescence at 365 nm as well as birefringence, making it suitable for diverse biomedical applications.

CNM-based hydrogels were also employed as bioinks to fabricate threads, films, scaffolds through 3D printing for wound dressing applications.[239,243–247] For example, the suitability of NFC-based hydrogels to fabricate 2D grids or 3D porous scaffolds through DIW for potential wound dressing application was reported by Rees et al.[245] The NFC was produced through a combination of carboxymethylation and periodate oxidation,

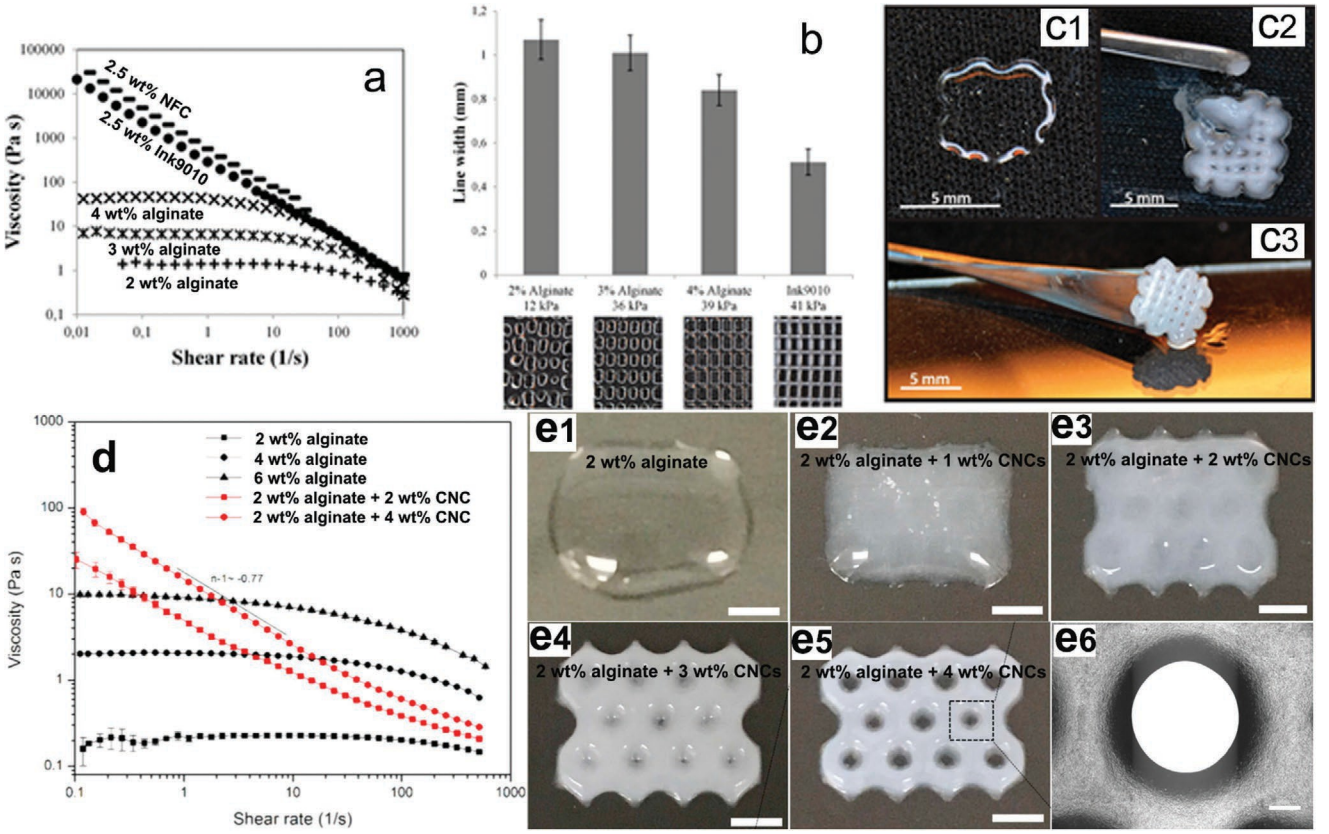

Figure 10. CNMs in inks for 3D printing biomedical constructs. a) Steady-state viscosity of pure alginate solution at concentrations of 2 wt% (+), 3 wt% (*) and 4 wt% (×), 2.5 wt% Ink9010 (●), and 2.5% E-NFC suspension (–). b) Change in line width and resolution of 3D printed large grids after addition of NFC. c1–c3) Digital images of small grids printed using: c1) 3 wt% alginate solution, c2) Ink9010, and c3) Ink9010 after crosslinked by $CaCl_2$ solution. Note: Ink9010 contains 90 wt% alginate and 10 wt% E-NFC. a–c) Reproduced with permission.[230] Copyright 2015, American Chemical Society. d) Steady-state viscosity of pure alginate solution and alginate/S-CNC ink at different concentrations. e1–e5) Digital images of 3D printed constructs using different ink formations (scale marker is 5 mm). e6) Enlarged image of the dashed area in (e5). d,e) Reproduced with permission.[250] Copyright 2018, Elsevier.

and hence it exhibited much smaller dimensions than those prepared from TEMPO oxidation. This enabled NFC to be 3D printed at a high concentration (i.e., 3.9 wt%) with suitable rheological properties (i.e., 10–0.1 Pa s@10–10^3 s^{-1}), creating a more solid 2D grid with defined tracks. A 3D scaffold was successfully printed using the carboxymethylated and periodate oxidized NFC, followed by crosslinking using $CaCl_2$ and freeze-drying. These findings provide strong evidence of the suitability of 3D printed C-NFC scaffolds as wound dressing materials.

4.1.2. Electronic Applications

3D printing for the rapid prototyping of structural electronics brings forth unprecedented flexibility in design, revolutionizing the electronics industry.[266] In this front, the use of CNM-based hydrogels as inks to 3D-printed electronics has attracted considerable attention. To achieve conductive functionality, conductive fillers are incorporated into CNM-based hydrogels, mainly including carbon nanoparticles, metallic nanoparticles, and conductive polymers.[229] In these hybrid inks, CNM additions serve as thickening agents for controlling printability and shape fidelity, and as dispersing, stabilizing or binding agents for conductive fillers, leading to superior physicochemical, thermal, mechanical, and electronic performance of 3D printed electric constructs. The pros and cons involved with the use of CNMs, a nonconductor, as part of a highly conductive system are well discussed.[267]

Various conductive fillers, including silver nanowires (AgNW),[257] $LiFePO_4$,[259] MXene,[260] and CNTs,[261,262] have been applied to formulate conductive inks together with CNMs for 3D printing of electronic devices. For instance, AgNW were compounded with CNMs to prepare conductive inks for 3D printing of disposable wireless ion sensors.[257] The AgNWs were randomly distributed in the printed NFC-AgNW ink, but they were oriented in the printed CNC-AgNW inks (**Figure 11**a–d), which can be attributed to different interactions between CNMs and AgNWs during the extrusion processes. The formulated NFC-AgNW ink displayed superior dynamic and steady-state shearing rheological properties. Under a 1 Pa shear stress, the G' reached ≈10^3 Pa (Figure 11e), allowing good printability through a rapid solidification after printing. Additionally, a typical shear-thinning behavior was observed, i.e., the viscosity gradually decreased from ≈10^5 to ≈10^{-4} Pa s with increase in shear rate from 10^{-3} to 10^3 s^{-1} (Figure 11f), enabling the ink to smoothly flow through small diameter nozzles under shear without clogging. A wireless sensor system, including inductor–capacitor circuits and ion selective membrane electrodes

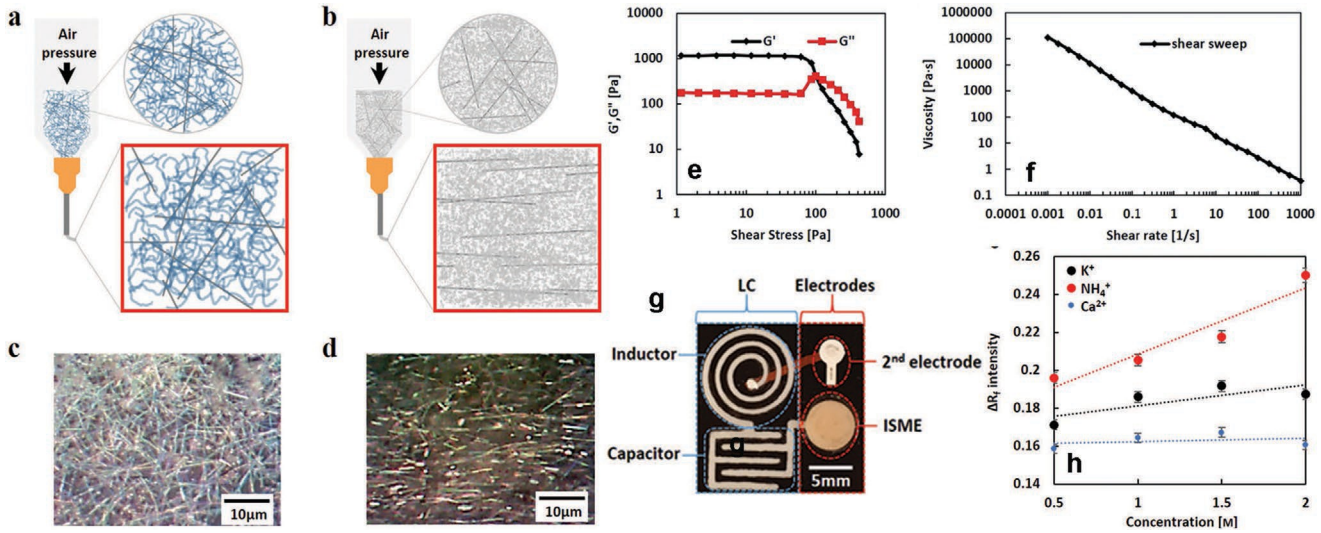

Figure 11. CNMs in inks for 3D printing electronic devices. a,b) Schematic illustration of printed NFC-AgNW and CNC-AgNW inks, respectively. c,d) Microscopy images of printed ink of 36 wt% AgNW in NFC and 30 wt% AgNW in CNC, respectively. e,f) Dynamic and steady-state rheological properties of NFC-AgNW ink, respectively. g) Configuration of printed IS-LC sensor. h) Change in resonant frequency (R_f) intensity of IS-LC sensor with NH_4^+ membrane as a function of NH_4^+ ion concentration. a–h) Reproduced with permission.[257] Copyright 2019, Wiley.

(Figure 11g) was 3D printed using the developed NFC-AgNW ink, which showed high selectivity of NH_4^+ ion (Figure 11h). In addition, post-treatments of 3D printed constructs, including carbonization[258] and in situ polymerization of conductive polymers[263] were reported to impart good electrical conductivity. For instance, honeycomb-like constructs based on C-NFC/alginate inks were printed and then functionalized through in situ polymerization of conductive poly(3,4-ethylenedioxythiophene) polystyrene sulfonate (PEDOT:PSS).[263] The functionalized sample showed an electrical conductivity of 5.7 S m^{-1}, exhibiting promising applications as energy storage materials, pressure and humidity sensors.

4.2. Materials for Oilfield and Construction Services

4.2.1. Drilling Fluids

Drilling fluids (DFs) are viscous, shear-thinning fluids that are used to facilitate the drilling operations for gas and oil extraction. During the drilling operations, DFs perform indispensable functions, primarily including carrying cuttings out of the wellbore, suspending cuttings, cooling drill bits, lubricating friction surfaces between drilling assembly and formation, maintaining wellbore stability, and minimizing formation damage.[268,269] Rheology and filtration are considered to be the two most important performance measures for water-based DFs (WDFs). CNMs with outstanding renewability and biodegradability, profound shear-thinning behavior, strong water-binding ability, and superior nanopore-plugging capacity can serve as next-generation rheological and filtration modifiers to formulate environmentally-friendly smart WDFs for oil and gas excavation (**Figure 12**a).

The presence of both UN-NFC and S-CNCs in bentonite-WDFs (BT-WDFs) dramatically increased the viscosity and yield stresses of BT-WDFs (Figure 12b,c).[77] The formulated S-CNC/BT-WDs had a higher viscosity compared with that of UN-NFC/BT-WDFs, despite the fact that the S-CNC suspension had much lower viscosity than the UN-NFC suspension at the same concentration level. Fluid microstructure analysis showed that highly negatively charged S-CNCs were attached to the surface of BT platelets (Figure 12d), creating a rigid "core–shell" structure (Figure 12e). A similar structure was, however, not observed for UN-NFC/BT-WDFs. The S-CNC/BT-WDFs also exhibited better filtration performance compared with NFC/BT-WDFs, i.e., less fluid loss volume, slower filtration speed, and thinner filter cake. These merits make S-CNCs preferable to UN-NFC for use as rheological modifiers and filtration controlling agents in BT-WDFs. The nature of CNCs' surface charge also showed a profound influence of the fluid behavior. It was revealed that the negatively charged C-CNCs were absorbed to the edge surface of BT platelets and acted as "bridges," connecting BT platelets via "edge-to-edge" association.[271] On the contrary, the positively charged CA-CNCs were attached to the face surface of BT platelets and acted as "cross-linking agents", stacking numerous layers of BT platelets through "face-to-face" association. As a consequence, the negatively charged C-CNC/BT-WDFs showed superior rheological properties (e.g., smother shear-thinning behavior, higher viscosity, and higher yield stress) as well as better filtration performances (e.g., lower fluid loss volume and thinner, more compact, and less permeable filter cake) compared with the positively charged CA-CNC/BT-WDFs.

To meet the requirements for unconventional formation excavation, thermo-thickening and salt-resistant CNC/BT-WDFs were developed through surface functionalization of CNCs. The thermo-thickening CNCs were manufactured by surface grafting of poly(2-acrylamido-2-methyl-1-propanesulfonic acid) and poly(N-isopropylacrylamide) through free-radical graft polymerization,[272] whereas poly(acrylamide) and poly(2-acrylamido-2-methyl-1-propanesulfonic acid) were coated on the surface of C-CNCs through in situ radical polymerization

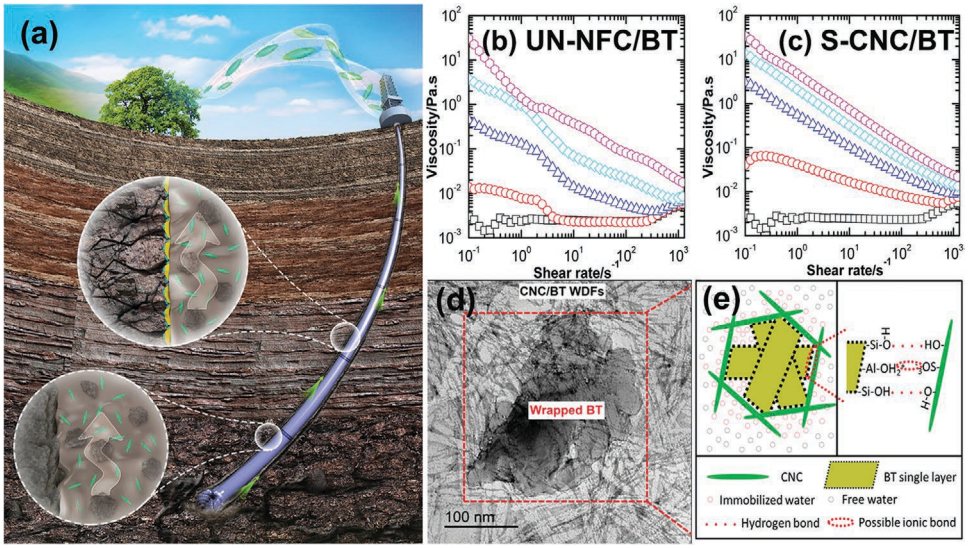

Figure 12. CNMs in WDFs. a) Schematic illustration on the application of CNMs as rheological and filtration modifiers in WDFs for oil and gas production. Reproduced under the terms of the CC-BY Creative Commons Attribution 4.0 International license (http://creativecommons.org/licenses/by/4.0/).[270] Copyright 2020, The Authors, published by American Chemical Society. b,c) Steady-state viscosity of UN-NFC/BT- and S-CNC/BT-WDFs at different concentrations: 0 wt% (black squares), 0.1 wt% (red circles), 0.25 wt% (blue triangles), 0.5 wt% (cyan diamonds) and 1.0 wt% (magenta hexagons), respectively. d) TEM image of S-CNC/BT-WDFs. e) Proposed surface interaction between S-CNCs and BT platelets. The concentration of BT was fixed at 3 wt%. b–e) Reproduced with permission.[77] Copyright 2015, American Chemical Society.

to synthesize salt-tolerant CNCs.[270] The combined use of polyaionic cellulose (PAC), a common filtration controlling agent, with CNMs (S-CNCs,[78] UN-NFC,[273] and LNFC,[274,275]) resulted in much improved rheological and filtration properties.

The development of low-bentonite or even bentonite-free WDFs helps provide high drilling rates, easy fluid control and maintenance, low friction in drilling assembly, thin filter cakes, and few pipe sticking problems. CNMs, especially NFC with outstanding rheological properties, can be utilized to partially or even fully replace BT in WDFs for the formulation of low-solid content or even bentonite-free WDFs.[193,276–278] Song et al. demonstrated that about half of the amount of BT (≈2.86 wt%) in a commercial WDF formulation can be utilized with the addition of a small amount of CNMs (≈0.30 wt%) while still maintaining good rheological properties.[276] Hall et al. formulated the bentonite-free WDFs using four types of NFC with different surface characteristics, i.e., UN-NFC, C-NFC, TO-NFC, and CA-NFC.[278] In comparison with the conventional rheological modifier (e.g., xanthan gum), NFC showed higher onset decomposition temperature as well as more stable rheology upon the temperature change.[175] Furthermore, the presence of anionic biopolymers gradually enhanced the rheology of NFC-WDFs;[193] whereas the maximum viscosities of nonionic biopolymer/NFC-WDFs were achieved when 0.1 wt% of nonionic biopolymers was incorporated. The bridging mechanism through adsorption of biopolymers chains on the surface of NFC was responsible for the enhanced rheological behaviors.

4.2.2. Cement Pastes

Concrete, made of cement and aggregates, is the most consumed material (second only to water) in the world. In oil fields, cementing is one of the most crucial processes in well construction to provide a hydraulic seal and zonal isolation, obtain a good cement-to-pipe bond, protect the casing from corrosion, and shut off water penetration into the well. A wide range of additives including supplementary cementitious materials, chemical admixtures and reinforcement fibers (including natural fibers at both micro and nano-scales) have been used to enhance strength, reduce cost, and speed up setting time and strength gain.[279–281]

The process of developing final concrete strength is closely related to the rheology of cementitious material.[282–284] In fact, the rheology is considered to be one of the most important factors for the high performance concrete for proper flowability and workability. The yield stress for the concrete is of critical importance to maintaining a uniform compounding of different additives, avoiding bleeding and segregation.[285] The rheology of concrete is influenced by many factors, e.g., water/cement ratio, cement grain shape and size, cement composition, mixing conditions, measuring instruments and experimental procedures, and the presence of additives such as water reducing agents, superplasticizers, and micro/nanofibers.

High quality CNM/cement composites have been developed, taking advantage of high surface area, superior water retention ability, tunable surface chemistry, outstanding rheological properties, and good mechanical properties of CNMs.[79,286–292] In the complex composite systems, CNMs interact with cement particles in pore solution, leading to altered rheology, setting time, and mechanical properties of the cementitious mixture. Using Type V cement with a water-cement ratio of 0.35, Cao et al. measured the influence of added S-CNCs on the yield stress of freshly mixed CNC–cement pastes (**Figure 13**a—black squares).[286] At low S-CNC loadings, the yield stresses decreased with the increase of S-CNC loading, which was attributable to

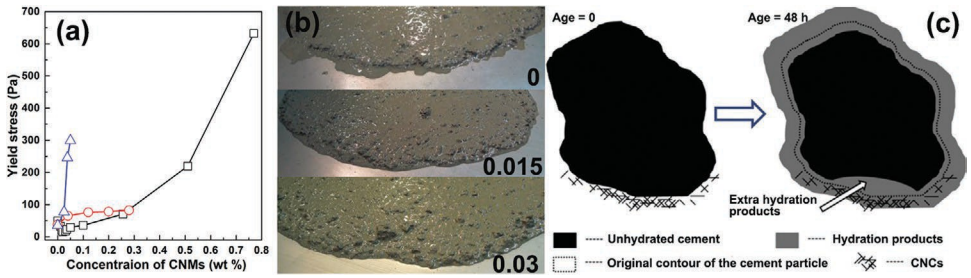

Figure 13. CNMs in cement pastes. a) Comparison on yield stress of CNM/cement pastes (black squares—S-CNC/cement pastes;[286] red circles— S-NFC/cement pastes;[79] blue triangles—UN-NFC/cement pastes[285]). b) Photos of stabilization of cement pastes containing 0, 0.015, and 0.03 wt% UN-NFC. c) Schematic illustration on the attachment of S-CNCs on the cement shell and improvement of hydration. b) Reproduced with permission.[285] Copyright 2017, EXILVA. c) Reproduced with permission.[286] Copyright 2015, Elsevier.

electrostatic stabilization and liberated entrapped water molecules. At higher S-CNC loadings, the yield stress increased linearly as the S-CNC loading was increased. This was attributed to possible S-CNC agglomeration in the pore solution, and the system with agglomerated S-CNCs requires higher forces to break the agglomeration. Increased yield stresses can possibly decrease cement flowability. Sun et al. studied the effect of S-NFC on flow, hydration, morphology, and strength of Type H oil well cement (OWC) with a water–cement ratio of 0.38.[79] Rheological modelling was done to fit the data using the Bingham plastic, Herschel–Bulkley, Vocadlo, and Vom Berg models. The Vom Berg model (Table 1) showed the best fit because of the adjustability of the three parameters to accurately capture yield stress and shear thinning response over the broadest range of compositions and shear rates. The addition of NFC at moderate levels increased the yield stress of the NFC-OWC slurry (Figure 13a—red circles) and degree of hydration and flexural strength of hydrated NFC/OWC samples. In another study,[231] UN-NFC, manufactured by mechanical disintegration with relatively large diameter and strong network, was shown to lead to more significant increase in yield stress in the cementitious system.[285] (Figure 13a—blue triangles). The increase in yield stress was beneficial to maintaining the stability of concrete and preventing segregation and bleeding (Figure 13b). Furthermore, the addition of S-CNCs increased the degree of hydration (DOH) of cement paste due to the combined influences of steric stabilization and short circuit diffusion.[286] S-CNCs were attached to the cement particles and present in the shell of the hydration product, leading to the formation of a path to transport water to the inner unhydrated cement core (Figure 13c).

4.2.3. Enhanced Oil Recovery

In recent years, nanofluid flooding has emerged as an effective strategy to enhance oil recovery. Some appealing features of CNMs, including nanoscale dimension, widely tunable rheological properties, highly hydrophilic surface nature, and easy chemical modification, enable them to serve as suitable flooding agents for EOR application.

Two types of TO-NFC with similar dimension but different surface charge densities (i.e., 0.72 and 1.51 meq g^{-1}) were compared for use in EOR.[124] Highly charged TO-NFC (NC-2) nanofluid had better salt tolerance and rheological properties over less charged TO-NFC (NC-1) nanofluid (**Figure 14**a), suggesting the superior sweep efficiency of NC-2. After being combined with oil, NC-2 not only reduced the interfacial tension more profoundly, but it also formed more stable emulsion in comparison to NC-1, indicating the better displacement efficiency of NC-2. With the visual EOR experiments using a micromodel (Figure 14b), it was shown that NC-2 nanofluid (Figure 14d) reached more oil saturation areas, and subsequently it swept and displaced a larger amount of oil than NC-1 nanofluid (Figure 14c). To overcome poor salt resistance, surface modification of TO-NFC through grafting of salt-resistant

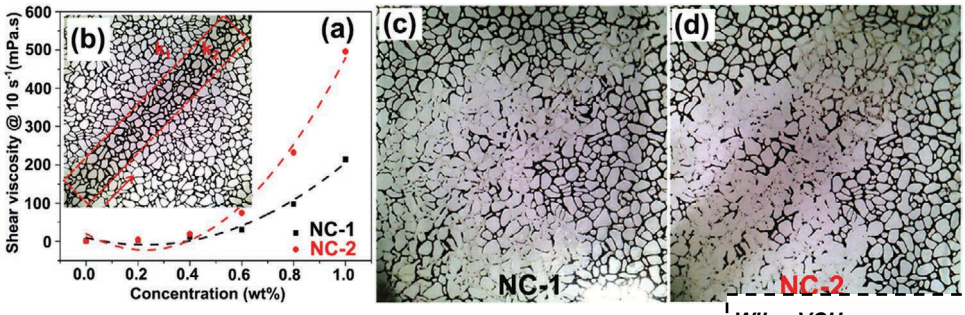

Figure 14. CNMs in enhanced oil recovery. a) Shear viscosity of TO-NFC nanofluids at different [illegible] b–d) Images of micromodel at initial oil saturation (b), and after NC-1 (c) and NC-2 (d) flooding, resp[illegible] direction of flooding; and the micromodel has a heterogeneous structure with two different permeabilit[illegible] permission.[124] Copyright 2016, American Chemical Society.

poly(2-acrylamido-2-methylpropane sulfonic acid) (PAMPS) and hydrophobic groups (HG) was carried out.[293–295] The presence of PAMPS and HG induced strong steric stabilization and electrostatic repulsion among TO-NFC and thereby prevented them from aggregation and precipitation in the presence of salts. As a consequence, the PAMPS and HG modified NFC (NC-KYSS) nanofluid showed more stable rheology upon adding salts when compared to nanofluids of neat TO-NFC (NC) and PAMPS modified NFC (NC-KY). Furthermore, NC-KYSS was effective in reducing interfacial tension with oil, converting the wettability of rock from oil-wet to water-wet, and creating stable oil-in-water emulsion. The oil recovery was further optimized by tailoring the injected volume, media permeability and oil viscosity.[296]

Foam flooding is another prospective EOR technique, which utilizes foam produced by a mixture of gas (e.g., hydrogen carbon, air, N_2, O_2 and CO_2) and foaming agents (e.g., surfactants) to sweep and displace oil from the reservoir.[297] In this process, the NC-KYSS helped stabilize the foam lamella generated by a mixture of air and the anionic surfactant alkyl polyglycoside (APG).[298] A 12% OOIP (original oil in place) increase in oil recovery was achieved using the NC-KYSS stabilized APG foam flooding compared with using the APG foam flooding. The work further revealed that: i) the NC-KYSS stabilized APG foam yielded larger flow resistance across the capillary than APG foam; and ii) the occurrence of "snap off" induced the NC-KYSS stabilized APG foam to generate finer bubbles, allowing them to reach the deep porous media.[299]

The feasibility of using S-CNCs as flooding agents for EOR was also demonstrated.[165] The sandstone injectivity of S-CNCs in 17×10^{-3} m (≈1000 ppm) NaCl brine was studied through core flooding experiments at room temperature. During the entire flooding process, the effluent viscosity barely changed, indicating the good injectivity of S-CNC nanofluid. However, the change in pressure (ΔP) steadily increased as more S-CNC nanofluids were injected. This was ascribed to the trapping of agglomerated S-CNCs inside the core or at the inlet of flooding setup, which was also confirmed by permeability measurements of the core. The injectivity was also dependent on the S-CNC concentration. S-CNC nanofluids with concentration ranging from 0.5 to 2 wt% showed good injectivity in sandstone under low salinities.

For practical application in oil wells, S-CNC nanofluids encounter several physical and chemical challenges, e.g., long retention time (>1 month), high temperature (>100 °C), fluctuating pH (5–9), and high salinity (>1000 ppm). Preliminary assessment showed that 0.5 wt% S-CNC in deionized water and in a 1000 ppm NaCl brine were stable within the pH range from 5 to 9 as well as within the temperature range from 50 °C to 90 °C.[174] Upon aging treatment at higher temperatures for several days (e.g., 120 °C and 7 d), both thermal oxidation and acid hydrolysis took place, which caused the exposure of more hydroxyl groups, resulting in a substantial increase in viscosity. This feature was advantageous for EOR application, because a low initial viscosity benefited injection, but subsequent thickening due to aging treatment during transportation in porous media promoted the oil sweep performance. The long-term thermal resistance of S-CNC nanofluids can be enhanced by adding sodium chloride, cesium formate and sodium formate through the complexion and radical scavenging effects of chloride and formate ions.[174,175] Subsequently, the sandstone injectivity and oil recovery performance of 0.5 wt% S-CNC in 17×10^{-3} m (≈1000 ppm) NaCl brine were examined at temperatures ranging from 60 °C to 120 °C.[300] Rheological measurements on the effluent samples revealed that the majority of S-CNCs were propagated through the porous media at all investigated temperatures, since there was little change in the viscosity of CNC nanofluids before and after flooding. The injection of 11 PV 0.5 wt% S-CNC nanofluids at 90 °C resulted in a 3.4% OOIP increase in oil recovery as a result of log-jamming of S-CNCs in pore throats and flow diversion. Additionally, the sandstone wettability alteration using formation water was crucially important to achieve superior microscopic sweep efficiency. The addition of S-CNCs for wettability alteration increased oil recovery from 51.0% to 69.4%.

4.3. Food Additives

Emulsions, including oil-in-water (O/W) and water-in-oil (W/O), are very popular in the food industry. Conventionally, emulsifiers are used to stabilize small oil or water droplets against coalescence. CNMs show a great potential use as suspending, thickening, gelling, stabilizing agents in some emulsion-based food products, helping maintain their structural stability without dripping and sagging.

The use of UN-NFC to stabilize oils in food was first demonstrated in a large number of emulsion-based food products, e.g., salad dressings, cake frostings, sauces, whipped topping, and gravies.[301] More recent work indicated that plant- or wood-derived NFC also provided superior shape retention performance to the frozen dessert and ice cream in a combination with soy protein isolate (SPI).[302–304] With increase in UN-NFC loading (i.e., decrease in SPI/NFC ratio from 1/0, to 20/1, 15/1, 10/1 and 7/1), the G' of SPI/UN-NFC mixture gradually increased, indicating that the presence of UN-NFC in SPI enhanced the viscoelastic properties (**Figure 15**a1). The viscoelastic properties are relevant to the stabilizing ability, and subsequently the SPI/UN-NFC sample at a ratio of 7/1 was used as an antisagging additive in the ice cream. Melting experimental results demonstrated that the addition of SPI/UN-NFC slowed down the melting rate of ice cream due to the superior water holding and structural stabilizing capacity of NFC (Figure 15a2).

The work on structural stabilizing mechanism of NFC in O/W emulsions revealed that UN-NFC was present as individualized fibrils or/and created stiff networks at the oil/water interface, preventing oil droplets from coalescence.[306] However, the degree of stabilization was strongly dependent on the oil type, NFC characteristics, as well as formulation and condition of the emulsion. The higher the contact between NFC and oil droplets, the higher the yield stress is, leading to superior stabilization. To obtain highly stable emulsions, NFC was further used in combination with biopolymers (e.g., guar gum,[307] and CNCs[308]), and surfactants (e.g., sorbitan monolaurate, glycerol monooleate,[309] and sodium dodecyl sulfate[310]) as costabilizers. The combined use of NFC and other stabilizers resulted in strong steric or electrostatic repulsion forces between oil droplets and hence generated more stable O/W emulsions, as

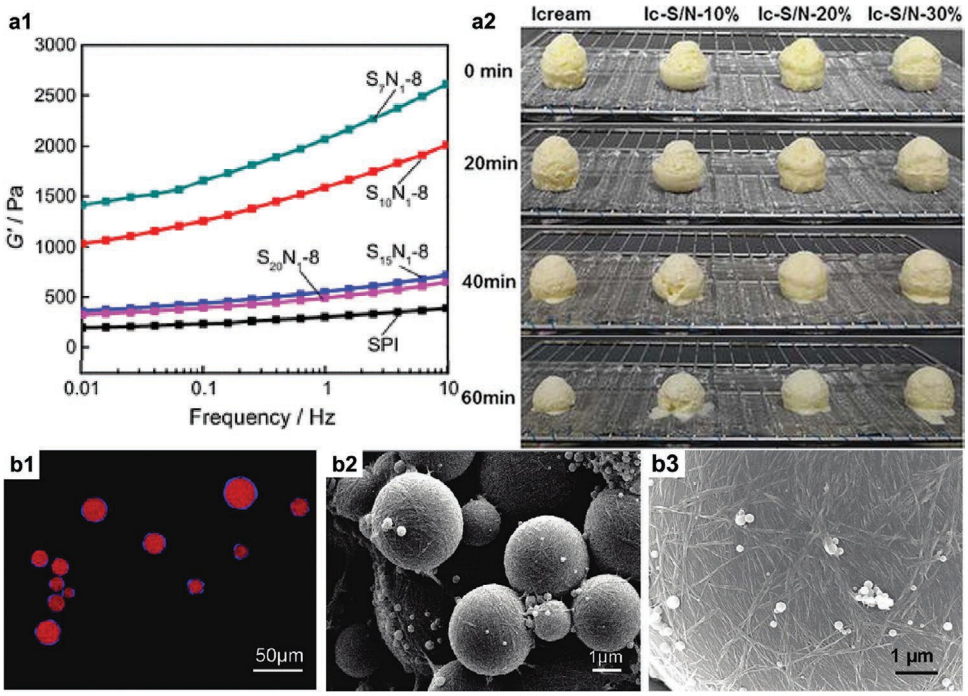

Figure 15. CNMs in food products. a) Stabilization of ice cream using SPI/UN-NFC mixture, where S and N are for SPI and UN-NFC, respectively—a1) *G*′of SPI/UN-NFC mixtures at different ratios (e.g., S_xN_y), and a2) melting phenomena of S_7/N_1-stabilized ice cream at different SPI/UN-NFC loadings from 0 to 30 wt%. Reproduced with permission.[303] Copyright 2015, Springer Nature. b) Stabilization [illegible] laser scanning microscopy image of hexadecane droplets, and b2,b3) SEM image of styrene Pickering [illegible] duced with permission.[305] Copyright 2011, American Chemical Society.

indicated by increases of both viscosity and dynamic modulus. On the other hand, to stabilize the W/O emulsions, NFC was also hydrophobized through silylation with chlorodimethyl isopropylsilane,[306,311] and esterification with organic aids (e.g., acetic acid, hexanoic acid, and dodecanoic acid).[312] Those hydrophobic modifications improved the dispersion state of NFC in the oil phase, leading to better stabilizing ability as well.

Short, rod-shape S-CNCs have been used to stabilize O/W emulsions to form so-called "Pickering emulsions".[305] S-CNCs were shown to accumulate at the oil/water interface to create a steric barrier against the coalescence of oil droplets (Figure 15b). As a result, the S-CNC-stabilized hexadecane/water emulsions exhibited monodispersed oil droplets with an average diameter of around 4 μm, stable for several months. The surface charge density and aspect ratio of S-CNCs played a vital role in the stability of Pickering emulsions.[313,314] S-CNCs with lower surface charge density and higher aspect ratio had the best stabilizing ability. The increase in surface charge density of S-CNCs resulted in enhanced electrostatic repulsion between adjacent S-CNCs, which destabilized the oil/water interface.[313] Desulfonation treatment in alkaline solution and screening the electrostatic repulsion using counter-ions were shown to be two efficient methods to overcome the bottleneck of highly charged S-CNCs. The surfactant-free nature of Pickering emulsions made them very appealing for use in food, cosmetic, personal care, and medical products in which surfactants might have detrimental effects on our human body.

CNC-stabilized Pickering emulsions have been increasingly studied recently with different types of oils and with costabilizers. For inst[illegible]e, CNCs were combined with some water-soluble polyme[illegible]rs (e.g., hydroxyethyl cellulose, methyl cellulose[315] and tan[illegible]ic acid[215]), cationic surfactants (e.g., didecyldimethylammo[illegible]ium bromide, cetyltrimethylammonium bromide,[316] and ethyl lauroyl arginate[317]), ionic surfactants (e.g., sodium dodecyl [illegible]sulfonate[318]) and macromolecular surfactants (e.g., amine-terminated polystyrene[319]) to further enhance their stabilizing ability for long-term storage. The presence of methyl cellulose endowed temperature-responsive viscoelastic properties to S-CNC-stabilized emulsion. At a frequency of 0.1 Hz, the value of *G*′ increased by three orders of magnitude as the temperature was elevated above the cloud point by an amount in the range 50–60 °C.[315] Hydrophobic modification of CNCs was also carried out through grafting of a wide range of small molecules (e.g., lauroyl chloride,[320] isophorone diisocyanate,[321] n-octadecyl isocyanate,[322] alkylamines,[323–325] stearyltrimethylammonium chloride,[326] stearic acid,[327] vinyl acetate and vinyl cinnamate,[328,329] bovine serum albumin,[330] octenyl succinic anhydride,[331] cinnamate,[332] and phenyltrimethyl ammonium chloride[333]), aiming at preparing highly stable emulsions with tiny droplets. The reduction in droplet size helped enhance the bioavailability of the encapsulated ingredients during digestion.[334]

4.4. Coatings

The ability of CNMs to stabilize emulsions makes them highly applicable in coatings. A typical coating is a viscous system,

comprising three components: functional filler, binder, and solvent. The processing and application of aqueous coatings necessitate a high degree of control of flow, and hence the rheological properties must be tuned according to the specific purpose.[335]

4.4.1. Paper Coatings

The suitability of NFC as rheological modifiers in the aqueous coating formulation for paper products has been extensively evaluated, for example, using TO-NFC as rheological modifiers, calcium carbonate, and kaolin as pigments, carboxylic butadiene–styrene latex as synthetic binders, and polyamine polyurea resin as water-resistant agents.[336] The presence of TO-NFC increased the viscosity at low shear rates, but TO-NFC had no obvious influence on viscosity at high shear rates due to the superior shear-thinning behavior of TO-NFC. The enhanced low shear rate viscosity was advantageous for sagging prevention. Meanwhile, stable viscosity at high shear rate ensured their good flowability during the high-speed coating process. As a consequence, with increase in TO-NFC loading in the coating formulation, the coated paper exhibited improved surface strength, smoothness, and air barrier properties. Combined UN-NFC and TO-NFC were used to partially replace CMC in an aqueous paper coating formulations with ground calcium carbonate, kaolin clay, CMC, and styrene acrylic latex.[218,219,337,338] In the system, NFC functioned as a water-binding, gel-forming component rather than as a flocculating and thickening agent, such as CMC. In comparison with CMC-containing coatings, the UN-NFC-containing coatings showed lower viscosity and elasticity, as well as slower network recovery after coating (**Figure 16**a), suggesting that the UN-NFC-containing coatings had a better leveling performance, but worse anti-sagging capacity. To balance the two, the combined use of NFC and CMC in paper coating formulation was studied.[338–340] CMC performed as a dispersing agent for NFC, leading to better water retention and stronger immobilization, which could notably improve the potential for high NFC content and gloss top coating.

The use of CNCs as rheological modifiers in the aqueous coating formulation for paper products has received less attention, probably owing to the relatively low viscosity. For example, the addition of S-CNCs from 0.6 to 1.0 wt% was shown to have no obvious influence on the viscosity of paper coating formulation.[341] However, the relatively low viscosity nature of S-CNCs enables them to be used in the preparation of high-solids content coatings, yielding thick layers on the surface substrates. A sustainable coating system based on 7.5–10 wt% S-CNCs, 1–2.5 wt% montmorillonite or kaolin, 0–2 wt% soy protein and 0–0.2 wt% alkyl ketene dimer was successfully formulated for packaging paper coating.[342] Interestingly, when S-CNCs were partially replaced by clay and other ingredients, the viscosity was lowered, which further offered the possibility of preparing high solid content coatings. Despite the fact that as high as 7.5–10 wt% S-CNCs were applied, uniform distribution and compact packing of fillers were observed from the coated surface, leading to remarkable improvement on liquid/gas barrier properties, stiffness and oil/grease resistance. Liu et al. compared the rheological properties of aqueous coatings containing calcium carbonate, kaolin, starch, and three types of CNCs,

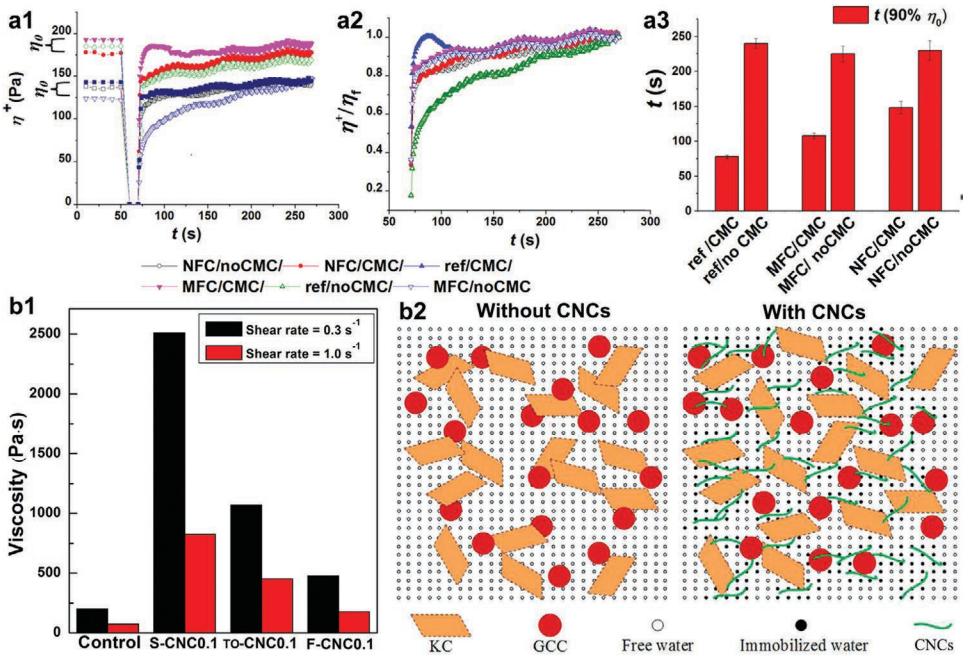

Figure 16. CNMs in paper coatings. a) UN-NFC as rheological modifiers in paper coatings—a1) transient viscosity curves as a function of time, a2) reduced transient curves as a function of time, and a3) time required for 90% recovery in transient viscosity in the third interval low shear regime after high shear in the second interval, to the initial dynamic viscosity. a) Reproduced with permission.[219] Copyright 2014, Degruyter. b) CNCs as rheological modifiers in paper coatings—b1) viscosity of control (coating + 0.4 pph CMC), S-CNC0.1 (coating + 0.1 pph SCNCs), TO-CNC0.1 (coating + 0.1 pph TO-CNC) and F-CNC0.1 (coating + 0.1 pph F-CNCs), and b2) proposed surface interaction among different components in coatings without and with CNCs. b) Reproduced with permission.[343] Copyright 2017, American Chemical Society.

i.e., S-CNCs, TO-CNCs and formic acid-hydrolyzed CNCs (F-CNCs).[343] The length of CNCs increased in the following order: S-CNCs<TO-CNCs<F-CNCs; whereas their surface charge density increased in the opposite order: F-CNCs<TO- CNCs<S-CNCs. These differences led to distinctive rheo- logical properties of their suspensions and coatings. Among them, the S-CNC-containing coating showed the highest vis- cosity (Figure 16b1), which could be ascribed to the formation of strong surface interaction among S-CNCs, clay, and water molecules (Figure 16b2). This result highlights that effects of the surface chemistry of CNCs are predominant in the rheological modification of coatings over the dimension of CNCs.

4.4.2. Wood Coatings

The main component in wood coatings is polymeric binder, e.g., acrylates, polyurethanes, alkyds (oil-modified polyester resins), and epoxies.[344] Considering the environmental effects, waterborne polymer emulsions (e.g., water-based acrylic resin and water-based polyurethane) are preferred. Among the published work, the influence of UN-NFC on the viscosity of four commercially available binders in form of acrylate polymer emulsions was studied.[104] The viscosity of UN-NFC/acrylate mixture was shown to be dominated by UN-NFC, and the type of acrylate polymer emulsions had little impact (**Figure 17**a). The resultant UN-NFC/polymer composite films showed higher tensile strength and Young's modulus but lower elongation at break than neat acrylate films.[344] However, the mechanical properties of both neat acrylate and composite films were deteriorated after aging through artificial weathering. To overcome this weathering issue, inorganic UV absorbers (ZnO nanoparticles) were included.[345] In the developed coating system, UN-NFC not only functioned as rheological modifiers, but also acted as stabilizers, which prevented ZnO nanoparticles from agglomeration. Artificial weathering experimental results confirmed that the weathering resistance of UN-NFC/acrylate coating was improved as more ZnO nanoparticles were added (Figure 17b). The dimension and surface chemistry of CNMs play an important role in the rheology of aqueous coating as well as final performance of dried film.[107,346] TO-NFC and TO-MCC with larger dimensions and higher aspect ratio improved the viscosity and dynamic properties of acrylic resin more effectively than S-CNCs and TO-CNCs, demonstrating the possibility to tune the flowability of coatings through controlling the dimension and surface chemistry of CNMs.[107] Surface modification of UN-NFC with γ-aminopropyltriethoxysilane (APS) was shown to result in significant improvement in the $G'$of UN-NFC/acrylate/polyurethane copolymer emulsion, leading to improvement in light transmittance and mechanical performance of coating film.[346]

The improved rheology of waterborne polymer coatings by CNMs is advantageous for the prevention of settling, syneresis and dripping, which usually take place in neat waterborne coatings. For example, a comparative investigation on the accelerated stability of acrylic based exterior flat paints containing UN-NFC and HEC was performed over 2 weeks at 49 °C. In comparison with HEC, UN-NFC prevented settling and syneresis problems more effectively, leading to more homogenous distribution (Figure 17c1).[285] UN-NFC additions avoided the dripping problems of coatings due to the high viscosity at rest and superior thixotropic property of UN-NFC (Figure 17c2).

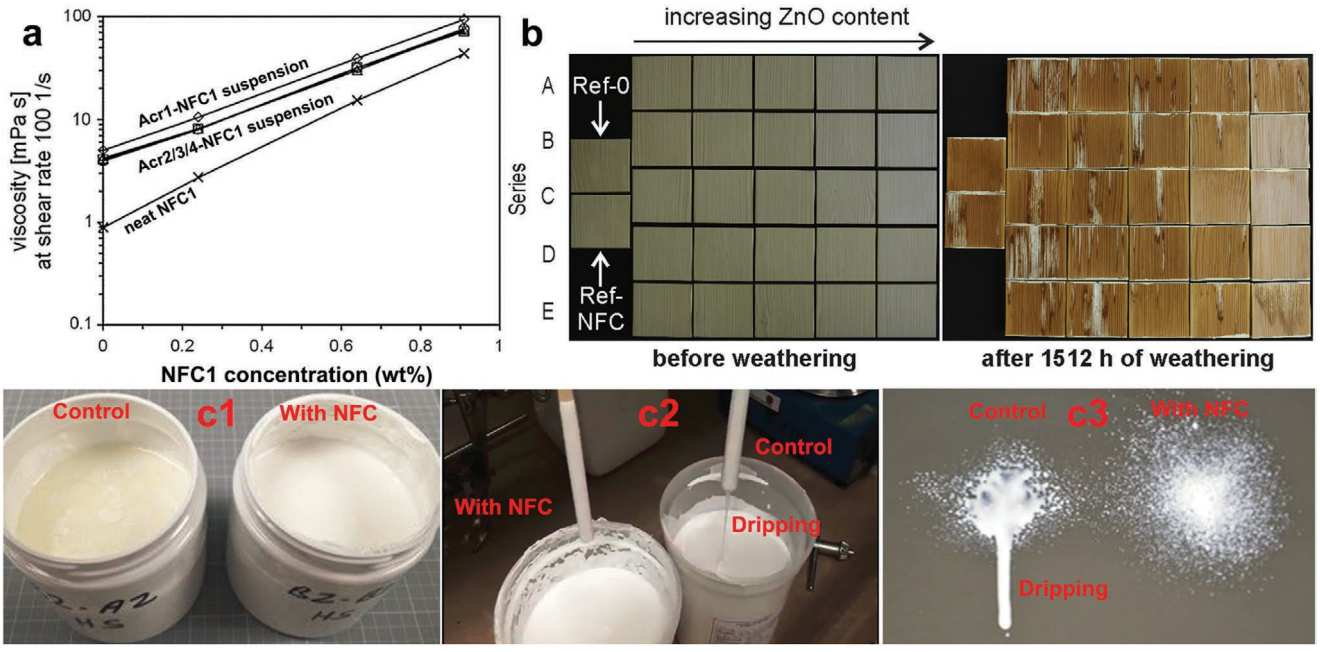

Figure 17. CNMs in wood coatings, cosmetics and personal care products. a) Viscosity of UN-NFC/acrylate emulsions as functions of UN-NFC concentration and type of acrylate. Reproduced with permission.[104] Copyright 2014, Springer Nature. b) Photographs of wood specimens coated with UN-NFC/acrylate emulsion without and with ZnO nanoparticles before and after weathering. Reproduced with permission.[345] Copyright 2015, Elsevier. c) UN-NFC (Exilva, Borregaard) as stabilizers in: c1) acrylic based exterior flat paint, as well as c2) anti-dripping agents in coating and c3) sprayable sunscreen. c) Reproduced with permission.[285] Copyright 2017, EXILVA.

Similar results were seen with regenerated CNMs from wood pulp and MCC to control the sagging phenomena of water-borne acrylic latex after spraying.[347]

4.4.3. Polymer Coatings

Functional polymer coatings are prevailing in many industrial sectors from packaging materials to electronics. A roll-to-roll manufacturing process to coat S-CNCs and S-CNC/PVA suspensions on the surface of polyester films produced superior gas barrier films for food packaging applications.[348,349] The viscosity of the coating system had a significant influence on the defect formation in the system. A good balance between S-CNC concentration, roller speed and web speed is needed to obtain defect-free coatings. Furthermore, the alignment of S-CNCs in dried films was dependent on the viscosity of the coating system. Screen printing and bar coating techniques were used to coat TO-NFC/silver nanowire suspension on the surface of polyester films, producing conductive films for electronic devices.[350,351] TO-NFC functioned as thickening and stabilizing agents for silver nanowire suspensions. The presence of 1 wt% TO-NFC in 1 wt% silver nanowire suspension led to 100-fold increase in viscosity at a low shear rate of 0.1 s^{-1}, which fulfilled the rheology requirements for screen printing. TO-NFC also provided better stability for silver nanowire suspensions, preventing the nanowires from aggregation and reorganization and leading to superior electric conductivity.

4.5. Cosmetics and Personal Care Products

CNMs show great potential in cosmetics and personal care products (e.g., toothpaste, sunscreen, shampoo, lotion, conditioner, lipstick, nail polish, and mascara) for enhanced processabilty, performance and customer's acceptance. CNMs with high viscosity at rest, high shear-thinning behavior, and strong thixotropic properties can be used as natural thickeners in the formulation of these products.[352] For instance, UN-NFC was successfully used as thickeners in a sprayable sunscreen formulation containing TiO_2 pigment. The presence of only 0.3% UN-NFC in the formation not only helped spray a larger area more evenly, but also effectively avoided the dripping issue (Figure 17c3).[285] Additionally, because of its elastic fiber network, UN-NFC can provide better skin feel compared with conventional stabilizers, which usually give sticky texture and skin feel. CNMs are also good stabilizers to entrap the oil droplets from coalescence and suspend the oil droplets from sedimentation. In addition, they can function as dispersants to aid in wetting out the pigments, to stabilize the pigments from agglomerates, and to inhibit settling, leading to more economic use of pigments in the formulation of lipstick, nail polish and mascara.

5. Conclusions and Perspectives

CNMs have emerged as effective rheological modifiers for fluids and gel-based applications. CNM's widely tailorable viscosity, high viscosity at rest, profound shear-thinning and thixotropic properties, high water retention capacity, and superior ability to stabilize emulsions are essential attributes for rheological modification. However, CNMs present a wide spectrum of particle morphologies, properties and surface chemistries, which affect the rheology, colloidal behavior and self-assembly of CNMs. It is thus essential to have a comprehensive and accurate characterization of the CNMs prior to their use.

The flocculation of NFC, the lyotropic phase of CNCs, and their shear-induced orientation are critically relevant for CNMs' rheological behaviors. Additionally, rheological properties of CNMs are influenced by test protocols (e.g., rheometer geometry, shear rate, and time), their inherent properties (e.g., concentration, morphology, and surface characteristics), suspension environments (e.g., ionic strength, pH, temperature, magnetic and electric strength, and water-soluble polymer interactions), and post processing (i.e., drying and redispersion). Recent advances in establishing quantitative understanding of these parameters have led to a variety of applications of CNMs. These applications include: i) multicomponent ink formulation for 3D printing of biomedical, electronic and other emerging devices; ii) fluid formation for drilling oil and gas wells as well as enhanced oil recovery; iii) cement formulation for stabilizing oil wells and construction through enhancing yield stresses, preventing segregation and bleeding phenomena without affecting the workability; iv) food ingredients as suspending, thickening and gelling agents; and v) compositions for coatings, cosmetics, and personal care products as thickening agents.

Although significant developments have been made using CNMs as rheological modifiers, limitations still exist that tend to prevent their widespread use in applications. These limitations include: i) high costs for as-made suspensions (e.g., production, drying, shipping, and storage); ii) high material variability in size, shape, surface chemistry, and composition; iii) strong process influence of CNM's rheology (e.g., ionic strength, pH, and temperature); and iv) unknown long-term risk to humans and ecosystems. As a consequence, the following efforts should be made for future development in this field: i) thorough-characterization of CNMs[353] prior to their rheological application; ii) increased use of industrially made CNMs for academic research to help better understand and improve the quality of commercial CNMs; iii) combined use of CNMs with other water-soluble polymers for enhanced processability (i.e., drying and redispersion) and functionalities; iv) understanding of long-term safety and regulating issues to minimize potential hidden risks; and v) development and improvement of test standards for CNMs. Overall, the potential of CNMs as rheological modifiers has not been completely explored yet, and there are still large opportunities in this area. We anticipate that the present review helps boost future research and development related to rheological modification using CNMs in a broader range of industrial sectors, leading to new fluid/material advances in the near future.

Acknowledgements

The authors acknowledge financial support from U.S. Endowment and USDA Forest Service [E17-23, United States], Louisiana Board of Regents

[LEQSF(2020-23)-RD-B-02, United States], Jiangsu Agriculture Science and Technology Innovation Fund [CX(20)3054, China], and Jiangsu Specially-Appointed Professor Program (Nanjing, China).

Conflict of Interest

The authors declare no conflict of interest.

Keywords

cellulose nanocrystals, cellulose nanomaterials, fluid application, nanofibrillated cellulose, rheology

Received: September 4, 2020
Revised: November 1, 2020
Published online:

[1] M. M. Falinski, D. L. Plata, S. S. Chopra, T. L. Theis, L. M. Gilbertson, J. B. Zimmerman, *Nat. Nanotechnol.* **2018**, *13*, 708.
[2] F. Jiang, T. Li, Y. Li, Y. Zhang, A. Gong, J. Dai, E. Hitz, W. Luo, L. Hu, *Adv. Mater.* **2018**, *30*, 1703453.
[3] R. J. Moon, A. Martini, J. Nairn, J. Simonsen, J. Youngblood, *Chem. Soc. Rev.* **2011**, *40*, 3941.
[4] Y. Habibi, L. A. Lucia, O. J. Rojas, *Chem. Rev.* **2010**, *110*, 3479.
[5] Y. Habibi, *Chem. Soc. Rev.* **2014**, *43*, 1519.
[6] F. Rol, M. N. Belgacem, A. Gandini, J. Bras, *Prog. Polym. Sci.* **2019**, *88*, 241.
[7] K. Heise, G. Delepierre, A. King, M. Kostiainen, J. Zoppe, C. Weder, E. Kontturi, *Angew. Chem., Int. Ed.* **2021**, *60*, 66.
[8] H. Kargarzadeh, J. Huang, N. Lin, I. Ahmad, M. Mariano, A. Dufresne, S. Thomas, A. Gałęski, *Prog. Polym. Sci.* **2018**, *87*, 197.
[9] C. M. Clarkson, S. M. El Awad Azrak, E. S. Forti, G. T. Schueneman, R. J. Moon, J. P. Youngblood, *Adv. Mater.* **2020**, online, 2000718.
[10] K. J. De France, K. G. Yager, K. J. W. Chan, B. Corbett, E. D. Cranston, T. Hoare, *Nano Lett.* **2017**, *17*, 6487.
[11] R. Ajdary, B. L. Tardy, B. D. Mattos, L. Bai, O. J. Rojas, *Adv. Mater.* https://doi.org/10.1002/adma.2001085.
[12] A. W. Carpenter, C.-F. de Lannoy, M. R. Wiesner, *Environ. Sci. Technol.* **2015**, *49*, 5277.
[13] C. Gómez H., A. Serpa, J. Velásquez-Cock, P. Gañán, C. Castro, L. Vélez, R. Zuluaga, *Food Hydrocolloids* **2016**, *57*, 178.
[14] H. M. C. Azeredo, M. F. Rosa, L. H. C. Mattoso, *Ind. Crops Prod.* **2017**, *97*, 664.
[15] M. Kaushik, A. Moores, *Green Chem.* **2016**, *18*, 622.
[16] G. R. Meseck, A. S. Terpstra, M. J. MacLachlan, *Curr. Opin. Colloid Interface Sci.* **2017**, *29*, 9.
[17] D. Zhao, Y. Zhu, W. Cheng, W. Chen, Y. Wu, H. Yu, *Adv. Mater.* https://doi.org/10.1002/adma.202000619.
[18] H. Zhu, W. Luo, P. N. Ciesielski, Z. Fang, J. Y. Zhu, G. Henriksson, M. E. Himmel, L. Hu, *Chem. Rev.* **2016**, *116*, 9305.
[19] X. Du, Z. Zhang, W. Liu, Y. Deng, *Nano Energy* **2017**, *35*, 299.
[20] W. Chen, H. Yu, S.-Y. Lee, T. Wei, J. Li, Z. Fan, *Chem. Soc. Rev.* **2018**, *47*, 2837.
[21] H. Oguzlu, C. Danumah, Y. Boluk, *Curr. Opin. Colloid Interface Sci.* **2017**, *29*, 46.
[22] O. Nechyporchuk, M. N. Belgacem, F. Pignon, *Biomacromolecules* **2016**, *17*, 2311.
[23] M. A. Hubbe, P. Tayeb, M. Joyce, P. Tyagi, M. Kehoe, K. Dimic-Misic, L. Pal, *BioResources* **2017**, *12*, 9556.
[24] A. García, A. Gandini, J. Labidi, N. Belgacem, J. Bras, *Ind. Crops Prod.* **2016**, *93*, 26.
[25] M. Jonoobi, R. Oladi, Y. Davoudpour, K. Oksman, A. Dufresne, Y. Hamzeh, R. Davoodi, *Cellulose* **2015**, *22*, 935.
[26] D. Trache, M. H. Hussin, M. K. M. Haafiz, V. K. Thakur, *Nanoscale* **2017**, *9*, 1763.
[27] O. Nechyporchuk, M. N. Belgacem, J. Bras, *Ind. Crops Prod.* **2016**, *93*, 2.
[28] R. J. Moon, G. T. Schueneman, J. Simonsen, *JOM* **2016**, *68*, 2383.
[29] L. Brinchi, F. Cotana, E. Fortunati, J. M. Kenny, *Carbohydr. Polym.* **2013**, *94*, 154.
[30] ISO, Standard Terms and Their Definitions for Cellulose Nanomaterials (ISO/AWI TS 20477 Nanotechnologies, Underdevelopement), **2017**, https://www.iso.org/standard/68153.html, (accessed: November 2020).
[31] H. P. S. Abdul Khalil, Y. Davoudpour, M. N. Islam, A. Mustapha, K. Sudesh, R. Dungani, M. Jawaid, *Carbohydr. Polym.* **2014**, *99*, 649.
[32] I. Siró, D. Plackett, *Cellulose* **2010**, *17*, 459.
[33] N. Chen, J. Y. Zhu, Z. Tong, *Cellulose* **2016**, *23*, 2573.
[34] F. Martoïa, C. Perge, P. J. J. Dumont, L. Orgéas, M. A. Fardin, S. Manneville, M. N. Belgacem, *Soft Matter* **2015**, *11*, 4742.
[35] A. Naderi, T. Lindström, J. Sundström, G. Flodberg, J. Erlandsson, *Nord. Pulp Pap. Res. J.* **2016**, *31*, 364.
[36] J. Desmaisons, E. Boutonnet, M. Rueff, A. Dufresne, J. Bras, *Carbohydr. Polym.* **2017**, *174*, 318.
[37] H. Kangas, P. Lahtinen, A. Sneck, A.-M. Saariaho, O. Laitinen, E. Hellen, *Nord. Pulp Pap. Res. J.* **2014**, *29*, 129.
[38] G. Henriksson, A. Nutt, H. Henriksson, B. Pettersson, J. Ståhlberg, G. Johansson, G. Pettersson, *Eur. J. Biochem.* **1999**, *259*, 88.
[39] T. Saito, S. Kimura, Y. Nishiyama, A. Isogai, *Biomacromolecules* **2007**, *8*, 2485.
[40] M. Jonoobi, J. Harun, M. Mishra, K. Oksman, *BioResources* **2009**, *4*, 626.
[41] I. A. Sacui, R. C. Nieuwendaal, D. J. Burnett, S. J. Stranick, M. Jorfi, C. Weder, E. J. Foster, R. T. Olsson, J. W. Gilman, *ACS Appl. Mater. Interfaces* **2014**, *6*, 6127.
[42] L. Chen, Q. Wang, K. Hirth, C. Baez, U. P. Agarwal, J. Y. Zhu, *Cellulose* **2015**, *22*, 1753.
[43] D. Bondeson, A. Mathew, K. Oksman, *Cellulose* **2006**, *13*, 171.
[44] S. Beck-Candanedo, M. Roman, D. G. Gray, *Biomacromolecules* **2005**, *6*, 1048.
[45] S. Dong, M. J. Bortner, M. Roman, *Ind. Crops Prod.* **2016**, *93*, 76.
[46] M. Roman, W. T. Winter, *Biomacromolecules* **2004**, *5*, 1671.
[47] S. C. Espinosa, T. K... **2013**, *14*, 1223.
[48] Y. Habibi, A.-L. Go... A. Dufresne, *J. Mate...*
[49] L. Zhou, H. He, M.-... *Polym.* **2016**, *153*, 4...
[50] A. Osorio-Madraz..., M. Eder, M. Rueggeberg, J. K. Pandey, M. J. Harrington, Y. ... Nishiyama, J.-L. Putaux, C. Rochas, I. Burgert, *Biomacromolecules* **2012**, *13*, 850.
[51] S. Elazzouzi-Hafraoui, Y. Nishiyama, J.-L. Putaux, L. Heux, F. Dubreuil, C. Rochas, *Biomacromolecules* **2007**, *9*, 57.
[52] K. Hyun, M. Wilhelm, C. O. Klein, K. S. Cho, J. G. Nam, K. H. Ahn, S. J. Lee, R. H. Ewoldt, G. H. McKinley, *Prog. Polym. Sci.* **2011**, *36*, 1697.
[53] A. Abbasi Moud, M. Kamkar, A. Sanati-Nezhad, S. H. Hejazi, U. Sundararaj, *Cellulose* **2020**, *27*, 5729.
[54] M. Danesh, D. Mauran, S. Hojabr, R. Berry, M. Pawlik, S. G. Hatzikiriakos, *Phys. Fluids* **2020**, *32*, 093103.
[55] E. C. Bingham, *An Investigation of the Laws of Plastic Flow*, US Government Printing Office, Washington D.C., USA **1917**.
[56] G. W. Govier, K. Aziz, *The Flow of Complex Mixtures in Pipes*, Van Nostrand Reinhold Company, New York **1972**.
[57] N. Casson, in *Rheology of Disperse Systems* (Ed: C. C. Mill), Pergamon Press, London, UK **1959**, p. 84.

[58] W. H. Herschel, R. Bulkley, *Kolloid-Z.* **1926**, *39*, 291.
[59] A. W. Sisko, *Ind. Eng. Chem.* **1958**, *50*, 1789.
[60] W. Heinz, *Mater. Prüfung* **1959**, *1*, 311.
[61] S. Mizrahi, Z. Berk, *J. Texture Stud.* **1972**, *3*, 69.
[62] R. E. Robertson, H. A. Stiff Jr., *Soc. Pet. Eng. J.* **1976**, *16*, 31.
[63] J. J. Vocadlo, M. Moo Young, *Can. Inst. Food Technol. J.* **1969**, *2*, 137.
[64] W. Vom Berg, *Mag. Concr. Res.* **1979**, *31*, 211.
[65] S. B. Ellis, *Thesis. Lafayette College, Easton, PA, USA; cited in: R. S. Brodkey, The Phenomena of Fluid Motions*, Courier Corporation, Chelmsford, MA, USA **1995**.
[66] L. Onsager, *Phys. Rev.* **1932**, *40*, 1028.
[67] R. Simha, *J. Phys. Chem.* **1940**, *44*, 25.
[68] G. K. Batchelor, *J. Fluid Mech.* **1970**, *44*, 419.
[69] A. M. Wierenga, A. P. Philipse, *Colloids Surf., A* **1998**, *137*, 355.
[70] I. M. Krieger, T. J. Dougherty, *Trans. Soc. Rheol.* **1959**, *3*, 137.
[71] A. Celzard, V. Fierro, R. Kerekes, *Cellulose* **2009**, *16*, 983.
[72] M.-C. Li, Q. Wu, K. Song, S. Lee, Y. Qing, Y. Wu, *ACS Sustainable Chem. Eng.* **2015**, 3, 821.
[73] E. Lasseuguette, D. Roux, Y. Nishiyama, *Cellulose* **2008**, *15*, 425.
[74] A. Karppinen, A.-H. Vesterinen, T. Saarinen, P. Pietikäinen, J. Seppälä, *Cellulose* **2011**, *18*, 1381.
[75] G. C. Ciftci, P. A. Larsson, A. V Riazanova, H. H. Øvrebø, L. Wågberg, L. A. Berglund, *Cellulose* **2020**, *27*, 9227.
[76] G. Lenfant, M.-C. Heuzey, T. G. M. van de Ven, P. J. Carreau, *Rheol. Acta* **2017**, *56*, 51.
[77] M.-C. Li, Q. Wu, K. Song, Y. Qing, Y. Wu, *ACS Appl. Mater. Interfaces* **2015**, *7*, 5006.
[78] M.-C. Li, Q. Wu, K. Song, C. F. De Hoop, S. Lee, Y. Qing, Y. Wu, *Ind. Eng. Chem. Res.* **2016**, *55*, 133.
[79] X. Sun, Q. Wu, S. Lee, Y. Qing, Y. Wu, *Sci. Rep.* **2016**, *6*, 31654.
[80] B. P. Sutliff, A. Das, J. Youngblood, M. J. Bortner, *Carbohydr. Polym.* **2020**, *231*, 115735.
[81] M. Bercea, P. Navard, *Macromolecules* **2000**, *33*, 6011.
[82] Y. Boluk, R. Lahiji, L. Zhao, M. T. McDermott, *Colloids Surf., A* **2011**, *377*, 297.
[83] J. Araki, M. Wada, S. Kuga, T. Okano, *Colloids Surf., A* **1998**, *142*, 75.
[84] S. Iwamoto, S. Lee, T. Endo, *Polym. J.* **2013**, *46*, 73.
[85] Q. Wu, X. Li, S. Fu, Q. Li, S. Wang, *Cellulose* **2017**, *24*, 3255.
[86] T. Sato, A. Teramoto, *Macromolecules* **1991**, *24*, 193.
[87] A. Lu, U. Hemraz, Z. Khalili, Y. Boluk, *Cellulose* **2014**, *21*, 1239.
[88] B. Peng, J. Tang, P. Wang, J. Luo, P. Xiao, Y. Lin, K. C. Tam, *Cellulose* **2018**, *25*, 3229.
[89] E. Saarikoski, T. Saarinen, J. Salmela, J. Seppälä, *Cellulose* **2012**, *19*, 647.
[90] A. Karppinen, T. Saarinen, J. Salmela, A. Laukkanen, M. Nuopponen, J. Seppälä, *Cellulose* **2012**, *19*, 1807.
[91] T. Saarinen, S. Haavisto, A. Sorvari, J. Salmela, J. Seppälä, *Cellulose* **2014**, *21*, 1261.
[92] A. I. Koponen, J. Lauri, S. Haavisto, T. Fabritius, *Appl. Sci.* **2018**, 8, 755.
[93] D. W. De Kort, S. J. Veen, H. Van As, D. Bonn, K. P. Velikov, J. P. M. Van Duynhoven, *Soft Matter* **2016**, *12*, 4739.
[94] E. E. Ureña-Benavides, G. Ao, V. A. Davis, C. L. Kitchens, *Macromolecules* **2011**, *44*, 8990.
[95] X. M. Dong, T. Kimura, J.-F. Revol, D. G. Gray, *Langmuir* **1996**, *12*, 2076.
[96] T. Ebeling, M. Paillet, R. Borsali, O. Diat, A. Dufresne, J.-Y. Cavaillé, H. Chanzy, *Langmuir* **1999**, *15*, 6123.
[97] W. J. Orts, L. Godbout, R. H. Marchessault, J.-F. Revol, *Macromolecules* **1998**, *31*, 5717.
[98] H.-N. Xu, Y.-Y. Tang, X.-K. Ouyang, *Langmuir* **2016**, *33*, 235.
[99] N. Yoshiharu, K. Shigenori, W. Masahisa, O. Takeshi, *Macromolecules* **1997**, *30*, 6395.
[100] S. Shafiei-Sabet, W. Y. Hamad, S. G. Hatzikiriakos, *Langmuir* **2012**, *28*, 17124.
[101] T. Saarinen, M. Lille, J. Seppälä, *Annu. Trans. – Nord. Rheol. Soc.* **2009**, *17*, 121.
[102] O. Nechyporchuk, M. N. Belgacem, F. Pignon, *Cellulose* **2015**, *22*, 2197.
[103] S. Shafiei-Sabet, W. Y. Hamad, S. G. Hatzikiriakos, *Cellulose* **2014**, *21*, 3347.
[104] F. Grüneberger, T. Künniger, T. Zimmermann, M. Arnold, *Cellulose* **2014**, *21*, 1313.
[105] Q. Wu, Y. Meng, S. Wang, Y. Li, S. Fu, L. Ma, D. Harper, *J. Appl. Polym. Sci.* **2014**, 131, 76.
[106] Y. Xu, A. D. Atrens, J. R. Stokes, *J. Colloid Interface Sci.* **2017**, *496*, 130.
[107] L. Du, T. Zhong, M. P. Wolcott, Y. Zhang, C. Qi, B. Zhao, J. Wang, Z. Yu, *Cellulose* **2018**, *25*, 2435.
[108] T. Moberg, K. Sahlin, K. Yao, S. Geng, G. Westman, Q. Zhou, K. Oksman, M. Rigdahl, *Cellulose* **2017**, *24*, 2499.
[109] H. A. Barnes, *J. Non-Newtonian Fluid Mech.* **1995**, *56*, 221.
[110] S. S. Vadodaria, A. J. Onyianta, D. Sun, *Cellulose* **2018**, *25*, 5535.
[111] O. Nechyporchuk, M. N. Belgacem, F. Pignon, *Carbohydr. Polym.* **2014**, *112*, 432.
[112] M. Schenker, J. Schoelkopf, P. Gane, P. Mangin, *Cellulose* **2018**, *25*, 961.
[113] M. Iotti, Ø. W. Gregersen, S. Moe, M. Lenes, *J. Polym. Environ.* **2011**, *19*, 137.
[114] P. Rezayati Charani, M. Dehghani-Firouzabadi, E. Afra, A. Shakeri, *Cellulose* **2013**, *20*, 727.
[115] M. Mohtaschemi, K. Dimic-Misic, A. Puisto, M. Korhonen, T. Maloney, J. Paltakari, M. J. Alava, *Cellulose* **2014**, *21*, 1305.
[116] A. Naderi, T. Lindström, in *Cellulose and Cellulose Derivatives: Synthesis, Modification and Applications* (Ed: M. I. H. Mondal), Nova Science Publishers, Inc.,, Hauppauge, New York **2015**, p. 187.
[117] M. Pääkkö, M. Ankerfors, H. Kosonen, A. Nykänen, S. Ahola, M. Österberg, J. Ruokolainen, J. Laine, P. T. Larsson, O. Ikkala, T. Lindström, *Biomacromolecules* **2007**, *8*, 1934.
[118] G. Agoda-Tandjawa, S. Durand, S. Berot, C. Blassel, C. Gaillard, C. Garnier, J.-L. Doublier, *Carbohydr. Polym.* **2010**, *80*, 677.
[119] T. Saito, T. Uematsu, S. Kimura, T. Enomae, A. Isogai, *Soft Matter* **2011**, *7*, 8804.
[120] R. Tanaka, T. Saito, T. Hänninen, Y. Ono, M. Hakalahti, T. Tammelin, A. Isogai, *Biomacromolecules* **2016**, *17*, 2104.
[121] N. Quennouz, S. M. Hashmi, H. S. Choi, J. W. Kim, C. O. Osuji, *Soft Matter* **2016**, *12*, 157.
[122] L. Jowkarderis, T. G. M. van de Ven, *Carbohydr. Polym.* **2015**, *123*, 416.
[123] M. J. Lundahl, M. Berta, M. Ago, M. Stading, O. J. Rojas, *Eur. Polym. J.* **2018**, *109*, 367.
[124] B. Wei, Q. Li, F. Jin, H. Li, C. Wang, *Energy Fuels* **2016**, *30*, 2882.
[125] A. Naderi, T. Lindström, J. Sundström, *Cellulose* **2014**, *21*, 1561.
[126] A. Naderi, T. Lindström, T. Pettersson, *Cellulose* **2014**, *21*, 2357.
[127] A. D. Haywood, V. A. Davis, *Cellulose* **2017**, *24*, 705.
[128] C. Qiao, G. Chen, J. Zhang, J. Yao, *Food Hydrocolloids* **2016**, *55*, 19.
[129] S. Onogi, T. Asada, in *Rheology*, (Eds: G. Astarita, G. Marrucci, L. Nicholais), Springer, New York **1980**, pp. 127–147.
[130] J. Li, J.-F. Revol, R. H. Marchessault, *J. Colloid Interface Sci.* **1996**, *183*, 365.
[131] R. L. Shogren, S. C. Peterson, K. O. Evans, J. A. Kenar, *Carbohydr. Polym.* **2011**, *86*, 1351.
[132] F. Bettaieb, O. Nechyporchuk, R. Khiari, M. F. Mhenni, A. Dufresne, M. N. Belgacem, *Carbohydr. Polym.* **2015**, *134*, 664.
[133] T. Abitbol, D. Kam, Y. Levi-Kalisman, D. G. Gray, O. Shoseyov, *Langmuir* **2018**, *34*, 3925.
[134] A. Lu, Y. Wang, Y. Boluk, *Carbohydr. Polym.* **2014**, *105*, 214.
[135] H. Liimatainen, M. Visanko, J. A. Sirviö, O. E. O. Hormi, J. Niinimaki, *Biomacromolecules* **2012**, *13*, 1592.
[136] H. Liimatainen, M. Visanko, J. Sirviö, O. Hormi, J. Niinimäki, *Cellulose* **2013**, *20*, 741.

[137] C. Eyholzer, A. Borges de Couraça, F. Duc, P. E. Bourban, P. Tingaut, T. Zimmermann, J. A. E. Månson, K. Oksman, *Biomacromolecules* **2011**, *12*, 1419.
[138] J. Araki, M. Wada, S. Kuga, T. Okano, *J. Wood Sci.* **1999**, *45*, 258.
[139] S. Shafeiei-Sabet, W. Hamad, S. Hatzikiriakos, *Rheol. Acta* **2013**, *52*, 741.
[140] M. Hasani, E. D. Cranston, G. Westman, D. G. Gray, *Soft Matter* **2008**, *4*, 2238.
[141] M.-C. Li, C. Mei, X. Xu, S. Lee, Q. Wu, *Polymer* **2016**, *107*, 200.
[142] L. Lewis, M. Derakhshandeh, S. G. Hatzikiriakos, W. Y. Hamad, M. J. MacLachlan, *Biomacromolecules* **2016**, *17*, 2747.
[143] T. Abitbol, H. Marway, E. D. Cranston, *Nord. Pulp Pap. Res. J.* **2014**, *29*, 46.
[144] R. Nigmatullin, R. Harniman, V. Gabrielli, J. C. Muñoz-García, Y. Z. Khimyak, J. Angulo, S. J. Eichhorn, *ACS Appl. Mater. Interfaces* **2018**, *10*, 19318.
[145] U. D. Hemraz, A. Lu, R. Sunasee, Y. Boluk, *J. Colloid Interface Sci.* **2014**, *430*, 157.
[146] F. Azzam, E. Siqueira, S. Fort, R. Hassaini, F. Pignon, C. Travelet, J.-L. Putaux, B. Jean, *Biomacromolecules* **2016**, *17*, 2112.
[147] J. Zhang, Q. Wu, M.-C. Li, K. Song, X. Sun, S.-Y. Lee, T. Lei, *ACS Sustainable Chem. Eng.* **2017**, *5*, 7439.
[148] J. R. McKee, S. Hietala, J. Seitsonen, J. Laine, E. Kontturi, O. Ikkala, *ACS Macro Lett.* **2014**, *3*, 266.
[149] X. Zhang, J. Zhang, L. Dong, S. Ren, Q. Wu, T. Lei, *Cellulose* **2017**, *24*, 4189.
[150] J. O. Zoppe, N. C. Ataman, P. Mocny, J. Wang, J. Moraes,H.-A. Klok, *Chem. Rev.* **2017**, *117*, 1105.
[151] B. V. Derjaguin, *USSR* **1941**, *14*, 633.
[152] J. H. Adair, E. Suvaci, J. Sindel, in *Encyclopedia of Materials* (Eds: K. H. J. Buschow, R. W. Cahn, M. C. Flemings, B. Ilschner, E. J. Kramer, S. Mahajan), Elsevier, Oxford, UK **2001**, pp. 1–10.
[153] E. Dinand, H. Chanzy, R. M. Vignon, *Food Hydrocolloids* **1999**, *13*, 275.
[154] K. Sim, J. Lee, H. Lee, H. J. Youn, *Cellulose* **2015**, *22*, 3689.
[155] Why does Microfibrillated Cellulose Tolerate Salts so Well? https://blog.exilva.com/why-does-microfibrillated-cellulose-tolerate-salts-so-well, (accessed: November 2020).
[156] M.-P. Lowys, J. Desbrières, M. Rinaudo, *Food Hydrocolloids* **2001**, *15*, 25.
[157] A. Naderi, T. Lindström, *Cellulose* **2014**, *21*, 3507.
[158] L. Jowkarderis, T. G. M. van de Ven, *Cellulose* **2014**, *21*, 2511.
[159] T. Moberg, M. Rigdahl, M. Stading, E. Levenstam Bragd, *Carbohydr. Polym.* **2014**, *102*, 409.
[160] H. Fukuzumi, R. Tanaka, T. Saito, A. Isogai, *Cellulose* **2014**, *21*, 1553.
[161] L. Geng, A. Naderi, Y. Mao, C. Zhan, P. Sharma, X. Peng, B. S. Hsiao, in *Nanocelluloses: Their Preparation, Properties, and Applications*, (Eds: U. P. Agarwal, R. H. Atalla, A. Isogai), American Chemical Society, Washington, DC, USA **2017**, pp. 113–132, SE-6.
[162] H. Dong, J. F. Snyder, K. S. Williams, J. W. Andzelm, *Biomacromolecules* **2013**, *14*, 3338.
[163] E. González-Labrada, D. G. Gray, *Cellulose* **2012**, *19*, 1557.
[164] G. Lenfant, M. C. Heuzey, T. G. M. van de Ven, P. J. Carreau, *Cellulose* **2015**, *22*, 1109.
[165] S. N. Molnes, I. P. Torrijos, S. Strand, K. G. Paso, K. Syverud, *Ind. Crops Prod.* **2016**, *93*, 152.
[166] Y. Qin, R. Chang, S. Ge, L. Xiong, Q. Sun, *Int. J. Biol. Macromol.* **2017**, *102*, 1073.
[167] P. Bertsch, S. Isabettini, P. Fischer, *Biomacromolecules* **2017**, *18*, 4060.
[168] Y. Xu, A. Atrens, J. R. Stokes, *Adv. Colloid Interface Sci.* **2020**, *275*, 102076.
[169] M. Chau, S. E. Sriskandha, D. Pichugin, H. Thérien-Aubin, D. Nykypanchuk, G. Chauve, M. Méthot, J. Bouchard, O. Gang, E. Kumacheva, *Biomacromolecules* **2015**, *16*, 2455.
[170] F. W. Herrick, R. L. Casebier, J. K. Hamilton, K. R. Sandberg, *J. Appl. Polym. Sci.: Appl. Polym. Symp.* **1983**.
[171] A. Naderi, T. Lindström, *Nord. Pulp Pap. Res. J.* **2016**, *31*, 354.
[172] X. M. Dong, D. G. Gray, *Langmuir* **1997**, *13*, 2404.
[173] H. Imura, K. Okano, *Jpn. J. Appl. Phys.* **1972**, *11*, 1440.
[174] S. N. Molnes, K. G. Paso, S. Strand, K. Syverud, *Cellulose* **2017**, *24*, 4479.
[175] E. B. Heggset, G. Chinga-Carrasco, K. Syverud, *Carbohydr. Polym.* **2017**, *157*, 114.
[176] J. Sugiyama, H. Chanzy, G. Maret, *Macromolecules* **1992**, *25*, 4232.
[177] K. J. De France, K. G. Yager, T. Hoare, E. D. Cranston, *Langmuir* **2016**, *32*, 7564.
[178] J.-F. Revol, L. Godbout, X.-M. Dong, D. G. Gray, H. Chanzy, G. Maret, *Liq. Cryst.* **1994**, *16*, 127.
[179] D. H. Kim, Y. S. Song, *Carbohydr. Polym.* **2015**, *126*, 240.
[180] K. Choi, C. Y. Gao, J. Do Nam, H. J. Choi, *Materials* **2017**, *10*, 1060.
[181] L. L. Xu, X. L. Shi, Q. L. Wang, *Mater. Sci. Forum* **2015**, *815*, 217.
[182] Z. Liu, P. Chen, Y. D. Liu, L.-M. Wang, H. J. Choi, *Curr. Smart Mater.* **2018**, *3*, 58.
[183] L. S. Sandell, P. Luner, *J. Appl. Polym. Sci.* **1974**, *18*, 2075.
[184] A. Lu, Y. Song, Y. Boluk, *Carbohydr. Polym.* **2014**, *114*, 57.
[185] V. K. LaMer, *Rev. Pure Appl. Chem.* **1963**, *13*, 112.
[186] P. Raj, S. Varanasi, W. Batchelor, G. Garnier, *J. Colloid Interface Sci.* **2015**, *447*, 113.
[187] M. D. Sikora, R. A. Stratton, *Tappi* **1981**, *64*, 97.
[188] H. Tanaka, A. Swerin, L. Ödberg, *Tappi J.* **1993**, *76*, 157.
[189] M. Ashmore, J. Hearn, F. Karpowicz, *Langmuir* **2001**, *17*, 1069.
[190] P. Jenkins, M. Snowden, *Adv. Colloid Interface Sci.* **1996**, *68*, 57.
[191] N. Pahimanolis, A. Salminen, P. A. Penttilä, J. T. Korhonen, L.-S. Johansson, J. Ruokolainen, R. Serimaa, J. Seppälä, *Cellulose* **2013**, *20*, 1459.
[192] M. H. J. Korhonen, A. Sorvari, T. Saarinen, J. Seppälä, J. Laine, *BioResources* **2014**, *9*, 3550.
[193] L. J. Hall, J. P. Deville, C. M. Santos, O. J. Rojas, C. S. Araujo, in *IADC/SPE Drilling Conf. and Exhibition*, Society of Petroleum Engineers, **2018**, SPE-[illegible].
[194] Y. Boluk, L. Zhao, V[illegible]
[195] H. Oguzlu, C. Danu[illegible]
[196] H. Oguzlu, Y. Boluk, [illegible]
[197] Y. Chen, C. Xu, J. [illegible] *Carbohydr. Polym.* **2017**, *157*, 303.
[198] S. Y. Ahn, Y. S. Song, [illegible] *Carbohydr. Polym.* **2016**, *151*, 119.
[199] C. E. Meree, G. T[illegible] Schueneman, J. C. Meredith, M. L. Shofner, *Cellulose* **2016**, *23*, 3001.
[200] P. Myllytie, S. Holappa, J. Paltakari, J. Laine, *Nord. Pulp Pap. Res. J.* **2009**, *24*, 125.
[201] A. Vesterinen, P. Myllytie, J. Laine, J. Seppälä, *J. Appl. Polym. Sci.* **2010**, *116*, 2990.
[202] H. Bian, L. Wei, C. Lin, Q. Ma, H. Dai, J. Y. Zhu, *ACS Sustainable Chem. Eng.* **2018**, *6*, 4821.
[203] C. Liu, M.-C. Li, W. Chen, R. Huang, S. Hong, Q. Wu, C. Mei, *Carbohydr. Polym.* **2020**, *246*, 116548.
[204] M. Imani, K. Dimic-Misic, M. Tavakkoli, O. J. Rojas, P. A. C. Gane, *Biomacromolecules* **2020**, *21*, 4123.
[205] H. Q. Lê, K. Dimic-Misic, L.-S. Johansson, T. Maloney, H. Sixta, *Cellulose* **2018**, *25*, 179.
[206] M. C. Iglesias, N. Shivyari, A. Norris, R. Martin-Sampedro, M. E. Eugenio, P. Lahtinen, M. L. Auad, T. Elder, Z. Jiang, C. E. Frazier, M. S. Peresin, *J. Wood Chem. Technol.* **2020**, *40*, 370.
[207] Y. Peng, D. J. Gardner, Y. Han, *Cellulose* **2012**, *19*, 91.
[208] N. Butchosa, Q. Zhou, *Cellulose* **2014**, *21*, 4349.
[209] V. Khoshkava, M. R. Kamal, *ACS Appl. Mater. Interfaces* **2014**, *6*, 8146.
[210] M. V. G. Zimmermann, C. Borsoi, A. Lavoratti, M. Zanini, A. J. Zattera, R. M. C. Santana, *J. Reinf. Plast. Compos.* **2016**, *35*, 628.
[211] W. Abdallah, M. R. Kamal, *Cellulose* **2018**, *25*, 5711.
[212] C. Eyholzer, N. Bordeanu, F. Lopez-Suevos, D. Rentsch, T. Zimmermann, K. Oksman, *Cellulose* **2010**, *17*, 19.

[213] K. Ben Azouz, E. C. Ramires, W. Van den Fonteyne, N. El Kissi, A. Dufresne, *ACS Macro Lett.* **2012**, *1*, 236.
[214] M. Hietala, S. Sain, K. Oksman, *Cellulose* **2017**, *24*, 2177.
[215] Z. Hu, H. S. Marway, H. Kasem, R. Pelton, E. D. Cranston, *ACS Macro Lett.* **2016**, *5*, 185.
[216] K. Missoum, J. Bras, M. N. Belgacem, *Biomacromolecules* **2012**, *13*, 4118.
[217] S. Beck, J. Bouchard, R. Berry, *Biomacromolecules* **2012**, *13*, 1486.
[218] K. Dimic-Misic, P. A. C. Gane, J. Paltakari, *Ind. Eng. Chem. Res.* **2013**, *52*, 16066.
[219] K. Dimic-Misic, T. Salo, J. Paltakari, P. Gane, *Nord. Pulp Pap. Res. J.* **2014**, *29*, 253.
[220] C. K. Chua, C. H. Wong, W. Y. Yeong, *Standards, Quality Control, and Measurement Sciences in 3D Printing and Additive Manufacturing*, Academic Press, San Diego, CA, USA **2017**.
[221] P. S. Gungor-Ozkerim, I. Inci, Y. S. Zhang, A. Khademhosseini, M. R. Dokmeci, *Biomater. Sci.* **2018**, *6*, 915.
[222] M. Guvendiren, J. Molde, R. M. D. Soares, J. Kohn, *ACS Biomater. Sci. Eng.* **2016**, *2*, 1679.
[223] S. Sultan, G. Siqueira, T. Zimmermann, A. P. Mathew, *Curr. Opin. Biomed. Eng.* **2017**, *2*, 29.
[224] C. C. Piras, S. Fernández-Prieto, W. M. De Borggraeve, *Biomater. Sci.* **2017**, *5*, 1988.
[225] G. Chinga-Carrasco, *Biomacromolecules* **2018**, *19*, 701.
[226] P. Gatenholm, H. Martinez, E. Karabulut, M. Amoroso, L. Kölby, K. Markstedt, E. Gatenholm, I. Henriksson, in *3D Printing and Biofabrication*, (Eds: A. Ovsianikov, J. Yoo, V. Mironov), Springer, Berlin, Germany **2018**, pp. 331–352.
[227] W. Xu, X. Wang, N. Sandler, S. Willför, C. Xu, *ACS Sustainable Chem. Eng.* **2018**, *6*, 5663.
[228] Q. Wang, J. Sun, Q. Yao, C. Ji, J. Liu, Q. Zhu, *Cellulose* **2018**, *25*, 4275.
[229] F. Hoeng, A. Denneulin, J. Bras, *Nanoscale* **2016**, *8*, 13131.
[230] K. Markstedt, A. Mantas, I. Tournier, H. Martínez Ávila, D. Hägg, P. Gatenholm, *Biomacromolecules* **2015**, *16*, 1489.
[231] H. M. Ávila, S. Schwarz, N. Rotter, P. Gatenholm, *Bioprinting* **2016**, *1*, 22.
[232] D. Nguyen, D. A. Hägg, A. Forsman, J. Ekholm, P. Nimkingratana, C. Brantsing, T. Kalogeropoulos, S. Zaunz, S. Concaro, M. Brittberg, *Sci. Rep.* **2017**, *7*, 658.
[233] T. Möller, M. Amoroso, D. Hägg, C. Brantsing, N. Rotter, P. Apelgren, A. Lindahl, L. Kölby, P. Gatenholm, *Plast. Reconstr. Surg. - Global Open* **2017**, *5*, e1227.
[234] M. Müller, E. Öztürk, Ø. Arlov, P. Gatenholm, M. Zenobi-Wong, *Ann. Biomed. Eng.* **2017**, *45*, 210.
[235] I. Henriksson, P. Gatenholm, D. A. Hägg, *Biofabrication* **2017**, *9*, 015022.
[236] K. Markstedt, A. Escalante, G. Toriz, P. Gatenholm, *ACS Appl. Mater. Interfaces* **2017**, *9*, 40878.
[237] Y. Jiang, X. Xv, D. Liu, Z. Yang, Q. Zhang, H. Shi, G. Zhao, J. Zhou, *BioResources* **2018**, *13*, 5909.
[238] S. Shin, S. Park, M. Park, E. Jeong, K. Na, H. J. Youn, J. Hyun, *BioResources* **2017**, *12*, 2941.
[239] H. Mertaniemi, C. Escobedo-Lucea, A. Sanz-Garcia, C. Gandía, A. Mäkitie, J. Partanen, O. Ikkala, M. Yliperttula, *Biomaterials* **2016**, *82*, 208.
[240] V. C. F. Li, A. Mulyadi, C. K. Dunn, Y. Deng, H. J. Qi, *ACS Sustainable Chem. Eng.* **2018**, *6*, 2011.
[241] G. Chinga-Carrasco, N. V Ehman, J. Pettersson, M. E. Vallejos, M. W. Brodin, F. E. Felissia, J. Håkansson, M. C. Area, *ACS Sustainable Chem. Eng.* **2018**, *6*, 4068.
[242] V. Kuzmenko, E. Karabulut, E. Pernevik, P. Enoksson, P. Gatenholm, *Carbohydr. Polym.* **2018**, *189*, 22.
[243] C. Xu, B. Zhang Molino, X. Wang, F. Cheng, W. Xu, P. Molino, M. Bacher, D. Su, T. Rosenau, S. Willför, G. Wallace, *J. Mater. Chem. B* **2018**, *6*, 7066.
[244] W. Xu, B. Z. Molino, F. Cheng, P. J. Molino, Z. Yue, D. Su, X. Wang, S. Willför, C. Xu, G. G. Wallace, *ACS Appl. Mater. Interfaces* **2019**, *11*, 8838.
[245] A. Rees, L. C. Powell, G. Chinga-Carrasco, D. T. Gethin, K. Syverud, K. E. Hill, D. W. Thomas, *Biomed Res. Int.* **2015**, *2015*, 925757.
[246] G. Chinga-Carrasco, N. V Ehman, D. Filgueira, J. Johansson, M. E. Vallejos, F. E. Felissia, J. Håkansson, M. C. Area, *Addit. Manuf.* **2019**, *28*, 267.
[247] J. Leppiniemi, P. Lahtinen, A. Paajanen, R. Mahlberg, S. Metsä-Kortelainen, T. Pinomaa, H. Pajari, I. Vikholm-Lundin, P. Pursula, V. P. Hytönen, *ACS Appl. Mater. Interfaces* **2017**, *9*, 21959.
[248] R. Ajdary, S. Huan, N. Zanjanizadeh Ezazi, W. Xiang, R. Grande, H. A. Santos, O. J. Rojas, *Biomacromolecules* **2019**, *20*, 2770.
[249] V. C.-F. Li, C. K. Dunn, Z. Zhang, Y. Deng, H. J. Qi, *Sci. Rep.* **2017**, *7*, 8018.
[250] Y. Wu, Z. Y. W. Lin, A. C. Wenger, K. C. Tam, X. S. Tang, *Bioprinting* **2018**, *9*, 1.
[251] N. B. Palaganas, J. D. Mangadlao, A. C. C. de Leon, J. O. Palaganas, K. D. Pangilinan, Y. J. Lee, R. C. Advincula, *ACS Appl. Mater. Interfaces* **2017**, *9*, 34314.
[252] A. Khabibullin, M. Alizadehgiashi, N. Khuu, E. Prince, M. Tebbe, E. Kumacheva, *Langmuir* **2017**, *33*, 12344.
[253] B. A. Frost, B. P. Sutliff, P. Thayer, M. J. Bortner, E. J. Foster, *Front. Bioeng. Biotechnol.* **2019**, *7*, 280.
[254] C. Jia, H. Bian, T. Gao, F. Jiang, I. M. Kierzewski, Y. Wang, Y. Yao, L. Chen, Z. Shao, J. Y. Zhu, *ACS Appl. Mater. Interfaces* **2017**, *9*, 28922.
[255] S. Sultan, A. P. Mathew, *Nanoscale* **2018**, *10*, 4421.
[256] Y. Jiang, J. Zhou, Z. Yang, D. Liu, X. Xv, G. Zhao, H. Shi, Q. Zhang, *J. Mater. Sci.* **2018**, *53*, 11883.
[257] T. Kim, C. Bao, M. Hausmann, G. Siqueira, T. Zimmermann, W. S. Kim, *Adv. Electron. Mater.* **2019**, *5*, 1800778.
[258] Y. Shao, D. Chaussy, P. Grosseau, D. Beneventi, *Ind. Eng. Chem. Res.* **2015**, *54*, 10575.
[259] D. Cao, Y. Xing, K. Tantratian, X. Wang, Y. Ma, A. Mukhopadhyay, Z. Cheng, Q. Zhang, Y. Jiao, L. Chen, *Adv. Mater.* **2019**, *31*, 1807313.
[260] W. Cao, C. Ma, D. Mao, J. Zhang, M. Ma, F. Chen, *Adv. Funct. Mater.* **2019**, *29*, 1905898.
[261] K. M. O. Håkansson, I. C. Henriksson, C. de la Peña Vázquez, V. Kuzmenko, K. Markstedt, P. Enoksson, P. Gatenholm, *Adv. Mater. Technol.* **2016**, *1*, 1600096.
[262] Y. Li, H. Zhu, Y. Wang, U. Ray, S. Zhu, J. Dai, C. Chen, K. Fu, S. Jang, D. Henderson, *Small Methods* **2017**, *1*, 1700222.
[263] H. Françon, Z. Wang, A. Marais, K. Mystek, A. Piper, H. Granberg, A. Malti, P. Gatenholm, P. A. Larsson, L. Wågberg, *Adv. Funct. Mater.* **2020**, *30*, 1909383.
[264] C. L. Ventola, *Pharm. Ther.* **2014**, *39*, 704.
[265] Z. Tehrani, H. R. Nordli, B. Pukstad, D. T. Gethin, G. Chinga-Carrasco, *Ind. Crops Prod.* **2016**, *93*, 193.
[266] E. Macdonald, R. Salas, D. Espalin, M. Perez, E. Aguilera, D. Muse, R. B. Wicker, *IEEE Access* **2014**, *2*, 234.
[267] H. Zhang, C. Dou, L. Pal, M. A. Hubbe, *BioResources* **2019**, *14*, 7494.
[268] A. S. Apaleke, A. A. Al-Majed, M. E. Hossain, in *North Africa Technical Conf. and Exhibition*, Society of Petroleum Engineers, **2012**, SPE-149555.
[269] Z. Vryzas, V. C. Kelessidis, [illegible]
[270] M.-C. Li, Q. Wu, J. [illegible] *tainable Chem. Eng.* **2**
[271] M.-C. Li, S. Ren, X. [illegible] Zhang, L. Dong, T. Lei, S. Lee, Q. Wu, *ACS Appl. Nano Mater.* **20**[illegible]8, *1*, 7039.
[272] M.-C. Li, Q. Wu, T. [illegible]ei, C. Mei, X. Xu, S. Lee, J. Gwon, *Energy Fuels* **2020**, *34*, 8206.
[273] M.-C. Li, Z. Tang, C[illegible] Liu, R. Huang, M. S. Koo, G. Zhou, Q. Wu, *Ind. Eng. Chem. Res.* **2020**, *59*, 14352.

[274] Y. Villada, M. C. Iglesias, N. Casis, E. Erdmann, M. S. Peresin, D. Estenoz, *Cellulose* **2018**, *25*, 7091.
[275] C. Liu, M. Li, C. Mei, W. Chen, J. Han, Y. Yue, S. Ren, A. D. French, G. M. Aita, G. Eggleston, Q. Wu, *Ind. Crops Prod.* **2020**, *150*, 112378.
[276] K. Song, Q. Wu, M. Li, S. Ren, L. Dong, X. Zhang, T. Lei, Y. Kojima, *Colloids Surf., A* **2016**, *507*, 58.
[277] K. Song, Q. Wu, M.-C. Li, A. K. Wojtanowicz, L. Dong, X. Zhang, S. Ren, T. Lei, *J. Nat. Gas Sci. Eng.* **2016**, *34*, 1403.
[278] L. J. Hall, J. P. Deville, C. S. Araujo, S. Li, O. J. Rojas, in *SPE Int. Conf. on Oilfield Chemistry*, Society of Petroleum Engineers, ~~Mont-gomery,~~ **2017**, SPE-184576.
[279] F. Pacheco-Torgal, S. Jalali, *Constr. Build. Mater.* **2011**, *25*, 575.
[280] F. Ridi, E. Fratini, P. Baglioni, *J. Colloid Interface Sci.* **2011**, *357*, 255.
[281] C. F. Ferraris, K. H. Obla, R. Hill, *Cem. Concr. Res.* **2001**, *31*, 245.
[282] G. Sant, C. F. Ferraris, J. Weiss, *Cem. Concr. Res.* **2008**, *38*, 1286.
[283] P. F. G. Banfill, *Rheology of Fresh Cement and Concrete: Proceedings of an International Conference*, CRC Press, Liverpool **1990**, 2014.
[284] C. Hu, F. de Larrard, *Cem. Concr. Res.* **1996**, *26*, 283.
[285] *Microfibrillated Cellulose and Rheology Modification*, Borregaard, Sarpsborg, Norway **2017**; https://response.exilva.com/free-ebook-microfibrillated-cellulose-and-rheology-modifications (accessed: November 2020).
[286] Y. Cao, P. Zavaterri, J. Youngblood, R. Moon, J. Weiss, *Cem. Concr. Compos.* **2015**, *56*, 73.
[287] Y. Cao, P. Zavattieri, J. Youngblood, R. Moon, J. Weiss, *Constr. Build. Mater.* **2016**, *119*, 71.
[288] X. Sun, Q. Wu, J. Zhang, Y. Qing, Y. Wu, S. Lee, *Mater. Des.* **2017**, *114*, 92.
[289] L. Jiao, M. Su, L. Chen, Y. Wang, H. Zhu, H. Dai, *PLoS One* **2016**, *11*, e0168422.
[290] O. Onuaguluchi, D. K. Panesar, M. Sain, *Constr. Build. Mater.* **2014**, *63*, 119.
[291] R. Mejdoub, H. Hammi, J. J. Suñol, M. Khitouni, A. M 'nif, S. Boufi, *J. Compos. Mater.* **2017**, *51*, 2491.
[292] S. Peters, T. Rushing, E. Landis, T. Cummins, *Transp. Res. Rec. J. Transp. Res. Board* **2010**, 25.
[293] Y. Wen, B. Wei, D. Cheng, X. An, Y. Ni, *Cellulose* **2017**, *24*, 731.
[294] B. Wei, Y. Xue, Y. Wen, J. Li, *J. Bioresour. Bioprod.* **2016**, *1*, 186.
[295] Q. Li, B. Wei, L. Lu, Y. Li, Y. Wen, W. Pu, H. Li, C. Wang, *Fuel* **2017**, *207*, 352.
[296] B. Wei, L. Qinzhi, Y. Wang, K. Gao, W. Pu, L. Sun, in *SPE Improved Oil Recovery. Conf., Society of Petroleum Engineers*, **2018**, SPE-190283.
[297] S. Farnazeh, M. Sohrabi, *Soc. Pet. Eng.* **2013**, SPE-164917.
[298] B. Wei, H. Li, Q. Li, Y. Wen, L. Sun, P. Wei, W. Pu, Y. Li, *Langmuir* **2017**, *33*, 5127.
[299] B. Wei, Y. Wang, Y. Wen, X. Xu, C. Wood, L. Sun, *J. Ind. Eng. Chem.* **2018**.
[300] S. N. Molnes, A. Mamonov, K. G. Paso, S. Strand, K. Syverud, *Cellulose* **2018**, *25*, 2289.
[301] A. F. Turbak, F. W. Snyder, K. R. Sandberg, *J. Appl. Polym. Sci.: Appl. Polym. Symp.* **1983**, *2*, 37.
[302] H. Yano, K. Abe, Y. Kase, S. Kikkawa, Y. Onishi, *WO2013039110A1* **2012**.
[303] L. Sun, W. Chen, Y. Liu, J. Li, H. Yu, *Cellulose* **2015**, *22*, 2619.
[304] J. Velásquez-Cock, A. Serpa, L. Vélez, P. Gañán, C. Gómez Hoyos, C. Castro, L. Duizer, H. D. Goff, R. Zuluaga, *Food Hydrocolloids* **2019**, *87*, 204.
[305] I. Kalashnikova, H. Bizot, B. Cathala, I. Capron, *Langmuir* **2011**, *27*, 7471.
[306] K. Xhanari, K. Syverud, G. Chinga-Carrasco, K. Paso, P. Stenius, *J. Colloid Interface Sci.* **2011**, *356*, 58.
[307] L. Golchoobi, M. Alimi, S. Shokoohi, H. Yousefi, *J. Texture Stud.* **2016**, *47*, 403.
[308] L. Bai, S. Huan, W. Xiang, O. J. Rojas, *Green Chem.* **2018**, *20*, 1571.
[309] A. Lif, P. Stenstad, K. Syverud, M. Nydén, K. Holmberg, *J. Colloid Interface Sci.* **2010**, *352*, 585.
[310] S. Huan, S. Yokota, L. Bai, M. Ago, M. Borghei, T. Kondo, O. J. Rojas, *Biomacromolecules* **2017**, *18*, 4393.
[311] M. Andresen, P. Stenius, *J. Dispersions Sci. Technol.* **2007**, *28*, 837.
[312] K.-Y. Lee, J. J. Blaker, R. Murakami, J. Y. Y. Heng, A. Bismarck, *Langmuir* **2014**, *30*, 452.
[313] I. Kalashnikova, H. Bizot, B. Cathala, I. Capron, *Biomacromolecules* **2012**, *13*, 267.
[314] I. Kalashnikova, H. Bizot, B. Cathala, I. Capron, *Soft Matter* **2013**, *9*, 95.
[315] Z. Hu, T. Patten, R. Pelton, E. D. Cranston, *ACS Sustainable Chem. Eng.* **2015**, *3*, 1023.
[316] Z. Hu, S. Ballinger, R. Pelton, E. D. Cranston, *J. Colloid Interface Sci.* **2015**, *439*, 139.
[317] L. Bai, W. Xiang, S. Huan, O. J. Rojas, *Biomacromolecules* **2018**, *19*, 1674.
[318] S. A. Kedzior, H. S. Marway, E. D. Cranston, *Macromolecules* **2017**, *50*, 2645.
[319] Y. Li, X. Liu, Z. Zhang, S. Zhao, G. Tian, J. Zheng, D. Wang, S. Shi, T. P. Russell, *Angew. Chem.* **2018**, *130*, 13748.
[320] A. G. Cunha, J.-B. Mougel, B. Cathala, L. A. Berglund, I. Capron, *Langmuir* **2014**, *30*, 9327.
[321] A. J. Svagan, A. Musyanovych, M. Kappl, M. Bernhardt, G. Glasser, C. Wohnhaas, L. A. Berglund, J. Risbo, K. Landfester, *Biomacromolecules* **2014**, *15*, 1852.
[322] J. Guo, W. Du, Y. Gao, Y. Cao, Y. Yin, *Colloids Surf., A* **2017**, *529*, 634.
[323] M. Visanko, H. Liimatainen, J. A. Sirviö, J. P. Heiskanen, J. Niinimäki, O. Hormi, *Biomacromolecules* **2014**, *15*, 2769.
[324] J. Ojala, J. A. Sirviö, H. Liimatainen, *Chem. Eng. J.* **2016**, *288*, 312.
[325] Y. Zhang, V. Karimkhani, B. T. Makowski, G. Samaranayake, S. J. Rowan, *Macromolecules* **2017**, *50*, 6032.
[326] D. Saidane, E. Perrin, F. Cherhal, F. Guellec, I. Capron, *Philos. Trans. R. Soc., A* **2016**, *374*, 20150139.
[327] W. Du, J. Guo, H. Li, Y. Gao, *ACS Sustainable Chem. Eng.* **2017**, *5*, 7514.
[328] G. Sèbe, F. Ham-Pichavant, G. Pecastaings, *Biomacromolecules* **2013**, *14*, 2937.
[329] A. Werner, V. Schm... 6064.
[330] F. Liu, J. Zheng, C.-... *loids* **2018**, *82*, 96.
[331] Q.-H. Chen, J. Zhe... *Hydrocolloids* **2018**, *75*, 125.
[332] Z. Zhang, K. C. Ta... *Eng.* **2018**, *6*, 2583.
[333] X. Gong, Y. Wang, ... Chen, *Carbohydr. Polym.* **2017**, *169*, 295.
[334] L. Salvia-Trujillo, O... Martín-Belloso, D. J. McClements, *Nanomaterials* **2016**, *6*, 17.
[335] R. R. Eley, *Rheol. Rev.* **2005**, *2005*, 173.
[336] Y. Xu, Y. Kuang, P. J. Salminen, G. Chen, *BioResources* **2016**, *11*, 4342.
[337] T. Salo, K. Dimic-Misic, P. Gane, J. Paltakari, *Nord. Pulp Pap. Res. J.* **2015**, *30*, 165.
[338] K. Dimic-Misic, C. Ridgway, T. Maloney, J. Paltakari, P. Gane, *Transp. Porous Media* **2014**, *103*, 155.
[339] K. Oh, J.-H. Lee, W. Im, A. Rajabi Abhari, H. L. Lee, *Ind. Eng. Chem. Res.* **2017**, *56*, 9569.
[340] S. M. M. Mousavi, E. Afra, M. Tajvidi, D. W. Bousfield, M. Dehghani-Firouzabadi, *Prog. Org. Coat.* **2018**, *122*, 207.

[341] D. Zhou, Y. Tang, N. Zhang, J. Zhang, D. Liu, *Dig. J. Nanomater. Biostruct.* **2014**, *9*, 305.
[342] P. Tyagi, M. A. Hubbe, L. Lucia, L. Pal, *Cellulose* **2018**, *25*, 3377.
[343] C. Liu, H. Du, L. Dong, X. Wang, Y. Zhang, G. Yu, B. Li, X. Mu, H. Peng, H. Liu, *Ind. Eng. Chem. Res.* **2017**, *56*, 8264.
[344] F. Grüneberger, T. Künniger, T. Zimmermann, M. Arnold, *J. Mater. Sci.* **2014**, *49*, 6437.
[345] F. Grüneberger, T. Künniger, A. Huch, T. Zimmermann, M. Arnold, *Prog. Org. Coat.* **2015**, *87*, 112.
[346] Y. Tan, Y. Liu, W. Chen, Y. Liu, Q. Wang, J. Li, H. Yu, *ACS Sustainable Chem. Eng.* **2016**, *4*, 3766.
[347] Y. Jiang, Y. Zhang, L. Ding, B. Wang, Z. Chen, Y. Zhong, L. Zhang, Z. Mao, H. Xu, X. Sui, *Prog. Org. Coat.* **2018**, *123*, 146.
[348] R. A. Chowdhury, C. Clarkson, J. Youngblood, *Cellulose* **2018**, *25*, 1769.
[349] R. A. Chowdhury, C. Clarkson, V. A. Apalangya, S. M. N. Islam, J. P. Youngblood, *Cellulose* **2018**, *25*, 2547.
[350] F. Hoeng, A. Denneulin, N. Reverdy-Bruas, G. Krosnicki, J. Bras, *Appl. Surf. Sci.* **2017**, *394*, 160.
[351] F. Hoeng, A. Denneulin, G. Krosnicki, J. Bras, *J. Mater. Chem. C* **2016**, *4*, 10945.
[352] R. Blell, Why will MFC show potential in cosmetic applications in 2016, https://blog.exilva.com/why-will-mfc-show-potential-in-cosmetic-applications-in-2016 **2016**, (accessed: November 2020).
[353] E. J. Foster, R. J. Moon, U. P. Agarwal, M. J. Bortner, J. Bras, S. Camarero-Espinosa, K. J. Chan, M. J. D. Clift, E. D. Cranston, S. J. Eichhorn, *Chem. Soc. Rev.* **2018**, *47*, 2609.

Mei-Chun Li received his Ph.D. (2013) in applied chemical engineering from Korea University of Technology and Education, South Korea. He was then employed as a lecturer in Korea University of Technology and Education, and later as a postdoctoral research scientist in Louisiana State University, USA. Currently, he is a full professor at Nanjing Forestry University, China. He was awarded as Jiangsu Distinguished Professor in 2019. His interests cover the application of cellulose nanomaterials in drilling fluids, 3D printing inks, and polymer composites.

Qinglin Wu is currently Gordon Cain Chair of Agriculture and Roy O. Martin Sr. Professor at the Louisiana State University (LSU) Agricultural Center. He is a member of International Academy of Wood Science (IAWS) and EU Academy of Sciences (EUAS). He holds a Ph.D. degree in wood science and engineering from Oregon State University (USA) and an M.S. degree in mechanical engineering from University of Tasmania (Australia). His research focus on sustainable cellulose nanomaterials as building blocks for composites, fluids, and energy storage materials.